Volume 19, Number 4

October, 1965

SOVIET ATOMIC ENERGY

АТОМНАЯ ЭНЕРГИЯ
(ATOMNAYA ÉNERGIYA)

TRANSLATED FROM RUSSIAN

CONSULTANTS BUREAU

Declassified and Approved For Release 2013/03/15 : CIA-RDP10-02196R000700020004-2

CRYSTALLOGRAPHY

THE GROWTH OF CRYSTALS

A. V. Shubnikov and N. N. Sheftal', Series Editors

This continuing series on crystal growth represents the work of Soviet scientists for the most part originally presented at the All-Union Conferences on Crystal Growth held at the Institute of Crystallography in Moscow.

Volume 4

These 42 papers deal with experimental studies on growth (in part, nucleation) of crystals and monocrystalline films, liquid crystals, the production of monocrystals of various materials, the search for ways of growing new crystals, important aspects of crystal growth, and surveys for ferroelectric crystals. Includes two papers on crystal symmetry by Sheftal' especially expanded and revised for this edition. Translated from Russian.

CONTENTS: **Experimental Studies:** Production of crystallization nuclei in the presence of a seed crystal • Relation of impurity effects in crystal growth to pH of solution • Growth of epitaxial germanium films from supercooled droplets • Effects of pH on the shape of ammonium dihydrogen phosphate crystals • Production of crystallization nuclei at the surface of an aqueous solution by a spark discharge • Equilibrium shape of a crystal in relation to the bulk free energy • The effects of borax on the rate of growth of alum crystals from solution • Transfer of defects in a deformed seed to the grown crystal • Anisotropy in the melting of o-nitrophenol crystals in the saturated vapor of camphor • Formation of skeletal cavities in lithium fluoride crystals • Conical structures on crystals • Frost patterns on windows • Growth form and properties of liquid crystals of thiazine dyes • Vitrified liquid-crystal films • Growth of monocrystalline nematic films • **Growth of Monocrystals and Auxiliary Studies:** Growth and piezoelectric properties of crystals of acenaphthene • Aspects of the growth of monocrystals of potassium dihydrogen phosphate • Some changes in a method of growing crystals from melts • Growth of calcite monocrystals under hydrothermal conditions • Crystallization of a film between parallel growing germanium dendrites • Growth of lead sulfide monocrystals by Tamman's method • Twin structure of germanium dendritic strips • Growth of crystals of silicon carbide from the vapor state • Growth forms of crystals of germanium and silicon grown from gaseous solution • Morphology of needle, whisker, and strip crystals of silicon • Oxidation of crystals of ferrites with the spinel structure during growth by Verneuil's method • Growth of crystals during reciprocating motion in a solution • Growth of potassium niobate crystals on seeds from a potash melt • Zinc sulfide crystals grown from a melt • Growth of Cr_2O_3 monocrystals by Verneuil's method • **Survey Work and Growth Methods:** Crystallization of zincite under hydrothermal conditions • Crystallization of cadmium sulfide from solutions in cadmium halides • Possibility of production of crystals of montroydite (HgO) under hydrothermal conditions • Crystallization of alkaline-earth molybdates under hydrothermal conditions • Hydrothermal synthesis of trigonal silicates and germanates of zinc • **Reviews:** The search for new ferroelectrics and antiferroelectrics not belonging to the oxide group • Production of monocrystals of gallium arsenide • Isomorphism and ferroelectric properties • Oriented overgrowth (epitaxis) of crystalline materials • **Miscellaneous:** *N. N. Sheftal':* The determination of symmetry • The physical meaning of symmetry • **Diary:** *N. N. Sheftal' and E. N. Slavnova:* Exchange of experience in studies on crystal growth.

206 pages 1966 $20.00

Also available:

Volume 3

368 pages 1962 $25.00

Volume 2

178 pages 1960 $16.00

Volume 1

295 pages 1958 $15.00

(c/b) **CONSULTANTS BUREAU** 227 West 17th Street, New York, New York 10011

SOVIET ATOMIC ENERGY

A translation of **ATOMNAYA ÉNERGIYA,**
a publication of the Academy of Sciences of the USSR

Volume 19, Number 4 October, 1965

CONTENTS

Annual Subscription: $95 **Single Issue: $30** **Single Article: $15**

CONTENTS (continued)

The Russian press date (podpisano k pechati) of this issue was 10/9/1965. Publication therefore did not occur prior to this date, but must be assumed to have taken place reasonably soon thereafter.

PLASMA JET DEFLECTION IN MAGNETIC FIELDS

(UDC 533.9)

V. F. Demichev, V. D. Matyukhin, A. V. Nikologorskii, and V. M. Strunnikov

Translated from Atomnaya Énergiya, Vol. 19, No. 4, pp. 329-335, October, 1965
Original article submitted February 20, 1965

We investigated the motion of plasma jets in a quadripole magnetic field produced by four current conductors whose axial lines were bent through 90° (the curvature radius was 30 cm). The maximum strength of the magnetic field in the "slit" between the current conductors was 6 kOe. The plasma jet, which was produced by means of a coaxial gun, was injected along the axis of the magnetic system. The magnetic system was adequate for deflecting the plasma jet, which had an initial velocity of 8×10^6 cm/sec and a maximum concentration before deflection of 2×10^{15} cm^{-3}. The jet velocity was equal to 7×10^6 cm/sec. In spite of the considerable loss of particles (due to the presence of slits in the magnetic system), the ion concentration in the jet beyond the turn attained 2×10^{14} cm^{-3}, while the over-all number of particles was as large as $\sim 10^{17}$.

As a result of deflection, it was possible to eliminate completely the neutral gas accompanying the jet and to obtain virtually totally ionized plasma. The optimum value of the magnetic field's strength was ~3 kOe.

The method of injection of plasma blobs into magnetic traps is widely used in investigations in the field of high-temperature plasma physics. The blobs that can presently be obtained by means of certain types of plasma injectors may have very high directional velocities (up to 10^8 mm/sec) and considerable densities $10^{12} - 10^{15}$ cm^{-3}. However, direct utilization of these blobs in traps is very complicated due to the incomplete ionization of plasma in the blob, the presence of impurities of extraneous elements, and the nonmonochromaticity of the directional velocities of blob particles. In connection with this, attempts are being made at eliminating neutral atoms and impurities from blobs by means of external magnetic fields. In particular, deflection of the plasma jet in a curvilinear magnetic field can be used for this purpose. The motion of plasma jets in curvilinear fields is also interesting in itself, since jet deflection may be found necessary for filling traps with a complex magnetic field geometry.

Magnetic fields produced by means of a bent solenoid were used in [1-5] for deflecting plasma jets. The results obtained in these experiments indicate that, under certain conditions, the hydrogen component of plasma can propagate with a concentration of up to 10^{13} cm^{-3} along a curved magnetic field with a strength of 1-2 kOe. It was found in this case that the heavy-ion impurities were eliminated from the plasma. The purification is apparently connected with polarizing electric fields [6], which arise in plasma as a result of the centrifugal and the gradient drifts. However, the presence of such fields limits the concentration of the plasma as it propagates along the curved field. The fact that the authors of [1-5] succeeded in deflecting plasma with a comparatively high concentration was a consequence of the partial neutralization of polarizing fields by the currents flowing over the plasma jet and closing the circuits either through the source or the metallic diaphragms or the plasma duct walls which were in contact with the plasma.

In order to transmit plasma with higher concentration and velocity values through a bent solenoid (which is of practical interest), it is necessary to increase the strength of the magnetic field and to neutralize to a greater extent the polarizing fields. However, this greatly reduces the purification effect, i.e., the plasma retains a large amount of impurities, the mass composition of which is completed with heavy and slow ions [3].

For plasma jet deflection, L. A. Artsimovich has suggested the use of magnetic fields produced by a system of conductors in which the current directions alternate. The present article provides the results of an experimental investigation of the motion of dense plasma jets in a magnetic field produced by a system of four current conductors

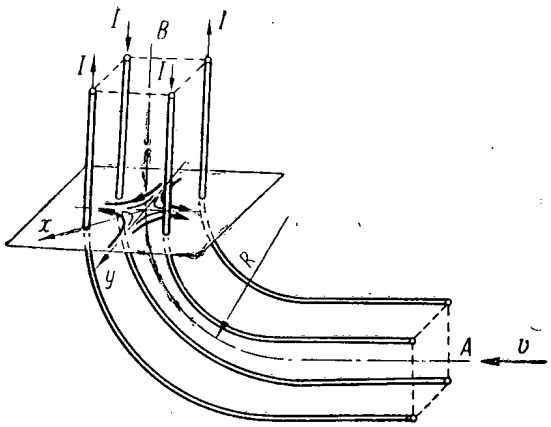

Fig. 1. Conductor system used for producing the magnetic field (the arrow indicates the direction of plasma jet injection).

(Fig. 1). The middle sections of the conductors were bent through 90°. The field strength in such a system is equal to zero along the axial line AB;* with increasing distance from this line, the field increases in correspondence with the expression:

$$H = \frac{0,2kI}{a} \cdot \frac{(r/a)^{k/2-1}}{1 \pm (r/a)^k},$$

where k is the number of conductors, I is the current intensity, and a is the distance between the axial line of the system and the conductor.†

As it is deflected from the axis, the plasma jet experiences the force of excess magnetic pressure in a direction opposite to the deflection. If the gradient of the magnetic field is sufficiently large for the excess pressure to compensate the centrifugal force, the plasma jet will be able to move along a curvilinear path near the AB axis. As a rough approximation, this condition can be expressed thus:

$$\frac{\rho v^2}{R} \approx \frac{1}{4\pi} H \frac{dH}{dr},$$

where $\rho = \sum_i M_i n_i$ is the density of plasma, v is the velocity of directional motion of a volume element of the plasma jet, and R is the turning radius. Estimates made on the basis of this expression indicate that the chosen configuration of the magnetic field could secure the deflection of plasma jets with very high velocity and plasma concentration values. For instance, in a field with a gradient of $\sim 10^3$ Oe/cm, a jet moving at a velocity of 10^7 cm/sec should be deflected with a concentration of 10^{16} cm^{-3}. However, due to the field's diffusion in plasma and the presence of slits in the magnetic system, the thus obtained plasma densities would actually have much lower values.

EXPERIMENTAL DEVICE AND INVESTIGATIVE METHOD

The schematic diagram of the device used in our experiments is shown in Fig. 2. The hydrogen plasma jet from the coaxial injector 1 passes through the porcelain cylinder 2 and the quartz cylinder 4 and enters the space between the bent current conductors 11, where it is deflected 90° from its initial direction. In order to eliminate the effect of the plasma duct walls, the curvilinear section of the current conductors is enclosed in a large vacuum volume 6. In the deflection zone, the current conductors are insulated from the plasma; they pass through Dural tube sections with vacuum sealing at the ends. Besides the bent section, the current conductors have two rectilinear sections, one ahead and one beyond the turn (both sections have a length of 30 cm). The curvature radius of the axial line is also equal to 30 cm. The spacing between adjacent current conductors is 9.2 cm. Each current conductor consists of two insulator-separated coaxial copper tubes, which are connected in such a manner that the current passes twice through the entire system. A capacitor battery C_3, which has a capacitance of 1500 μF, serves as the current source for the magnetic system. The battery is switched on by means of the vacuum discharger D_3.

The maximum strength of the magnetic field in the slit between the conductors was 6 kOe. (The value H of the magnetic field's strength that figures in the text and in the drawings pertains to this location.) The maximum value of the magnetic field's gradient near the axis attained 1.6 kOe/cm. The period of field change was equal to 0.82 msec; the jet was injected in the field at the instant of time corresponding to the maximum of the field, so that its strength remained virtually constant during the process.

*In fact, the zero field line does not coincide with the axial line on the system due to the curvature of the conductors. However, the shift of these lines is small (~3 mm), and we shall, therefore, neglect it.

† The minus sign in this expression corresponds to a change of the field in the x direction, while the plus sign corresponds to a change in the y direction (see Fig. 1).

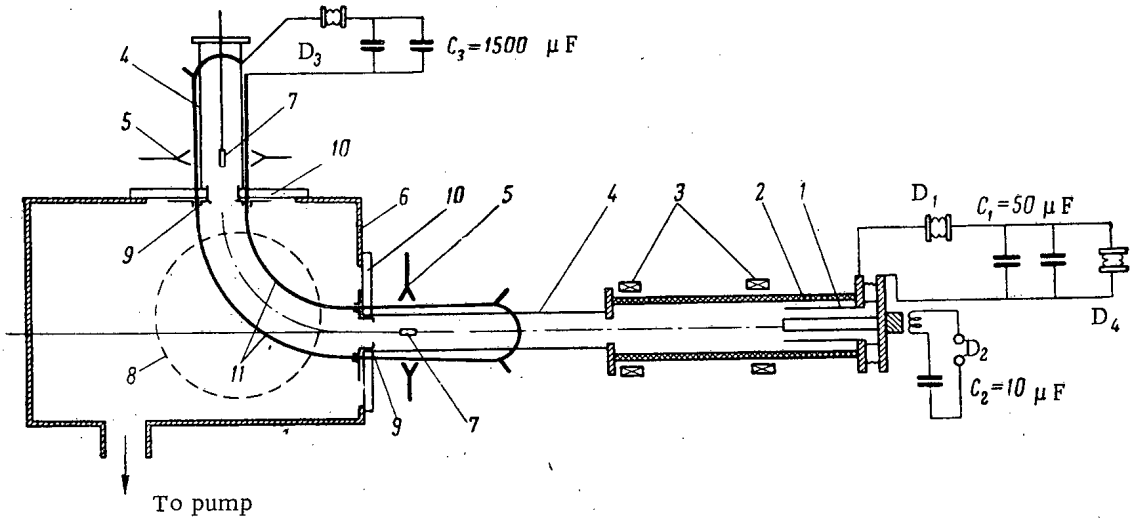

Fig. 2. Schematic diagram of the experimental device: 1) injector; 2) porcelain plasma duct (diameter: 120 mm); 3) measuring magnetic field coils; 4) quartz plasma duct (diameter: 90 mm); 5) UHF antennas; 6) vacuum volume (50 × 50 × 70 cm^3); 7) location at which the electric probes, calorimeters, and thermoprobes are installed; 8) observation window; 9) stainless-steel diaphragms (thickness, 0.1 mm; opening diameter, 60 mm); 10) plastic insulators; 11) current conductors for producing the magnetic field.

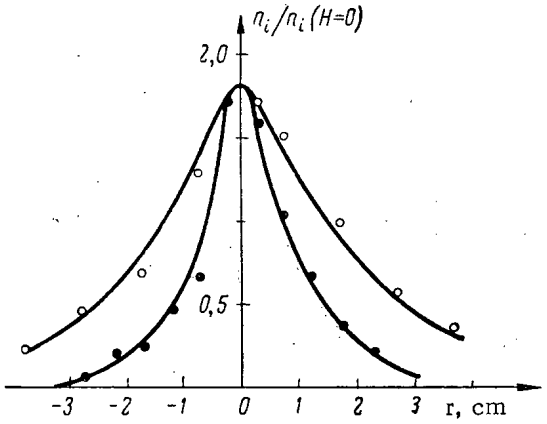

Fig. 3. Distribution of the ion concentration over the transverse cross section of the plasma jet in a field with H = 3 kOe: ● and ○) n_i distributions along the x and y axes, respectively.

A coaxial electrodynamic injector was used as the plasma source [7]. The operating conditions chosen for the injector ensured the following plasma jet parameters: The maximum directional velocity (the front velocity) was $v_{fr} = 10^7$ cm/sec; the velocity of the central jet portion, which had the highest density, was $v = 8 \cdot 10^6$ cm/sec; the maximum plasma density was $(1.5-2) \cdot 10^{15}$ cm^{-3}; the electron temperature at the concentration maximum was $T_e \approx 5$ eV; the length of the jet at the time of entrance into the magnetic field was L ≈ 50 cm. Besides the hydrogen lines, the plasma spectrum also contained the lines of carbon, copper, and other elements. The intensities of the carbon line C II 4276 A and the copper line Cu I 5218 A were comparable to the intensity of H_β, which indicate that the hydrogen plasma contained a considerable percentage of impurities.

Various experimental methods were used in the measurements. The high-speed photographing of the process was performed by means of an SFR camera. The velocity of the plasma jet and its density and temperature were measured by means of double electric and diamagnetic probes. The plasma energy was determined by using the calorimetric method and a thermoprobe [8]. The light radiation of the plasma jet was investigated by means of a spectrograph and a UM-2 monochromator with a photomultiplier adapter. Microwave diagnostics (λ = 4 mm and λ = 8 mm) was used for measuring the electron concentration and calibrating the electric probes.

EXPERIMENTAL RESULTS

The passage of plasma through the magnetic field created by the rectilinear current conductor sections was investigated in the preliminary experiments. The aim of this investigation was to ascertain the efficiency of the chosen magnetic field configuration for the transportation of dense plasma jets. The results of the experiments performed can be briefly summarized as follows.

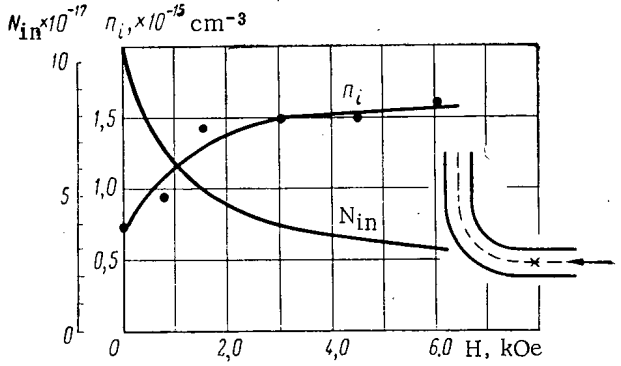

Fig. 4. Dependences of n_i and N_{in} before deflection on H (× is the point at which the n_i value was measured).

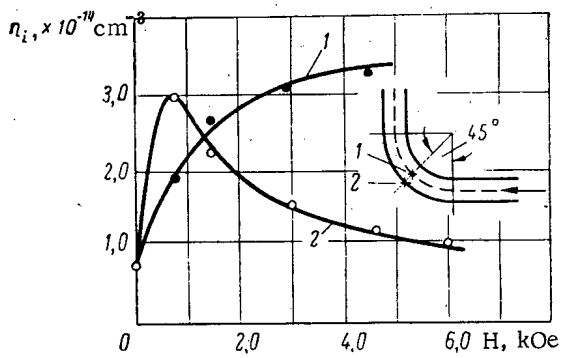

Fig. 5. Dependence of n_i at different points of the system on H: ×) position of the electric probes: probe 1 is located on the axis of the system; probe 2 is located in the magnetic slit at the middle between the current conductors.

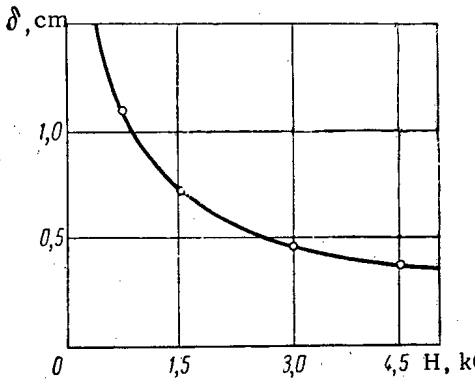

Fig. 6. Dependence of δ on the H value of the magnetic field. The measurements were performed at the point 2 (see Fig. 5).

As it becomes concentrated at the axis of the system, where H = 0, the plasma jet overcomes the rectilinear section of the field, whose length is 40 cm. For a field strength of 4.5 kOe, no changes in the velocity of the plasma jet's forward front are observed in this section. In this, the velocity of the region with the maximum concentration drops by 10-15%. The plasma density at the entrance to the field near the system's axis increases approximately by a factor of 2, after which it slowly decreases due to the leakage of plasma through the slits during its motion. The plasma cross section assumes the shape of a cross whose prongs are oriented along the magnetic field's lines of force. The effective diameter of the jet's central portion is approximately equal to 2.5 cm. It decreases with an increase in the field; the width of the prongs also decreases. The over-all number of particles in the jet that have traversed the rectilinear field section is much smaller than the number of particles in the incident jet. This can be explained mainly by the fact that the magnetic field configuration under investigation cuts out of the plasma jet, as it were, only its central region near the axis, where $\rho v^2/2 > H^2/8\pi$, while the peripheral regions of the jet are slowed down to a great extent in interaction with the transverse field, due to which their velocity drops. The leakage of plasma through the slits of the magnetic system also contributes to the reduction in the number of particles.

The ion density distribution over the transverse cross section of the plasma jet in the field is shown in Fig. 3. The density maximum is located at the axis of the system. The distribution is smoother along the magnetic field's lines of force than across the field. The results of the preliminary experiments have shown that the magnetic system under investigation can be considered as a satisfactory plasma duct for dense plasma jets.

G. A. Delone and M. M. Savchenko [9] also investigated the motion of plasma blobs in a quadripole magnetic field. They have shown that the rectilinear section of the quadripole field possesses good channeling properties for plasma with a density of $\sim 10^{12}$ cm^{-3}.

The experiments on deflecting plasma jets in a quadripole field were first performed by using a stainless-steel plasma duct, which was placed inside the magnetic system. However, the reflection of plasma from the duct walls was so intensive that it was impossible to separate the effect of plasma deflection by the magnetic field from the deflection effect due to reflection from the walls. In order to eliminate the effect of the walls, the curvilinear section of the magnetic system was enclosed in a large vacuum volume (see Fig. 2). Since, in this case, there were no walls in the deflection zone, only the magnetic field could cause the deflection of the plasma jet. All the experiments, the results of which are given below, were performed under these conditions.

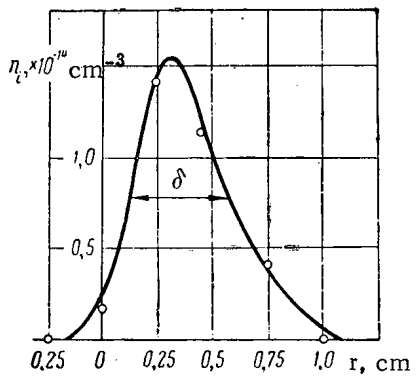

Fig. 7. Distribution of n_i across the magnetic slit for H = 3 kOe

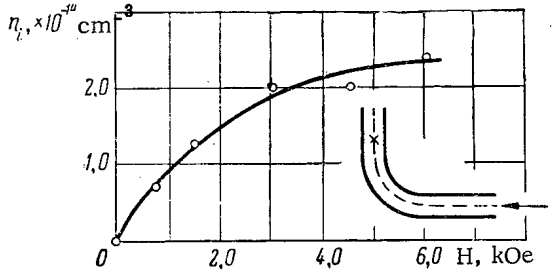

Fig. 8. Dependence of n_i in the jet after deflection on H (the probe is located at the system's axis at the point marked by the cross).

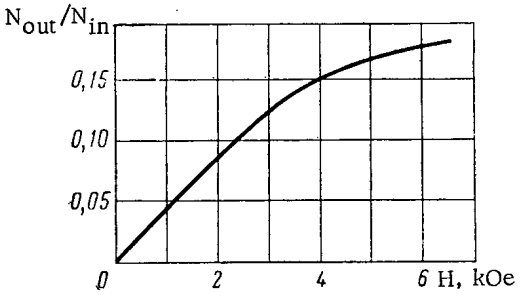

Fig. 9. Dependence of N_{out}/N_{in} on H.

Before reaching the deflection zone, the plasma jet passed through the rectilinear section of the field. With an increase in the field strength, the ion concentration in the jet near the system's axis increased before deflection. For H = 3 kOe, the concentration n_i attained $2 \cdot 10^{14}$ cm^{-3}, and it remained virtually unchanged with an additional increase in the field (Fig. 4). The total number N_{in} of ions entering the deflection zone was determined with respect to the measured transverse cross section of the plasma jet and its lengths and concentration. Figure 4 also shows the dependence of N_{in} on the magnetic field's strength. In spite of the increase in the concentration of ions in the jet, the N_{in} value decreases with an increase in the field; in this, an especially rapid decrease is observed in the case of relatively weak fields. This is mainly due to a sharp reduction in the cross-sectional area of the jet with an increase in the field strength.

High-speed photographing of the plasma passage through the curvilinear section of the magnetic field has shown that plasma overcomes this section in the form of a relatively fine jet without visible deviation from the system's axial line.

The curves (Fig. 5) showing the ion density variation at two different points of the magnetic system in dependence on the field strength make it possible to estimate the effect of the magnetic field on the deflection of plasma. The ion concentration at the magnetic system's axis monotonically increases with an increase in the field strength. The rate of this increase gradually diminishes and becomes insignificant for H $\geq$ 3 kOe. A sharp increase in the ion concentration, which is connected with plasma pinching, is observed initially with an increase in the field strength in the slit of the magnetic system (see curve 2 in Fig. 5), after which (for H > 1 kOe) the concentration decreases rather rapidly. For $\simeq$ 1.5 kOe, the ion concentration in the slit and at the system's axis are equal. With a further increase in the field strength, the ion concentration in the external slit continues to decrease, but it remains fairly high ($n_i \approx 10^{14}$ cm^{-3}) even at maximum strength(H = 6 kOe), which leads to considerable plasma losses due to leakage through the slit.

The ion concentration distribution along the radius in the deflection plane is nonsymmetric with respect to the axial line within the curvilinear section. As was to be expected, the concentration near the external slit is much higher than near the internal slit, especially in the case of weak fields. A reduction in asymmetry is observed with an increase in the field strength. A similar plasma distribution pattern in the transverse cross section was also observed in measuring the density of plasma energy by means of microcalorimeters.

The width δ of the slit through which plasma leaves the magnetic system depends on the magnetic field's strength (this dependence is given in Fig. 6). The δ value is defined as the half-width of the curve of the plasma density distribution across the slit (Fig. 7). Starting with H = 3 kOe, δ changes very little, which is apparently connected with the diffusion of the magnetic field in plasma. Therefore, for the assigned values of the plasma jet's velocity, density, and temperature at the entrance to the system, increasing the field strength beyond a certain given value (~3 kOe in our case) would be ineffective, since it would hardly reduce the plasma loss (see Figs. 5 and 6).

We should mention a peculiarity connected with plasma leakage through the slit. The curve of Fig. 7 representing the ion density in the slit is asymmetric with respect to the median deflection plane of the magnetic system. The maximum is shifted to a distance of ~0.3 cm toward the conductor in which the current direction coincides with the direction of the plasma jet's velocity. This effect is apparently connected with the drift of plasma in the crossed electric and magnetic fields. The electric polarization of plasma as it moves in a nonuniform transverse magnetic field [10].

After deflection, the plasma moved, as before deflection, in a field formed by rectilinear current conductors. The concentration of plasma, its energy, the over-all number of particles and their distribution over the transverse cross section, and the degree of plasma ionization were measured in this place. After deflection, the velocity of the densest portion of the jet was equal to 7×10^6 cm/sec.

In the absence of the field, the plasma deflection was not recorded by means of the ordinarily used methods. However, already for H = 300 Oe, the electron concentration in the plasma jet after deflection attained 1.7×10^{13} cm^{-3}. The dependence of the maximum ion concentration in the jet after deflection on the magnetic field's strength is shown in Fig. 8. The basic increase in concentration occurs as the field changes from 0 to 3 kOe. For H = 3 kOe, the concentration is equal to 2×10^{14} cm^{-3}, after which it increases very slowly with a further increase in the field strength, as can be seen from the figure.

The plasma density distribution over the transverse cross section is approximately the same as the distribution before deflection. However, the distribution in the deflection plane is somewhat asymmetric with respect to the system's axial line: The ion concentration decreases less sharply toward the external magnetic slit than toward the internal slit. The distribution of the plasma energy density has a similar shape in this plane. The mean transverse cross section of the plasma jet only slightly depends on the magnetic field's strength for H > 1 kOe; it is equal to 5-6 cm^2.

The over-all number N_{out} of particles that have been deflected increases with an increase in the field strength in spite of the fact that N_{in} decreases. Here, as in the case of the concentration value, the basic increase in N_{out} is observed as the field strength changes from 0 to 3 kOe. The dependence of the N_{out}/N_{in} ratio on the magnetic field's strength is shown in Fig. 9. The over-all number of deflected ions amounted to about 10% of N_{in}; it was equal to $\sim 5 \times 10^6$. In certain experiments, this value attained 10^{17}.

As the plasma jet moves along the curvilinear section of the magnetic system, the effect of elimination of neutral atoms from the plasma should take place. Neutral atoms, which are retained in the jet only as a result of charge-exchange collisions, will leave the surface layer of the jet, whose thickness is of the order of the charge-exchange range $\lambda = 1/n_i\sigma$, where σ is the resonance charge-exchange cross section. The effect of elimination of neutral atoms from the plasma is considerable when the λ value becomes comparable to the transverse dimensions of the jet as a result of the reduction in the ion concentration.

The checking of the elimination of neutral atoms from the plasma consists in determining the degree of ionization. One of the indirect methods used for rough estimates of the degree of ionization consisted in comparing the plasma energy measured by means of a thermoprobe or a calorimeter with the energy carried only by the ions. The ion energy was determined with respect to the measured distribution of the ion concentration along the jet and with respect to the ion velocities. According to this estimate, the degree of ionization amounted to ~100%, while the measurement error was ~20%. More accurate results were obtained by using the optical method. Since the ion concentration had been measured, the problem consisted in determining the concentration of neutral hydrogen atoms.

The method which we used made it possible to determine the upper limit of the neutral atom concentration n_0 with respect to the absolute intensity of the H_β line. This method consisted in the following. According to calculations, the distribution of the population of levels with principal quantum numbers $n \geq 3$ should obey the Boltzmann law in hydrogen plasma with an electron concentration $n_e \geq 10^{14}$ cm^{-3} and a temperature $T_e = 5$ eV. Consequently, the over-all concentration of excited atoms with $n \geq 3$ can be related to the intensity of the H_β line (n = 4) by means of the expression:

$$N = \frac{I_\beta}{A_{42} h\nu_{42}} \cdot \frac{\sum_{j=3}^{n^*} g_j e^{-\frac{\Delta E_{3j}}{T_e}}}{g_4 e^{-\frac{\Delta E_{34}}{T_e}}}.$$

Here, I_β is the intensity of the H_β radiation per unit volume of plasma, A_{42} is the Einstein coefficient of spontaneous radiation of the H_β line, ν_{42} is the frequency, g_j is the statistical weight of the level, n = j, and ΔE_{3j} is the difference between the energies of levels with n = 3 and n = j. The summation is performed up to the maximum principal quantum number n• corresponding to the maximum atomic radius R_{max} in the plasma, which, according to [11, 12], can be considered to be close to the Debye radius R_D. In our calculations, R_{max} was assumed to be equal to 0.7 R_D. The thus determined concentration N of excited atoms differed only slightly from n_0, since, according to calculations, more than 96% of all the neutral atoms were in the excited state with $n \geq 3$ in our case.

The concentration of neutral atoms, determined with respect to the absolute intensity of H_β was equal to $(1 \pm 0.7) \cdot 10^{12}$ cm^{-3}, which was less than one-hundredth of the ion concentration in the jet after deflection. Thus, it can be assumed that, after deflection, neutral hydrogen atoms are virtually completely eliminated from the plasma. The presence of the small number of neutral atoms in the jet is largely due to their entering the jet from the diaphragm and the quartz tube's walls as a result of interaction between them and the plasma flowing out the slits. A small percentage of the neutral atoms in the jet may also be the result of volume recombination.

A complete elimination of the neutral atoms of impurities should also take place in plasma deflection. Moreover, it seems that ionized impurity atoms are also eliminated to a certain extent from plasma after it has been deflected. This conclusion is reached, for instance, on the basis of the behavior of the C II 4267 A line intensity; after deflection, the intensity of C II is reduced by a factor of 500-1000.

Thus, the chosen configuration of the magnetic field proved to be a sufficiently effective system for deflecting plasma jets with a mean initial velocity of $8 \cdot 10^6$ cm/sec and a maximum initial density of $2 \cdot 10^{15}$ cm^{-3}. The plasma passed through the magnetic system near its axial line. The effective diameter of the plasma jet in the magnetic field was equal to ~2.5 cm, while its length was ~50 cm. The velocity of the jet's densest portion at the exit from the magnetic system was $7 \cdot 10^6$ cm/sec. In spite of the fact that the particle losses in plasma jet deflection were considerable due to the presence of slits, the magnetic system used made it possible to secure a plasma jet with a considerable concentration after deflection($n_i = 2 \cdot 10^{14}$ cm^{-3}), while the over-all number of particles was $\sim 10^{17}$. As a result of deflection, it was possible to eliminate the neutral gas accompanying the plasma jet and to obtain completely ionized plasma. The optimum value of the magnetic field's strength was 3 kOe.

The authors are deeply grateful to Academician L. A. Artsimovich for the suggested idea of the experiment his continued assistance during the work, and the discussion of the results. The authors are indebted to A. M. Andrianov for his continued interest in this project.

LITERATURE CITED

1. B. G. Safronov, V. S. Voitsenya, and I. I. Konovalov, ZhTF, 32, 678 (1962).
2. H. Eubank and T. Wilkerson, Phys. Fluids, 4, 1407 (1961).
3. H. Eubank and T. Wilkerson, Phys. Fluids, 6, 914 (1963).
4. V. S. Voitsenya et al., ZhTF, 34, 280 (1964).
5. G. M. Batanov et al., ZhÉTF, 46, 1915 (1964).
6. G. Schmidt, Phys. Fluids, 3. 961 (1960).
7. V. F. Demichev and V. D. Matyukhin, Dokl. AN SSSR, 150, 279 (1963).
8. Yu. G. Prokhorov et al., In the Collection: Plasma Diagnostics [in Russian], Moscow, Gosatomizdat (1963), p. 274.
9. G. A. Delone and M. M. Savchenko, ZhTF, 34, 1409 (1964).
10. I. I. Demidenko et al., ZhTF, 34, p. 1183.
11. H. Margenau and M. Lewis, Rev. Mod. Phys., 31, 595 (1959).
12. Ya. B. Zel'dovich and Yu. P. Raizer, Physics of Shock Waves and High-Temperature Hydrodynamic Phenomena [in Russian], Moscow, Fizmatgiz (1963).

THE INTERACTION OF A MODULATED FLOW WITH PLASMA

(UDC 533.9)

Ya. B. Fainberg and V. D. Shapiro

Translated from Atomnaya Énergiya, Vol. 19, No. 4,
pp. 336-342, October, 1965
Original article submitted December 28, 1964; revised May 4, 1965

The disturbance of longitudinal waves by the interaction of a modulated flow of electrons with plasma is investigated. Conditions are found for the generation of instabilities, and the frequency spectrum and increment of growth of the oscillations are calculated.

The majority of papers published on the theory of bunch instabilities deal mainly with the interaction of originally unmodulated beams of charged particles with plasma (see the literature cited in [1]). It is plain, however, that the modulation of a beam must essentially change the frequency spectrum and the growth increment of the oscillations generated, and also the effective beam and plasma temperature due to the oscillations. Preliminary modulation will destroy the particle phasing, necessary for the development of instabilities, for those oscillations with frequency and wavelength different from the modulation, and so this modulation will lead to the disruption of certain instabilities. At the same time the modulation aids in the development of instabilities with frequencies and wavelengths coinciding with those of the modulated frequency, since in this part of the spectrum the initial amplitude of the oscillations considerably exceed the fluctuation amplitude.

When an originally unmodulated beam interacts with plasma a wide wave packet with a relatively low field strength of the wave vector k in each harmonic is generated, but if the beam is modulated there will be strong resolution of the spectrum. We also note that, because of the phase grouping of the particles, caused by the modulation, the energy scattering due to the excitation may be considerably reduced, i.e., there will be a decrease in the effective temperature of the beam and the plasma. In addition to the change in the frequency spectrum and in the growth increments of the bunch instabilities, there will also be new instabilities connected with parametric resonance. The width of parametric resonance is small, however, and so the inhomogeneities and collisions in real systems will weaken these instabilities and sometimes eliminate them entirely. The above qualitative conclusions concerning the interaction of modulated beams with plasma (see also the paper [1] by one of the authors) are confirmed by the experimental results described in [2, 3].

Theoretical studies of the interaction of modulated beams with plasma have up to the present been limited to the consideration of the generation of oscillations in the approximations obtained with the assumption of a given current [4, 5]. In [6-8], parametric instabilities of a modulated electron beam without plasma were investigated by using a self-consistent approximation. To investigate parametric and bunch instabilities caused by the interaction of a modulated beam with plasma, we must consider the generation of oscillations in a self-consistent approximation.

In the present article, this problem is solved for the case when the beam is a periodic sequence of compensated bunches moving through plasma with a constant velocity U. All calculations were performed in a reference system related to the bunches. In such a system the density of a bunch when there are no oscillations varies according to the law

$$N_b = N_1 \sum_{n=-\infty}^{\infty} \sigma(z - \ln) - \sigma(z - \ln - a) = \begin{cases} N_1 & \text{at} \quad < z < \ln + a; \\ 0 & \text{at} \quad + a < z < l(n+1), \end{cases} \tag{1}$$

where

$$\sigma(z) = \begin{cases} 1 & \text{at} \quad z > 0; \\ 0 & \text{at} \quad z < 0; \end{cases}$$

N_1 is the constant density of particles inside a bunch; a is the dimension of bunches; l is the distance between bunches; the z axis is in the direction of the velocity U, the bunches are assumed to be infinitely wide and homogeneous in the two other directions. It is also assumed that the plasma is homogeneous when there are no oscillations (N_0 = const).

As basic equations for the description of the oscillations, we use the usual equations of one-dimensional hydrodynamics. By linearizing these equations relative to the oscillation amplitude we obtain in the range $-l + a < z < 0$, i.e., outside the bunch, a system of equations for the forced oscillations of the disturbed density n_0 and velocity v_0 of the plasma particles and of the electric field E of the oscillations:

$$\left.\begin{aligned} \left(i\omega + U\frac{d}{dz}\right)v_0 &= \frac{e}{m}E; \\ \left(i\omega + U\frac{d}{dz}\right)n_0 &= N_0\frac{dv_0}{dz}; \\ \frac{dE}{dz} &= -4\pi e n_0. \end{aligned}\right\} \tag{2}$$

We assume as usual that the dependence of n_0, v_0, and E on the time is described by a factor e^{-iwt}. For simplicity we consider only oscillations propagated in the direction of the inhomogeneity. The solution of (2) is of the form:

$$n_0 = A\exp\left[-i\left(\frac{\omega}{U}+\alpha\right)z\right] + B\exp\left[-i\left(\frac{\omega}{U}-\alpha\right)z\right];$$

$$v_0 = \frac{\alpha v}{N_0}\left\{A\frac{\exp\left[-i\left(\frac{\omega}{U}+\alpha\right)z\right]}{\frac{\omega}{U}+\alpha}\right.$$

$$\left. - B\frac{\exp\left[-i\left(\frac{\omega}{U}-\alpha\right)z\right]}{\frac{\omega}{U}-\alpha}\right\} + \frac{eC}{im\omega}; \quad E = -4\pi ie\left\{A\frac{\exp\left[-i\left(\frac{\omega}{U}+\alpha\right)z\right]}{\frac{\omega}{U}+\alpha}\right. \tag{3}$$

$$\left. + B\frac{\exp\left[-i\left(\frac{\omega}{U}-\alpha\right)z\right]}{\frac{\omega}{U}-\alpha}\right\} + C.$$

Here $\alpha = \frac{\Omega_0}{U}$; $\Omega_0^2 = \frac{4\omega N_0 e^2}{m}$; and A, B, and C are constants. From Flok's theorem, the dependence of n_0, v_0, and E on z is described by a function of the form $u_k(z)e^{-ikz}$, where $u_k(z)$ is a periodic function with period l; and k is the wave number. Hence for $a < z < l$ the relations (3) yield

$$n_0 = \left\{A\exp\left[-i\left(\frac{\omega}{U}+\alpha\right)(z-l)\right] + B\exp\left[-i\left(\frac{\omega}{U}-\alpha\right)(z-l)\right]\right\} \times \exp(ikl);$$

$$v_0 = \frac{\alpha v}{N_0}\left\{A\frac{\exp\left[-i\left(\frac{\omega}{U}+\alpha\right)(z-l)\right]}{\frac{\omega}{U}+\alpha} - B\frac{\exp\left[-i\left(\frac{\omega}{U}-\alpha\right)(z-l)\right]}{\frac{\omega}{U}-\alpha}\right\} \tag{4}$$

$$\times \exp(ikl) + \frac{eC}{im\omega}\exp(ikl);$$

$$E=-4\pi ie\left\{A\frac{\exp\left[-i\left(\frac{\omega}{U}+\alpha\right)(z-l)\right]}{\frac{\omega}{U}+\alpha}+B\frac{\exp\left[-i\left(\frac{\omega}{U}-\alpha\right)(z-l)\right]}{\frac{\omega}{U}-\alpha}\right\}\times\exp(ikl)+C\exp(ikl). \tag{4}$$

To find the equations giving the changes in n_0, v_0, and E through the bunches, we use the equations for the disturbances in density and velocity of both components and the disturbance in the electric field inside a bunch ($0 < z < a$):

$$\left(i\omega+U\frac{d}{dz}\right)v_0=\frac{e}{m}E;\qquad \left(i\omega+U\frac{d}{dz}\right)n_0=N_0\frac{dv_0}{dz};$$

$$i\omega v_1=\frac{e}{m}E+\frac{\gamma T}{mN_1}\cdot\frac{dn_1}{dz};\qquad i\omega n_1=N_1\frac{dv_1}{dz}; \tag{5}$$

$$\frac{dE}{dz}=-4\pi e(n_0+n_1).$$

Here the subscript "1" indicates quantities referred to the bunch and the subscript "0" indicates quantities referred to the plasma. By introducing a force proportional to the gradient of the pressure p = ynT in these equations, we take into account the thermal dispersion of the velocities of the particles in the bunch. The thermal motion inside the bunch must be taken into account since, for $T \neq 0$, a disturbance is transmitted from one boundary of a bunch to another not only by plasma particles with velocities in the direction of U, but also by particles of the bunch.

From (5) we obtain a fourth-order equation for n_1:

$$\left[\left(i\omega+U\frac{d}{dz}\right)^2+\Omega_0^2\right]\left[\omega^2+\frac{\gamma T}{m}\frac{d^2}{dz^2}\right]n_1-\Omega_1^2\left[i\omega+U\frac{d}{dz}\right]^2n_1=0. \tag{6}$$

When

$$\varepsilon=\frac{\Omega_0}{U}\sqrt{\frac{\gamma T}{m(\omega^2-\Omega_1^2)}}\ll 1 \tag{7}$$

Equation (6) breaks up into the two second-order equations

$$\frac{\gamma T}{m}\cdot\frac{d^2n_1}{dz^2}+(\omega^2-\Omega_1^2)n_1=0;\qquad \left(i\omega+U\frac{d}{dz}\right)^2n_1+\frac{\Omega_0^2}{1-\frac{\Omega_1^2}{\omega^2}}n_1=0. \tag{8}$$

In this case we obtain

$$n_1=\mathscr{E}\exp(i\lambda z)+F\exp(-i\lambda z)+M\exp\left[-i\left(\frac{\omega}{U}+\alpha_1\right)z\right]+K\exp\left[-i\left(\frac{\omega}{U}-\alpha_1\right)z\right], \tag{9}$$

where

$$\lambda=\sqrt{\frac{m}{\gamma T}(\omega^2-\Omega_1^2)};\quad \alpha_1=\frac{\Omega_0}{U\sqrt{1-\frac{\Omega_1^2}{\omega^2}}};\quad \Omega_1^2=\frac{4\pi e^2N_1}{m};$$

$\mathscr{E}$, F, M, and K are constants.

• This condition determines, in particular, the minimum value $\omega - \Omega_1$.

By using Eqs. (5) it is not difficult to express v_1, n_0, v_0, and E in terms of n_1. Then using (9) we obtain

$$\left.\begin{aligned}
v_1 &= \frac{\omega}{N_1}\left\{\frac{1}{\lambda}\left[\mathscr{E}\exp(i\lambda z) - F\exp(-i\lambda z)\right] - M\frac{\exp\left[-i\left(\frac{\omega}{U}+\alpha_1\right)z\right]}{\frac{\omega}{U}+\alpha_1}\right.\\
&\qquad\left. - K\frac{\exp\left[-i\left(\frac{\omega}{U}-\alpha_1\right)z\right]}{\frac{\omega}{U}-\alpha_1}\right\} + \frac{eG}{im\omega};\\
n_0 &= \frac{\omega^2-\Omega_1^2}{\Omega_1^2}\left\{M\exp\left[-i\left(\frac{\omega}{U}+\alpha_1\right)z\right] + K\exp\left[-i\left(\frac{\omega}{U}-\alpha_1\right)z\right]\right\}\\
&\qquad - \frac{\Omega_0^2}{\omega^2-\Omega_1^2}\cdot\frac{\gamma T}{mU^2}\left\{\mathscr{E}\exp(i\lambda z) + F\exp(-i\lambda z)\right\};\\
v_0 &= \frac{\omega^2-\Omega_1^2}{\Omega_1^2}\cdot\frac{\alpha_1 U}{N_0}\left\{M\frac{\exp\left[-i\left(\frac{\omega}{U}+\alpha_1\right)z\right]}{\frac{\omega}{U}+\alpha_1} - K\frac{\exp\left[-i\left(\frac{\omega}{U}-\alpha_1\right)z\right]}{\frac{\omega}{U}-\alpha_1}\right\}\\
&\qquad + \frac{eG}{im\omega} - \frac{\Omega_0^2}{\omega^2-\Omega_1^2}\cdot\frac{\gamma T}{mUN_0}\left\{\mathscr{E}\exp(i\lambda z) - F\exp(-i\lambda z)\right\};\\
E &= 4\pi ie\left\{\frac{1}{\lambda}\left[\mathscr{E}\exp(i\lambda z) - F\exp(-i\lambda z)\right] - \frac{\omega^2}{\Omega_1^2}\left[M\frac{\exp\left[-i\left(\frac{\omega}{U}+\alpha_1\right)z\right]}{\frac{\omega}{U}+\alpha_1}\right.\right.\\
&\qquad\left.\left. + K\frac{\exp\left[-i\left(\frac{\omega}{U}-\alpha_1\right)z\right]}{\frac{\omega}{U}-\alpha_1}\right]\right\} + G.
\end{aligned}\right\} \qquad (10)$$

In the formulas for n_0 and v_0, the amplitude of the rapidly oscillating terms $\sim\exp(\pm i\lambda z)$ is of the order of ε. In this case, however, when the dimensions of the bunch are sufficiently small compared to the wavelength of the plasma [see (14) below] and the first two terms of (10) insignificantly in a single bunch, the rapidly oscillating terms in the formulas for n_0 and v_0 can be important in the boundary conditions.

To find the constants in the solutions (9) and (10) we use the following boundary conditions on the surface of a bunch. We assume that the boundaries of a bunch (z = 0, z = a) are points of reversal of the particles in the bunch, i.e., for z = 0 and z = a the velocities of the particles of a bunch are zero:*

$$v_1(0) = 0; \qquad v_1(a) = 0. \qquad (11)$$

In this case electric charges do not accumulate on the boundaries of the bunch and, in view of the absence of surface charges, the electric field must be continuous for z = 0 and z = a:

$$E^{\text{int}}(0) = E^{-}(0); \qquad E^{\text{int}}(a) = E^{+}(a). \qquad (12)$$

Here and in the sequel the superscript "plus" indicates quantities to the right of a bunch and the superscript "minus" indicates quantities to the left of a bunch. When the electric field is continuous, the density of the plasma is also continuous on the boundaries:

$$n_0^{\text{int}}(0) = n_0^{-}(0); \qquad n_0^{\text{int}}(a) = n_0^{+}(a). \qquad (13)$$

In the following we will investigate only the case in which the dimension of bunches is small in comparison to the plasma wavelength, i.e.,

*By the same token we assume that the boundaries of a bunch remain fixed during the oscillations.

$$\delta = \frac{\omega a}{U} \ll 1. \tag{14}$$

It is in this case that the effect of the modulation of the beam on the development of bunch instability is most pronounced. Moreover we can assume that the smallness of ε will mean that

$$\varepsilon \left| \frac{1-\cos \lambda a}{\sin \lambda a} \cdot \frac{\omega_1^2 \omega_0}{(\omega^2-\omega_1^2)(\omega \pm \omega_0)} \right| \ll 1. \tag{14'}$$

We consider only terms of the lowest order in the parameters (14) and (14'); then by using (11)-(13) we can easily express the constants in the solution inside the bunch in terms of the values of n_0 and E outside the bunch:

$$\begin{aligned}
\mathscr{E} &= -\frac{\Omega_1^2}{2(\omega^2-\Omega_1^2)} \cdot \frac{\lambda}{\sin \lambda a} \left\{ n_0^-(0)\, a + \frac{E^-(0)}{4\pi e} [\exp(-i\lambda a) - 1] \right\}; \\
F &= -\frac{\Omega_1^2}{2(\omega^2-\Omega_1^2)} \cdot \frac{\lambda}{\sin \lambda a} \left\{ n_0^-(0)\, a + \frac{E^-(0)}{4\pi e} [\exp(i\lambda a) - 1] \right\}; \\
M &= \frac{\Omega_1^2}{\omega^2-\Omega_1^2} \left\{ \frac{1}{2i\alpha_1 a} [n_0^-(0) - n_0^+(a)] + \frac{n_0^-(0)}{2\alpha_1} \left(\alpha_1 + \frac{\omega}{U} \right) \right. \\
&\quad \left. + \frac{\Omega_0^2}{\omega^2-\Omega_1^2} \cdot \frac{\gamma T}{mU^2} [\mathscr{E}(e^{i\lambda a} - 1) + F(e^{-i\lambda a} - 1)] \frac{i}{2\alpha_1 a} \right\}; \\
K &= \frac{\Omega_1^2}{\omega^2-\Omega_1^2} \left\{ \frac{1}{2i\alpha_1 a} [n_0^+(a) - n_0^-(a)] - \frac{n_0^-(0)}{2\alpha_1} \left(\frac{\omega}{U} - \alpha_1 \right) \right. \\
&\quad \left. - \frac{\Omega_0^2}{\omega^2-\Omega_1^2} \cdot \frac{\gamma T}{mU^2} [\mathscr{E}(e^{i\lambda a} - 1) + F_1(e^{-i\lambda a} - 1)] \frac{i}{2\alpha_1 a} \right\}; \\
G &= \frac{m\omega^2}{eN_1} \frac{\Omega_1^2}{\omega^2-\Omega_1^2} \left\{ \frac{E^-(0)}{4\pi e} \left[1 + 2 \frac{\Omega_0^2 \Omega_1^2}{(\omega^2-\Omega_1^2)(\omega^2-\alpha_1^2 U^2)} \cdot \frac{1}{\lambda a} \right] \right. \\
&\quad \left. + \left[\frac{k\omega}{U} n_0^-(0) + \frac{1}{a} \left(n_0^+(a) - n_0^-(0) \right) \right] \frac{1}{\frac{\omega^2}{U^2} - \alpha_1^2} \right\}.
\end{aligned} \tag{15}$$

From (11)-(13) we also obtain a relation giving the variation of the electric field through the bunches:

$$\begin{aligned}
E^+(a) - E^-(0) - 4\pi e a (M+K) \left(1 - \frac{\omega^2}{\Omega_1^2} \right) \\
= 4\pi e a n_0^-(0).
\end{aligned} \tag{16}$$

Since $\frac{dE^-}{dz}(0) = -4\pi e n_0^-(0)$, it follows that (16) can be written:

$$E^+(a) - E^-(0) = \frac{dE^-}{dz}(0)\, a, \quad \text{i.e.} \quad E^+(a) = E^-(a). \tag{16'}$$

It follows from (16) that the discontinuity in the electric field through a bunch is determined only by the plasma density and is independent of the density in the bunch. This is explained by the fact that, when there are oscillations, a double layer type of structure is formed in a bunch and the total charge of a bunch remains zero.

To find the equation giving the discontinuity in the plasma-particle velocity through a bunch, we integrate the equation of motion of these particles inside the bunch. Using the condition that the velocity v_0 is continuous at the boundaries, we obtain

$$U [v_0^+(a) - v_0^-(0)] + i\omega \int_0^a v_0\, dz = \frac{e}{m} \int_0^a E\, dz. \tag{17}$$

Using the relation

$$i\omega v_0^-(z) + U \frac{dv_0^-}{dz} = \frac{e}{m} E^-(z),$$

we can write

$$U\left[(v_0^+(a)-v_0^-(a)\right]+i\omega\int_0^a (v_0-v_0^-)\,dz=\frac{e}{m}\int_0^a (E-E^-)\,dz. \tag{18}$$

In these formulas $v_0^-(z)$ and $E^-(z)$ are determined by the relations (3) and are continuations into the interior of the bunch ($0 < z < a$) of the previously obtained solutions to the left and right. Using the value of E obtained from (10) and the values of the constants $\mathcal{E}$, F, G, M, and K given by (15) and integrating with respect to z, we obtain

$$\frac{e}{m}\int_0^a [E(z)-E^-(z)]\,dz=-\frac{eE^-(0)}{m\lambda}\cdot\frac{\Omega_1^2}{\omega^2-\Omega_1^2}\left[2\frac{1-\cos\lambda a}{\sin\lambda a}-\lambda a\right]. \tag{19}$$

Here we have neglected small terms of the order $en_0^-a\sim\delta E^-$ compared with E^-. By using (11) we can similarly transform the other integral in (18):

$$\begin{aligned}\int_0^a [v_0(z)-v_0^-(z)]\,dz&=\frac{a^2}{2}\left[\frac{dv_0}{dz}(0)-\frac{dv_0^-}{dz}(0)\right]\\ &=\frac{1}{N_0}\left\{\frac{aU}{2}[n_0^-(0)-n_0^+(a)]+\frac{i\omega a^2}{2}n_0^-(0)\right\}\\ &\quad-\frac{a^2}{2}\cdot\frac{dv_0^-}{dz}(0)=\frac{aU}{2N_0}[n_0^-(a)-n_0^+(a)].\end{aligned} \tag{20}$$

From (19) and (20) we obtain our final equation for the variation of v_0 through a bunch:

$$\begin{aligned}v_0^+(a)-v_0^-(a)&=-\frac{eE^-(0)}{m\lambda U}\cdot\frac{\Omega_1^2}{\omega^2-\Omega_1^2}\Phi(\lambda a)\\ &\quad-i\frac{\omega a}{2N_0}[n_0^+(a)-n_0^-(a)],\end{aligned} \tag{21}$$

where

$$\Phi(\lambda a)=2\frac{1-\cos\lambda a}{\sin\lambda a}-\lambda a.$$

To obtain the equation giving the variation of n_0 inside a bunch, we integrate the continuity equation from 0 to a. This yields

$$\begin{aligned}i\omega\int_0^a n_0\,dz+U[n_0^+(a)-n_0^-(0)]\\ -N_0[v_0^+(a)-v_0^-(0)]=0,\end{aligned} \tag{22}$$

where the first term is proportional to a; we may thus consider only the lowest order terms in the parameter δ and in Eq. (22) we can make the approximation of replacing n_0 by n_0^- [see also (20)]. Then using the relation

$$i\omega n_0^-+U\frac{dn_0^-}{dz}-N_0\frac{dv_0^-}{dz}=0,$$

we obtain

$$n_0^+(a)-n_0^-(a)=\frac{N_0}{U}[v_0^+(a)-v_0^-(a)]. \tag{23}$$

• For the discontinuity in v_0, this integral yields a small correction $\sim\delta$ in (21) [see (21) and (23)] which we neglect in our calculations.

† Starting from (10) and (15), we can use some transformations to obtain (21) and (23) directly from the conditions for the continuity of v_0 at the boundary: $v_0^{int}(0)=v_0^-(0)$, $v_0^{int}(a)=v_0^+(a)$.

The relations (16'), (21) and (23) are the desired equations for the discontinuities in density and velocity of plasma particles in the electric field through a bunch. Substituting the values of E, n_0, and v_0 given by (3) and (4) in these equations, we obtain a system of equations for the constants A, B, and C, and from the condition that these equations be solvable when $\omega \neq \Omega_0$, $\exp(ikl) \neq 1$, we obtain the dispersion equation

$$w^2 - 2w(\cos \alpha l - \Delta \sin \alpha l) + 1 = 0. \tag{24}$$

Here

$$w = \exp\left[i\left(\frac{\omega}{U} + k\right)l\right] \quad \Delta = \frac{\Omega_0}{2\lambda U}\frac{\Omega_1^2}{\omega^2 - \Omega_1^2}\Phi(\lambda a).$$

When $\Delta = 0$ (the bunch ceases to exist), we obtain from (24) the relation $w = e^{\pm i\alpha l}$, i.e., $\omega = \pm\Omega_0 - kU + \frac{2\pi nU}{l}$ ($n = 0, \pm 1 \ldots$), and in the laboratory coordinate system ω coincides with $\pm\Omega_0$. We use (24) to study the generation of oscillations with a given k in the plasma-modulated wave system. In the laboratory coordinate system, the dispersion equation for the oscillation can be written

$$\sin\left[(\omega_л + \Omega_0)\frac{l}{2U}\right]\sin\left[(\omega_1 - \Omega_0)\frac{l}{2U}\right] + \frac{\omega_0}{4\lambda U}\cdot\frac{\Omega_1^2}{(\omega_1 - k_1 U)^2 - \Omega_1^2}F(\lambda a)\sin\frac{\Omega_0 l}{U} = 0. \tag{25}$$

In the transformation, we use the usual transformations ω_1 and $w + kU$, $k_1 = k$, where the subscript "1" refers to the laboratory coordinate system. In our calculations, however, we will omit this subscript, since all the following formulas refer only to the laboratory system.

We investigate only the case $\lambda a \gg 1$, for which the thermal motion in a bunch is unimportant. Since it follows from (14') that $\lambda a \neq \pi n$, we have the approximate relation $\Phi(\lambda a) \approx -\lambda a$. When the density in a bunch is sufficiently low and $\Omega_1 \ll \Omega_0$, the solution of Eq. (25) is written, as usual, in the form

$$\omega = kU + \varepsilon; \qquad |\varepsilon| \ll kU.$$

From (25) we have

$$\varepsilon^2 = \Omega_1^2\left\{1 + \frac{a\Omega_0}{4U} \times \frac{\sin\frac{\Omega_0 l}{U}}{\sin\left[\frac{kU + \Omega_0}{2}\cdot\frac{l}{U}\right]\sin\left[\frac{kU - \Omega_0}{2}\cdot\frac{l}{U}\right]}\right\}. \tag{26}$$

In the case under consideration, in which $\Omega_0 a/U \ll 1$, instability ($\varepsilon^2 < 0$) arises only in very restricted intervals of k (with lengths of the order of a/l):

$$\Omega_0\left(1 - \frac{a}{2l}\right) + 2\pi n\frac{U}{l} \leqslant kU < \Omega_0 + \frac{2\pi nU}{l}. \tag{27}$$

Hence during the interaction of a modulated beam with plasma, there will be considerable discharge of the spectrum of unstable values of k in comparison with the case of interaction of a continuous beam with plasma, in which all the k satisfying the condition $kU \leq \Omega_0$ are unstable. The increment of these waves is $kU \simeq \Omega_0 + \frac{2\pi nU}{l}$. Substituting $kU = \Omega_0 + \frac{2\pi nU}{l}$, and $\omega = kU + \varepsilon$ ($|\varepsilon| \ll kU$), in (25), we obtain for ε the equation:

$$\varepsilon[\varepsilon^2 - \Omega_1^2] = \frac{\Omega_0\Omega_1^2}{2}\cdot\frac{a}{l}. \tag{28}$$

For $\varepsilon \gg \Omega_1$ this equation yields

$$\varepsilon_1 = \frac{1}{2^{4/3}}\Omega_0^{1/3}\Omega_1^{2/3}\left(\frac{a}{l}\right)^{1/3}; \quad \varepsilon_{2,3} = \frac{1}{2^{4/3}}(-1 \pm i\sqrt{3})\,\Omega_0^{1/3}\Omega_1^{2/3}\left(\frac{a}{l}\right)^{1/3}, \tag{29}$$

i.e., the increment for resonance increases somewhat in comparison with the nonresonance case, but remains nonetheless smaller by a factor $\left(\frac{a}{l}\right)^{1/3}$ than for the case of an unmodulated beam. Formula (29) is applicable when $|\varepsilon| \gg \Omega_1$, that is, when $\frac{a}{l} \gg \frac{\Omega_1}{\Omega_0}$. In the other limiting case $\left(\frac{a}{l} \ll \frac{\Omega_1}{\Omega_0}\right)$ stabilization of the instability occurs at resonance:

$$\varepsilon_1 \approx \frac{\Omega_0 a}{2l}; \quad \varepsilon_{2,3} \approx \pm \Omega_1. \tag{30}$$

An investigation of the original Eq. (25) shows that instabilities arise only in very short intervals of variation of k:

$$\left.\begin{aligned} \Omega_0 + \Omega_1(1-\delta^{1/4}) + \frac{2\pi n U}{l} \leqslant kU < \Omega_0 \\ + \Omega_1(1+\delta^{1/4}) + \frac{2\pi n U}{l}; \\ \delta = \frac{\Omega_0^2 a^2}{\Omega_1^2 l^2} \ll 1, \end{aligned}\right\} \tag{31}$$

where the maximum increment is $\operatorname{Im} \varepsilon = \Omega_1 \frac{\delta^{1/4}}{2} \ll \Omega_1$. The condition $\lambda a \gg 1$, which must hold if thermal motion is to be neglected, takes the form:

$$a^2 \gg D^2, \tag{32}$$

for oscillation instabilities with k in the interval defined by (27), where $D = \sqrt{\frac{\gamma T}{4\pi e^2 N_1}}$ is the Debye radius in a bunch. In the case of resonance $\left(kU = \Omega_0 + \frac{2\pi n U}{l}\right)$ if $\frac{a}{l} \gg \frac{\Omega_1}{\Omega_0}$ and ε is determined by (29), thermal motion may be neglected for still smaller values of a:

$$a^2 \gg D^2 \left(\frac{\Omega_1 l}{\Omega_0 a}\right)^{2/3}. \tag{33}$$

Hence the validity of the approximate solution requires the assumption of the possibility of stabilizing bunch instabilities [1] by the use of external modulated fields.

The authors wish to thank V. I. Kurilko for his discussions of the results of this work.

LITERATURE CITED

1. Ya. B. Fainberg, Atomnaya énergiya, 11, 313 (1961).
2. I. F. Kharchenko and others. Supplement to the Journal "Yadernyi sintez" [in Russian], Chapter III, Vienna, MAGATÉ (1962), p. 1101.
3. A. K. Berezin and others. In the book: Material Presented at the International Conference on Accelerators [in Russian], Dubna (1963), Moscow Atomizkat (1964), p. 1023.
4. A. N. Kondratenko, Ukr. fiz. zh., VII, 371 (1962); Plasma Physics, No. 2, Kiev, Izd-vo AN UkSSR (1963), p. 176.
5. V. F. Aleksin and K. N. Stepanov, ZhTF, 34, 1210 (1964).
6. O. Rydbeck and B. Agdur, L'onde Electrique, 34, 499 (1954).
7. P. V. Bliokh and Ya. B. Fainberg, ZhTF, 26, 530 (1956).
8. V. D. Shapiro, Izv. vyssh. uchebn. zavedenii Radiofizika, No. 7, 736 (1964).

THE USE OF AN INTEGRATING COINCIDENCE γ-SPECTROMETER FOR ANALYZING A MIXTURE OF RADIOACTIVE ISOTOPES

(UDC 539.107)

V. A. Blinov, V. N. Dmitriev, and M. I. Kuznetsov

Translated from Atomnaya Énergiya, Vol. 19, No. 4,
pp. 342-346, October, 1965
Original article submitted October 10, 1964

The integrated γ-coincidence method is used for the selective detection of radioactive isotopes emitting cascade γ-quanta. This method enables the quantitative content of the isotopes to be determined, whose γ-radiation comprises 3-4% of the γ-radiation from the mixture, and also to be determined the quantitative content of the radioactive isotopes whose decay is accompanied by the emission of a positron, with subsequent emission of a γ-quantum.

In the quantitative analysis of a mixture of radioactive isotopes with a complex γ-spectrum, the determination of the area of the total absorption peaks is complicated because a large part of the total absorption peaks is superimposed on the continuous Compton scattering from high energy γ-quanta. Analysis of such γ-spectra by the method of successive graphical subtraction of the known spectral shape of the appropriate isotope gives good accuracy [1]. However, this method is very time consuming. A less laborious, but also less accurate, method is the method of measuring the amplitude of the total absorption peaks.

Methods have been suggested in certain papers which enable the contribution of scattered γ-quanta in the γ-spectrum to be reduced by means of spectrometers which have two or three crystals. In a spectrometer with a protective scintillator surrounding the primary crystal, the recording efficiency of the γ-quanta due to Compton scattering can be reduced significantly. Usually, the contribution from scattered γ-quanta is reduced by 50-60% [2-5]. In order to eliminate the recording of scattered γ-quanta, it is necessary to use large protective crystals. In addition, cumbersome cast iron or lead shielding is necessary.

The two-crystal γ-spectrometer designed by Thomas and Callew, with subtraction of the Compton scattering quanta and background requires complex and expensive equipment [6]. The NaI(Tl) and anthracene crystals used in it have different temperature coefficient and therefore it is necessary to maintain the crystals at a constant temperature. Hoogenboon [7], developed a two-crystal scintillation spectrometer with improved resolution for recording cascade γ-quanta and with accumulated amplitude control.

In this paper, it is proposed to use this method for analyzing a mixture of radioactive isotopes, and for increasing the reliability of operation and for eliminating the recording of integrated pulses, a fast-slow coincidence circuit is inserted. The block diagram of the equipment is shown in Fig. 1.

Positive pulses from the cathode followers of the scintillation detectors are fed to the control grid of the linear pulse integrator at an output of up to 30 V. The pulse from the output of the integrator is fed to the spectrometric nonoverloading amplifier. The amplified summed pulse enters the single-channel differential discriminator. The range of energies to be recorded is set by the bias and change of width of the discriminator window.

A PS-6 circuit is used as the fast-slow coincidence circuit. The resolving time of the fast coincidence circuit can be adjusted over the range $0.5 \cdot 10^{-9}$ to $5 \cdot 10^{-8}$ sec. The shaped pulses from the scintillation detectors are fed to the input of the fast coincidence circuit and, in the event of a coincidence, a signal is generated at the output which is fed to the slow coincidence circuit. The output pulses from the slow coincidence circuit, which control the input of the multichannel amplitude analyzer, are delayed relative to the pulses arriving from the cathode follower of the scintillation detector for the amplitude analysis by the time necessary for triggering the differential discriminator. Consequently, the pulses from the cathode follower are delayed by 1.5 μsec by means of the delay line without distortion of their amplitude distribution.

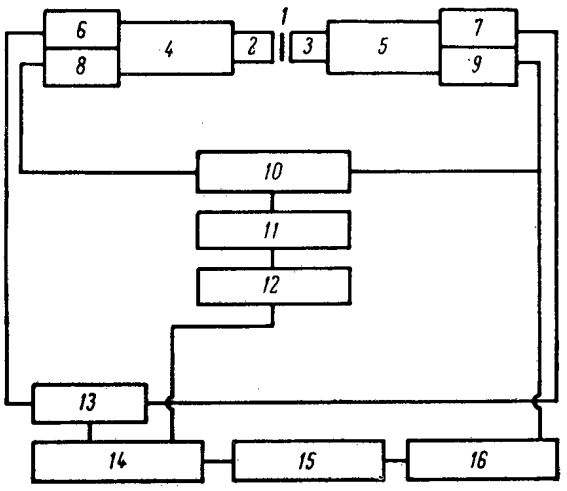

Fig. 1. Block diagram of integrating coincidence γ-spectrometer: 1) sample being studied; 2, 3) NaI(Tl) crystals; 4, 5) FEU-13 photomultipliers; 6, 7) pulse shapers; 8, 9) cathode followers; 10) linear integrator; 11) amplifier; 12) differential discriminator; 13) fast coincidence circuit with time resolution of 10^{-8} to 10^{-9} sec; 14) slow coincidence circuit; 15) AI-100 analyzer; 16) delay line.

Thus, the multichannel analyzer records only time-coincident pulses whose sum corresponds to the total energy emitted by two cascade γ-quanta. Only the total absorption peaks of the cascade γ-quanta are recorded. There is no Compton scattering. The recording efficiency of the coincident γ-quanta is identical.

Calibration of the spectrometer consists in determining the factors which will allow conversion from the areas of the total absorption peaks, referred to unit time of measurement, to the absolute activity of the radioisotope being studied and in determining the dependence of these factors on the weight and form of the samples. The calibration is carried out with radiochemically pure isotopes. In this case, it is not necessary to know the decay scheme of the isotopes and the quantum outputs of the individual γ-rays [1].

RESULTS OF THE EXPERIMENT

The Co^{60} isotope, in decaying, gives only one cascade with γ-quanta energies of 1.17 and 1.33 MeV [9]. The bias of the sum-discriminator is set according to the total energy emitted in the 2.5 MeV cascade and then the coincidence spectrum is plotted by summing for a different width of the discriminator window.

The spectra obtained are shown in Fig. 2. It can be seen that by reducing the window width the energy resolution of the spectrometer is improved, but the spectrometer efficiency in this case is reduced. Reduced widths of the discriminator window can be used for high sample activities or with a high background. It should be noted that with

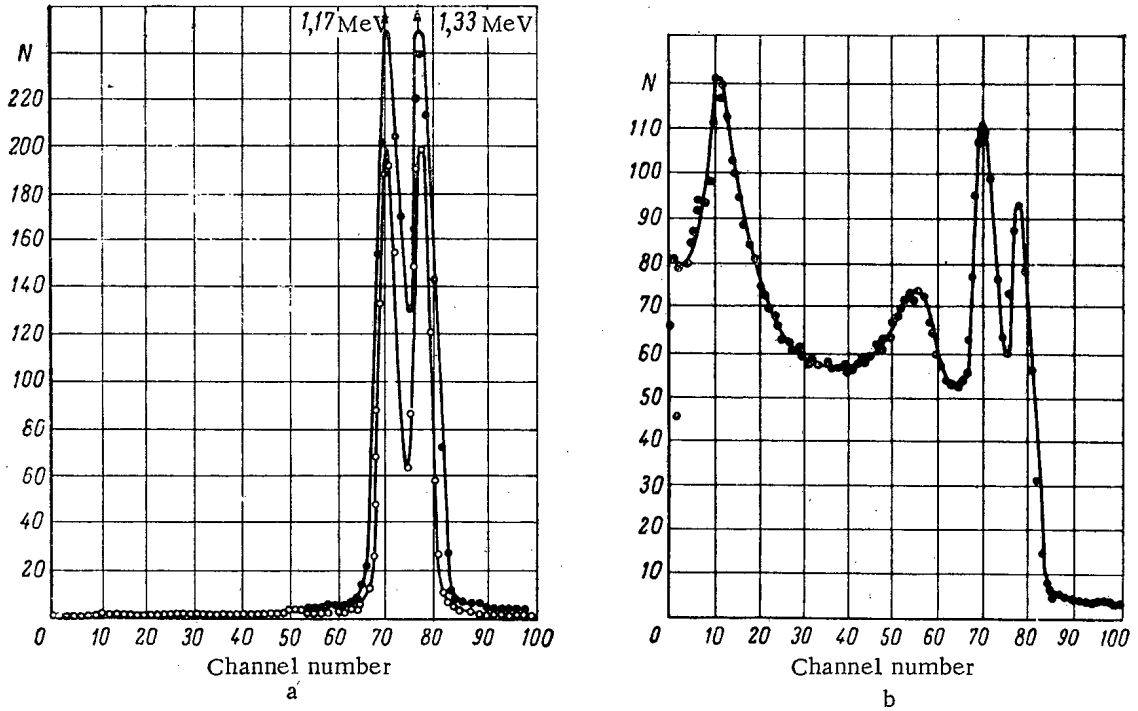

Fig. 2. Co^{60} spectrum with different channel widths: a) Co^{60} spectrum with a different channel width: ●— width of channel, IV, resolution 5.2%; O— channel width 5V, resolution 7%; b) usual spectrum of Co^{60} (N is the relative number of pulses).

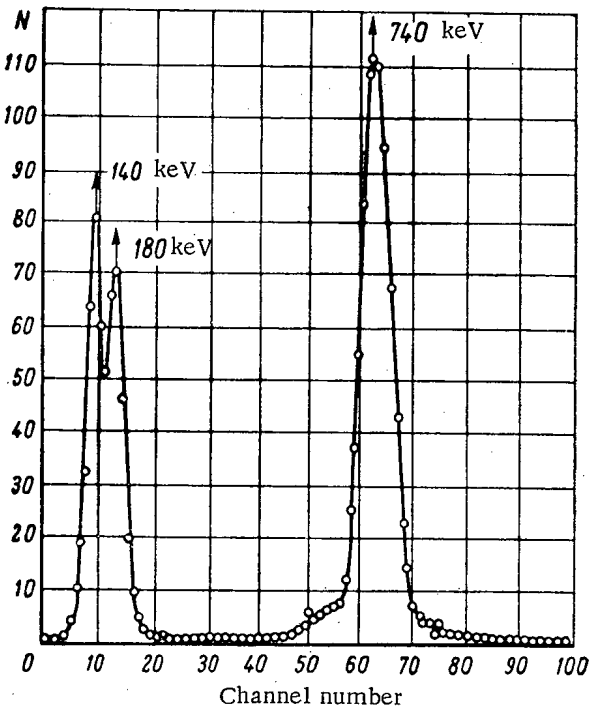

Fig. 3. Mo^{99} spectrum.

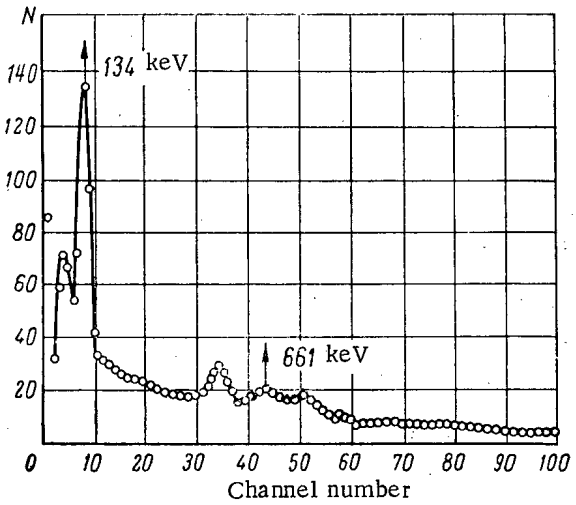

Fig. 4. Form of spectrum of a mixture of fission products with an age of about a year.

the correct adjustment of the spectrometer the areas of the peaks, corresponding to a single cascade transition, must be identical. The spectrum of Co^{60} is presented in Fig. 2 for comparison, plotted for the normal γ-spectrometer conditions.

For measuring Mo^{99} it is convenient to use the γ-quanta with energy of 740 keV, coincident with γ-quanta of energies 140 and 180 keV. The discriminator is set up on the average integrated energy of 900 keV. The spectrum of Mo^{99} is shown in Fig. 3. The shapes of the total absorption peaks can be distinguished in the spectrum, corresponding to energies of 140 and 180 keV which, in the normal spectrometer with a crystal of NaI(Tl) having a resolution with respect to Cs^{137} of about 10%, are not distinguishable. It can be seen from the figure that the areas of the peaks corresponding to energies of 740 and 140-180 keV are equal.

Similarly, the spectrometer is set up for measuring two isotopes having cascade γ-quanta. Figure 4 shows the spectrum of a mixture of fission products with an age of about a year, plotted under the normal γ-spectrometer conditions. In this mixture, only two long-lived isotopes are present which have cascade γ-quanta: Ru^{106} and Ce^{144}. In addition, Cs^{137} and Zr^{95} + Nb^{95} are present in the mixture. Even in this simple case, the use of the normal γ-spectrometer for the quantitative determination of the isotopes mentioned presents considerable difficulties. Figure 5 shows the spectra of Ru^{106} and Ce^{144}, plotted with an integrating coincidence γ-spectrometer.

Back-Scattering

In accordance with the Klein--Nishina formula, the energy distribution of scattered γ-quanta has a minimum [10] whose position depends on the initial energy of the γ-quanta. For γ-quanta with energies of 0.5 to 5 MeV this minimum is located in the energy region 0.17-0.24 MeV [8]. Therefore, because of backscattering in the materials surrounding the crystal, a peak is observed in this energy region in the nornal γ-spectrometer, which is often called the backscatter peak. If the differential sum discriminator is set on the energy of the γ-quanta, then in measurements with the integrating coincidence γ-spectrometer, as a result of backscatter, in one of the crystals a peak is recorded in the energy region of 0.17-0.24 MeV and in the other crystal a peak is recorded which is supplementary to the total energy of the γ-quantum being recorded. In order to measure samples with a high intensity of γ-radiation, backscatter can be eliminated almost completely by inserting a lead shield between the crystals (Fig. 6). For measuring weak samples, it is more suitable to operate without shielding; however, it is necessary to discriminate between peaks which are due to backscatter from peaks which are due to cascade γ-quanta. In the case, when the total energy of any cascade is equal to the energy of an individual γ-quantum present in a mixture of isotopes, the probability is small so that the energy of individual γ-quanta in the cascade will be equal to the energies of the peaks from backscatter.

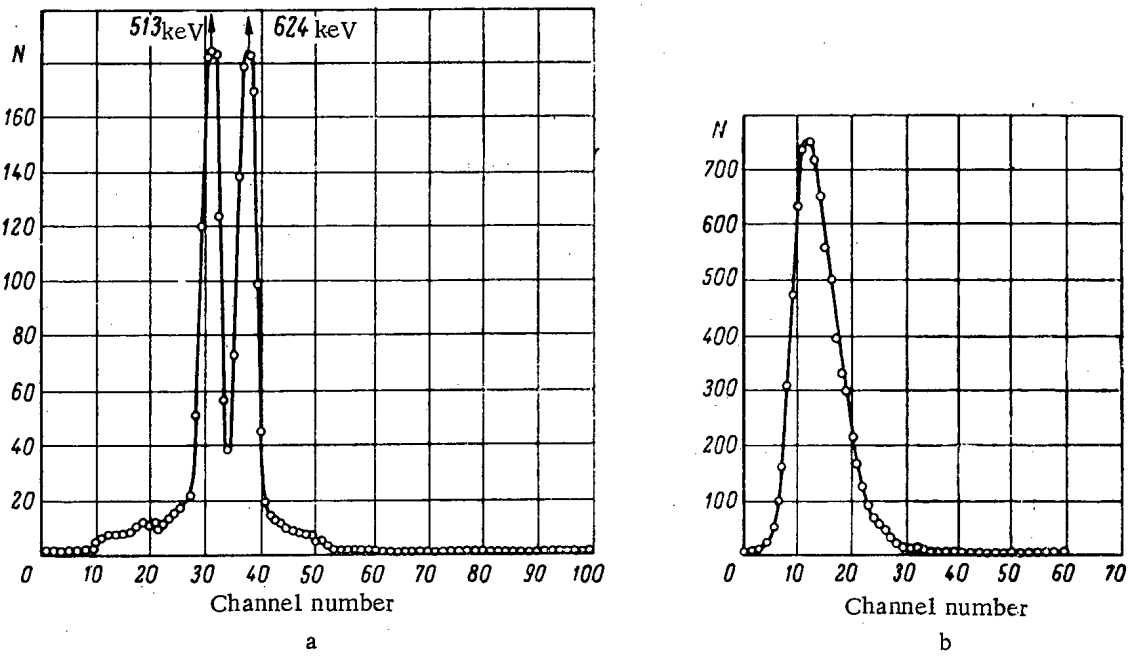

Fig. 5. Spectrum of Ru^{106} (a) and Ce^{144} (b) from a mixture of fission products.

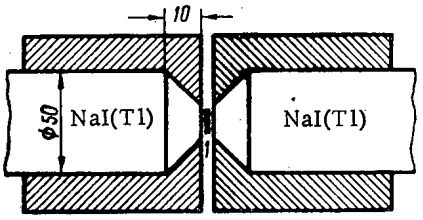

Fig. 6. Lead shielding from backscatter (1-sample).

Thus, the use of the integrating coincidence γ-spectrometer for analyzing a mixture of radioactive isotopes allows the quantitative content of Ce^{143}, Ce^{144}, Mo^{99}, I^{131}, I^{132}, Ru^{106}, Ba^{140}, La^{140}, Co^{60}, U^{235}, and other radioactive nuclei of isotopes which have cascade γ-quanta to be detected and determined.

In addition, by means of the spectrometer mentioned, the quantitative content can be determined of radioactive isotopes which decay with the emission of a positron and subsequent emission of a γ-quantum (for example, Na^{22}, which emits a positron and a γ-quantum with an energy of 1.28 MeV). In this case, the sum-discriminator is adjusted to an energy of 1.79 MeV, equal to the sum of the γ-quantum energy (1.28 MeV) and the annihilation quantum (0.51 MeV). The method described enables the content of radioactive isotopes to be reliably determined, which have a γ-emission amounting to 3-4% of the γ-emission of the mixture.

LITERATURE CITED

1. L. I. Gedeonov et al., Procedure for analyzing radioactive contamination by means of a scintillation gamma-spectrometer [in Russian], Leningrad, V. G. Khlopin Radium Institute (1963).
2. R. Albert, Rev. Scient. Instrum., 24, 1096 (1953).
3. K. Roulston and S. Nagvi, Rev. Scient. Instrum., 27, 230 (1956).
4. G. O'Kelly, N. Larar, and E. Eichler, Phys. Rev., 102, 233 (1956).
5. V. O. Vyazenskii et al., The Scintillation method in radiometry [in Russian], Moscow Gosatomizdat (1961).
6. D. Thomas and W. Callow, Nuclear Electronics Proceedings of the Intern. Symposium on Nuclear Electronics Organized by the French Society of Radioelectricians (1959), p. 17.
7. A. Hoogenboom, Nucl. Instrum., 3, 57 (1958).
8. J. Sharpe, Nuclear Radiation Detectors. Methuen's Monographs of Physical Subject. Late of Atomic Energy Res. Establishment., Harwell (1956).
9. B. S. Dzhelepov and L. K. Pekker, Decay schemes of radioactive nuclei [in Russian], Moscow-Leningrad, Izd-vo AN SSSR (1958).
10. E. Segré, Experimental Nuclear Physics [Russian translation], Vol. 1, Moscow, Izd-vo IL (1955).

THE USE OF THE P_n-APPROXIMATION IN THE DESCRIPTION OF THE DISTRIBUTION OF NEUTRONS IN AN ABSORBING ROD

(UDC 621.039.51.134)

I. V. Sergeev

Translated from Atomnaya Énergiya, Vol. 19, No. 4,
pp. 346-349, October, 1965
Original article submitted November 9, 1964

The system of nonlinear differential equations describing the distribution of neutrons in an absorbing rod in the P_n approximation is transformed into a system of integral equations more convenient for investigation. A method of solution based on the use of successive approximations is proposed.

The great majority of contemporary nuclear reactors are heterogeneous reactors with the nuclear fuel and the materials used for the compensation of excessive reactivity located in active zones in the form of separate rods. During the operation of a reactor the materials of the rod with large neutron capture cross sections are rapidly consumed, and the depth to which they are consumed in the center of an active zone and for rods with an absorbent that is consumed can reach 80% and higher. The variation of the internal interlocking coefficient can become so large that if it is neglected there will be large errors in the determination of the dependence of the multiplication coefficient on the time.

Many papers have been devoted to the determination of the dependence of the depth of the fuel consumption ([1, 2] for example). This dependence is usually obtained by using various artificial methods and simplifying assumptions which restrict the range of application of the resulting formulas. In the present article, we attempt to use exact transformations to reduce the P_n approximation for the nonstationary Boltzmann equation to a form more convenient for both numerical methods of solution and for approximate analytical solution (by successive approximations, for example).

For simplicity we consider only the plane case. With certain extra complications, the reasoning used below can be applied to the problem for cylindrical and spherical blocks.

The Basic Equations

To describe the behavior of neutrons in an infinite absorbing place we use the single-velocity Boltzmann equation for the neutron density N and the equation for fuel consumption:

$$\left.\begin{aligned} \frac{1}{v}\cdot\frac{\partial N}{\partial t} &= -\mu\frac{\partial N}{\partial x}-(\Sigma_c+\Sigma_s)\,N \\ &\quad+\frac{\Sigma_s}{2}\int_{-1}^{1} g(\mu',\ \mu)\,N(x,\ t,\ \mu')\,d\mu'; \\ \frac{1}{v}\cdot\frac{\partial \Sigma_c}{\partial t} &= -\sigma_c\Sigma_c\frac{1}{2}\int_{-1}^{1} N(x,\ t,\ \mu')\,d\mu'. \end{aligned}\right\} \tag{1}$$

Here v is the neutron velocity; $\mu = \cos\vartheta$ is the cosine of the angle between the velocity and the x axis; $g(\mu', \mu)$ is the probability that the direction of flight of a neutron will be turned by a collision through an angle (ϑ, ϑ'); the remaining notation is standard. In obtaining (1) it is assumed that there is only one isotope in the system which absorbs neutrons strongly (this assumption is not essential and it can be omitted if desirable) and that the quantity σ_c is independent of the time, i.e., the variation of the neutron spectrum in the rod can be neglected. To determine

a unique solution of the system (1) we must specify initial and boundary conditions (these conditions will not appear in the following reasoning and so they will be discussed only at the end of the article).

Following the usual method for obtaining the P_n approximation [3], we expand N and g in series of Legendre polynomials and terminate the series for N at the nth term:

$$N_n = \sum_{k=0}^{n} f_k(x,\ t)\, P_k(\mu); \quad g(\mu,\ \mu') = \sum_{k=0}^{\infty} (2k+1)\, c_k P_k(\cos\Phi),$$

where $\Phi = \vartheta - \vartheta'$.

After some transformations, we obtain instead of (1) a set of (n + 2) first order nonlinear differential equations:

$$\frac{1}{v}\cdot\frac{\partial f_k}{\partial t} = -\frac{k}{2k-1}\cdot\frac{\partial f_{k-1}}{\partial x} - \frac{k+1}{2k+3}\cdot\frac{\partial f_{k+1}}{\partial x} -$$

$$-\Sigma_c f_k - \Sigma_s f_k (1-c_k) \quad (k=0,\ 1,\ 2,\ \ldots,\ n;\ f_k = 0$$

$$\text{at} \quad k \geqslant n+1);\ \frac{1}{v}\cdot\frac{\partial \Sigma_c}{\partial t} = -\sigma_c \Sigma_c f_0. \tag{2}$$

We introduce the notation

$$\bar{u} = \begin{pmatrix} f_0 \\ \cdot \\ \cdot \\ \cdot \\ f_n \\ \Sigma_c \end{pmatrix}; \qquad \bar{\Phi} = \begin{pmatrix} -\Sigma_c f_0 - \Sigma_s (1-c_0) f_0 \\ \cdots\cdots\cdots\cdots \\ -\Sigma_c f_n - \Sigma_s (1-c_n) f_n \\ -\sigma_c \Sigma_c f_0 \end{pmatrix};$$

$$A = \begin{pmatrix} 0; & -\frac{1}{3}; & 0 \ldots & 0 \\ -1; & 0; & -\frac{2}{5} \ldots & 0 \\ \cdots\cdots & \cdots\cdots & \cdots\cdots & \cdots\cdots \\ 0 \ldots & & -\frac{n}{2n-1}; & 0;\ 0 \\ 0 \ldots & & 0; & 0;\ 0 \end{pmatrix}$$

and replace t by the new variable s = vt. Then (2) can be written in the vector-matrix form.

$$\frac{\partial \bar{u}}{\partial s} = A\frac{\partial \bar{u}}{\partial x} + \bar{\Phi}. \tag{3}$$

For further simplification we introduce the vector $\bar{v}$ defined by the relation [4]:

$$\bar{u} = B\bar{v}, \tag{4}$$

where the elements of the matrix B depend in general on the coordinates and the time. We assume that B^{-1} exists [the direct calculation of B for the system (2) confirms the validity of this assumption]. Substituting (4) in (3) and multiplying both sides of the resulting equation by B^{-1} we transform (3) into

$$\frac{\partial \bar{v}}{\partial s} = B^{-1}AB\frac{\partial \bar{v}}{\partial x} + B^{-1}\left(\bar{\Phi} + \frac{\partial B}{\partial x}\bar{v} - \frac{\partial B}{\partial s}\bar{v}\right).$$

We choose B so that it diagonalizes A:

$$B^{-1}AB = \Lambda,$$

where Λ is a diagonal matrix with elements $\lambda_{ik} = \lambda_i \delta_{ik}$. The quantities λ_i are the solutions of the characteristic equation

$$|A - \lambda I| = 0. \tag{5}$$

From (5) we determine the (n + 2) characteristic values and write them in the order of increasing magnitude. For odd n it is not difficult to show that one of the characteristic values of the matrix A is zero and the others are located symmetrically about zero. When we know the characteristic values of A we can find the elements of the matrix B:

$$AB = B\Lambda, \tag{6}$$

i.e.,

$$\sum_{l=1}^{n+2} a_{il} b_{lk} = \lambda_k b_{ik}; \quad k = 1, 2, \ldots, n+2.$$

Since the system (6) is homogeneous, the b_{ik} are determined up to an arbitrary factor. It also follows from (6) that all the b_{ik} are constant, since A and Λ are independent of x and s. Hence,

$$\frac{\partial B}{\partial x} = \frac{\partial B}{\partial s} = 0.$$

Thus Eq. (3) can be transformed into the equation:

$$\frac{\partial \bar{v}}{\partial s} = \Lambda \frac{\partial \bar{v}}{\partial x} + \Psi, \tag{7}$$

where $\Psi = B^{-1}\bar{\Phi}$.

Reduction to an Integral Equation

Equation (7) is equivalent to the differential equation system

$$\frac{\partial v_i(x, s)}{\partial s} = \lambda_i \frac{\partial v_i(x, s)}{\partial x} + \psi_i(v_i, x, s). \tag{8}$$

The functions ψ_i are nonlinear functions of the v_i; in the present case the nonlinearity is due to the presence in the ψ_i of a product of two of the v_i.

The further transformation of (8) is based on the properties of the characteristics of these equations [4]. The characteristics are the lines l_i in the (x, s) plane which are defined parametrically by the relation:

$$\omega_i(x, s) = c_i,$$

where the functions ω_i satisfy

$$\frac{\partial \omega_i}{\partial s} - \lambda_i \frac{\partial \omega_i}{\partial x} = 0. \tag{9}$$

Since the λ_i are constants, the characteristics of the system (8) are given by the very simple equations

$$\omega_i(x, s) = \lambda_i s + x = c_i.$$

The arbitrary constants c_i are obtained from the condition that the ith characteristic passes through the fixed point (x', s'). On this basis, we finally write the equations for the l_i in the form

$$\lambda_i(s - s') + (x - x') = 0 \text{ or } x = x' - \lambda_i(s - s'). \tag{10}$$

By considering the variation of any function f along a characteristic l_i and by using the properties of the characteristics, we can write the total derivative with respect to s of such a function in the form

$$\frac{df}{ds}=\frac{\partial f}{\partial s}+\frac{\partial f}{\partial x}\cdot\frac{dx}{ds}=\frac{\partial f}{\partial s}-\lambda_i\frac{\partial f}{\partial x}\ .$$

Thus all the derivatives in (8) can be expressed as total derivatives with respect to s along l_i, and this means that we can write the system (8)

$$\left.\frac{dv_i}{ds}\right|_{l_i}=\psi_i(v_i,\ x,\ s);\ i=1,\ 2,\ \ldots,\ n+2. \tag{11}$$

In (11) the independent variables x and s vary along l_i, i.e., they are related by the condition (10).

Integrating (11) with respect to s from 0 to s' along a characteristic l_i, we finally obtain

$$v_i(s',\ x')=v_i(0,\ x'+\lambda_i s')+\int_0^{s'}\psi_i\left[s,\ x'-\lambda_i(s-s')\right]ds;\ i=1,\ 2,\ \ldots,\ n+2. \tag{12}$$

The system of nonlinear differential Eqs. (2) has thus been transformed into the system of integral Eqs. (12). If the solution of (12) is known then the solution of (2) can be expressed as a linear combination of the functions v_i according to (4):

$$f_i=\sum_{k=1}^{n+2}b_{ik}v_k;\ i=1,\ 2,\ \ldots,\ n+2.$$

The Boundary Conditions and the Method of Solution

The solution of (12) exists and is unique if initial and boundary conditions are given. The specification of initial conditions is usually not difficult, since initially the absorbing material is usually uniformly distributed through the rod and the components of the vectors $\overline{u}$ and $\overline{v}$ for t = 0 are obtained from a static calculation [3]. The boundary conditions for even and odd harmonics are obtained by the usual method [3], but we must take into account the fact that the neutron flow in a reactor depends essentially on the coordinates and the time. Hence, in the solution of the equations describing the behavior of neutrons in the environment of a rod in the P_n approximation, the term denoting the neutron source must be multiplied by the appropriate function of the coordinates and the time. With sufficient accuracy for use in practice, we can use for this factor the quantity

$$\frac{\Phi_0(x)}{1-\sigma_s^{\Gamma}\Phi_0(x)\,t},$$

where $\Phi_0(x)$ describes the initial distribution of the neutron flow in the reactor and σ_s^{Γ} is the neutron capture cross section in the fuel.

The system (12) is more convenient for investigation and solution than the system (2). If a computer is used, programming will clearly be simpler with (12) than with (2), and the difference in the ease of programming will be greater when the dependence of the ψ_i on the v_i is relatively simple (a quadratic dependence) and when the ψ_i are not directly dependent on x and s. If an approximate analytic solution is required, it is convenient to use successive approximations as described below since (12) is a system of integral equations.

We assume that the solution of the systems (2) and (12) are known at the initial time t = 0, and also for very large times $t\to\infty$. We denote these solutions by $v_{i0}(x)$ and $v_{i\infty}(x)$. There is no difficulty in finding these solutions: We have already considered the case t = 0 (or s = 0), and the case $t\to\infty$ (or $s\to 0$), corresponds to the complete consumption of the absorbing isotope in which case the solution of the system (2) is simple. Knowing v_{i0} and $v_{i\infty}$, we use the first approximation

$$v_i^1(s,\ x)=h_1(s)\,v_{i0}(x)+h_2(s)\,v_{i\infty}(x), \tag{13}$$

where $h_1(s)$ and $h_2(s)$ are for the moment unknown functions satisfying the conditions $h_1(0)=h_2(\infty)=1$; $h_1(\infty)=h_2(0)=0$.

If the expression in (13) is substituted in the right-hand side of (12), then the second approximation is $v_i^2(s, x)$ on the left-hand side. We select $h_1(s)$ and $h_2(s)$ so that for different values of s and x the functions differ from the functions s and x $v_i^1(s, x)$ by the smallest amount possible. To make this selection easier, it is convenient to specify $h_1'(s)$ and $h_2(s)$ as explicit functions of s and the parameters:

$$h_1(s) = \sum_{k=1}^{M} \exp(-\alpha_k s);$$

$$h_2(s) = 1 - \sum_{k=1}^{N} \exp(-\beta_k s), \tag{14}$$

where α_k and β_k are unknown parameters that can be determined by the condition that the difference between v_i^1 and v_i^2 be small, and the numbers M and N depend on the concrete conditions of the problem. The resulting functions $h_1(s)$ and $h_2(s)$ are substituted in (13); the resulting expression is used in the calculation of the dependence of the interlocking on the time.

It can be shown by the usual methods [4] that, when the original approximation is expressed as in (13), the successive approximations converge to the actual solution, and a special choice of h_1 and h_2 will accelerate the convergence and will make even the first approximation sufficiently reliable. The assumed form of the initial approximations for v_i^1, h_1 and h_2 is not the only one possible, and different forms may be used to suit the concrete features of the problem.

The author must thank Academician A. K. Krasina of the Academy of Sciences BSSR for her interest in this work.

LITERATURE CITED

1. G. I. Toshinskii and A. G. Kalashinkov, In the Collection: Theory and Methods of Designing Nuclear Reactors [in Russian], edited by G. I. Marchuk, Moscow, Gosatomizdat (1962), p. 118.
2. A. Radkovskii, In the book: Trans. of the Second International Conference on the Peaceful Uses of Atomic Energy [Russian translation], Coll. Articles of Foreign Scientists, Vol. 3, Moscow, Atomizdat (1959), p. 717.
3. A. D. Galanin, The Theory of Nuclear Reactors Using Thermal Neutrons [in Russian], Moscow, Atomizdat (1959).
4. I. G. Petrovskii, Lectures on Partial Differential Equations [in Russian], Moscow, Fizmatgiz (1961), p. 92.

ELECTROPHORETIC FILTER CLEANS UP REACTOR WATER

(UDC 621.039.568)

V. D. Ganzha, A. I. Egorov, D. M. Kaminker, A. B. Kolyadin,
K. A. Konoplev, Yu. P. Saikov, and V. T. Sharov

Translated from Atomnaya Énergiya, Vol. 19, No. 4,
pp. 350-354, October, 1965
Original article submitted July 7, 1964; rivised April 10, 1965

Sparingly soluble hydrated aluminum oxide formed in the primary-loop water of the reactor in the A. F. Ioffe Physics and Engineering Institute of the Academy of Sciences, USSR, as a result of corrosion. An electrophoretic filter specially designed to clean up the water made it possible to completely clarify the primary-loop coolant. The filter has a total volume of 10.7 liters, low hydraulic drag, and is simple to service. The effective flowrate through the filter is 0.5 cubic meters per hour. The power drain is 0.3 kW.

It was reported in January 1962 that the water in the primary loop of the VVR-M reactor at the A. F. Ioffe Physics and Engineering Institute of the USSR Academy of Sciences had become turbid [1]. In July the turbidity of the water had worsened to such an extent that it began to interfere seriously with loading and transfer of fuel elements (fuel-handling operations are conducted under a 3.5 meter thick shielding layer of water).

The appearance of a suspension in the coolant water was a phenomenon observed at other reactors as well: at the Soviet RFT reactor, the Polish VVR-S reactor, where mechanical filters were employed to clarify the water [2], and at the Canadian NRU reactor, where the water was cleaned up by distillation [3].

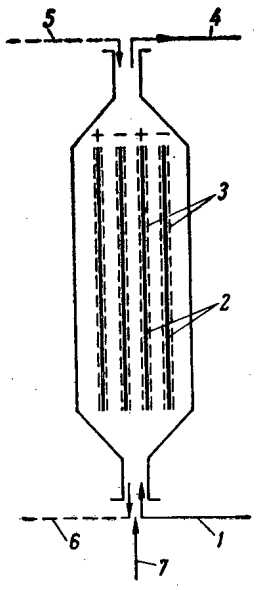

Fig. 1. Design of electrophoretic filter: 1) inlet for water and suspended particles; 2) electrodes; 3) membranes; 4) exit for clarified water and detonating gas bubbles; 5) water inlet for pulp overflow; 6) discharge of pulp; 7) compressed air in to clean membranes.

Characteristics of the Suspension

The suspension is made up of particles of hydrated aluminum oxide. The particulate dimensions vary over a wide range (from a millimicron to tens of microns) depending on the reactor operating conditions and on what purifying instruments are employed. The suspension forms as a result of corrosion of the aluminum used as structural material in the fuel element cladding and in the walls of the reactor vessel. The chemical composition of the suspension is very similar to the chemical composition of products deposited on the heat-transfer surface of the fuel elements (Table 1).

The concentration of suspended particles was found from the optical density of water. Observations of the increased optical density of the primary-loop water over several years yielded an estimate of the mean rate at which suspended particles are introduced into the water: $P = 1.9 \pm 0.3$ g per MWd. This rate of introduction of suspended particles corresponds to a rate of erosion of the aluminum cladding equal to $(0.41 \pm 0.06) \cdot 10^{-5}$ mm per MWd, assuming that only the heat-transfer surface of the fuel elements is subject to erosion.

Operating Principles of the Electrophoretic Filter

Strongly dispersed suspensions are usually stable in distilled water because of the electric charge on the particles. In our case, actually, it turned out that the particles acted upon by the electric

TABLE 1. Make-Upof Suspended Particles in Primary Coolant Water of FTI [Ioffe Institute] Reactor, and Make-Up of Sediment Scraped off Surface of FTI Fuel Element

Substance	Suspended particles, weight, %	Sediment scraped off fuel element surface, weight %
Al_2O_3	54.0	58.0
Fe_2O_3	2.5	4.5
SiO_2	1.8	2.5
Undetermined oxides	1.2	1.1
Moisture	3.0	3.0
Water of crystallization	33.4	33.2
Total	95.9	100.6

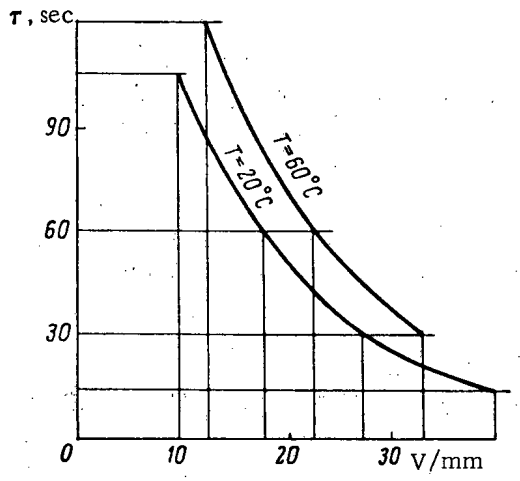

Fig. 2. Dependence of time of contact on field strength when $\xi \geq 0.9$; laboratory specimen.

field are drawn to the electrodes, most of the particles having positive charge.

Suppose that the suspension consists of particles of different size carrying like charges, that the flow of water between the plane electrodes is laminar, and that the particles reaching an electrode are retained there (Fig. 1). An elemental volume of the water passes through the filter in a time (known as time of contact)

$$\tau = \frac{V_f}{Q}, \tag{1}$$

where V_f is the volume of the filter; Q is the flowrate of water through the filter. In that time the particles moving at a speed

$$w = uE, \tag{2}$$

(u is the mobility of the particles; E is the field strength) advance toward the electrodes a distance

$$\Delta x = w\tau. \tag{3}$$

If $\Delta x \geq d$, where d is the interelectrode distance, then all the particles will be retained, and if $\Delta x < d$, then the concentration of the suspended particulates at the exit from the filter will be

$$\left.\begin{aligned} C' &= C\left(1 - \frac{uE\tau}{d}\right); \\ C' &= C(1 - \xi), \end{aligned}\right\} \tag{4}$$

where C is the concentration of the suspension at the filter entrance; ξ is the coefficient for water purified by the filter. In the case of plane electrodes

$$\xi = \frac{uU\tau}{d_2}, \tag{5}$$

and in the case of cylindrical electrodes

TABLE 2. Chemical Composition of Reactor Water at Filter Entrance and Filter Exit

Parameters	At entrance	At exit
Al_2O_3, mg /kg	3.0	0.0
Fe^{+3} mg/ kg	0.4	0.18
SiO_2, mg/kg	6.0	1.3
Oxidizability, mg O_2/ kg	0.96	2.96
Optical density	0.065	0.008

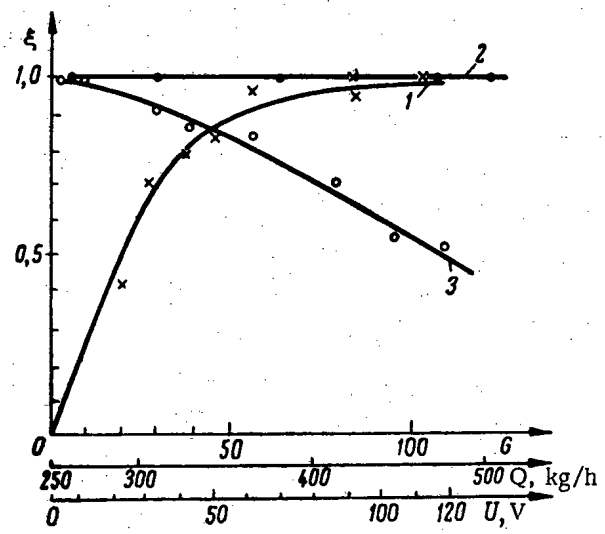

Fig. 3. Dependence of clean-up factor on voltage U across electrodes at Q = 250 kg/h, C = 7 mg/kg (curve 1), on flowrate Q at U = 110 V, C = 4 mg/kg (curve 2), and on the amount G of suspended particulates retained on the filter at Q = 500 kg/h, U = 110 V, C = 5 mg/kg (curve 3). (G is in grams.)

$$\xi = \frac{2uU\tau}{(R^2 - r^2)\ln\frac{R}{r}},$$

where U is the voltage across the electrodes; R and r are respectively radii of the outer and inner electrodes.

Specimen of an Electrophoretic Filter

A laboratory specimen of the electrophoretic filter was of cylindrical shape. The cathode was an outer tube of stainless steel, the anode was a platinized zirconium rod. The filter was 20 cm long, 0.75 cm in radius, and featured an annular space of 0.3 cm between the electrodes.

Caprone membranes were placed ahead of the electrodes to aid coagulation and filtration of the particulates. But pore size in the membranes is much larger than the size of suspended particles, so that when this tissue is used as a simple mechanical filter the water will not be cleaned successfully.

The relationship between the time of contact of the reactor water (at temperatures 20° and 60°C) and field strength when the clean-up factor is close to unity was found experimentally (Fig. 2). A certain flowrate of water through the filter was established, and then the minimum voltage across the electrodes at which the clean-up factor would be greater than or equal to 0.9 was selected. When these results are substituted into Eq. (5), we get: $u = (2.5 \pm 0.6) \cdot 10^{-5}$ cm^2/sec at 60°C, and $u = (5.1 \pm 1) \cdot 10^{-5}$ cm^2/sec at 25°C.

The computed values of u are not the true mobilities, however, since the effect of turbulence on the rate of cross-flow of the particles was not taken into consideration in the calculations (for example, the effect of the membranes on the field strength and on the fluid flow was ignored. Nevertheless, the values of u obtained made if possi- to design an electrophoretic filter capable of cleaning up the reactor water to the required level.

The characteristics graphed in Fig. 3 were taken at water flowrates from 15 to 240 ml/min, voltages, from 40 to 150 V, and currents from 42 to 260 mA.

To determine the capacity of the filter at steady state, the filter was connected up directly to a sampler in the reactor primary loop. At voltages 80 to 84 V, currents of 78 to 80 mA, and a flowrate of 26 g/min through the filter, the filter was operated for 32 h, i.e., 1500 volumes of water were passed through the filter. The clean-up factor remained at unity during the whole time. The experiment was terminated for reasons of radiation safety, since the suspended particulates had been sorbing the radioactive elements dissolved in the reactor water.

The chemical make-up of the water before and after filtration is shown in Table 2. The membranes were cleansed of coagulated particles by reversing the flow of water, with voltage shut off, in amounts equal to two to

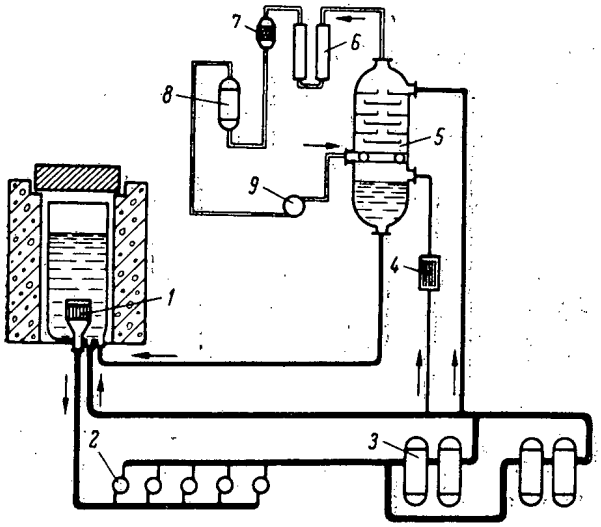

Fig. 4. Diagram showing inclusion of filter in reactor primary loop: 1) core; 2) pumps; 3) heat exchangers; 4) electrophoretic filter; 5) deaerator; 6 to 9) units included in loop to burn up detonating gas.

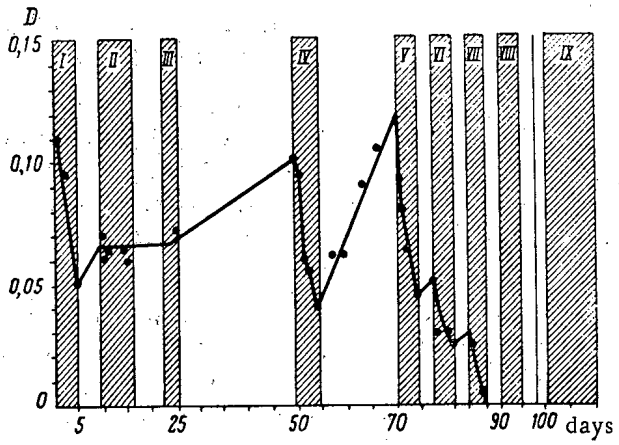

Fig. 5. Variation of optical density D of reactor water with time when the electrophoretic filter is put into service (shaded blocks indicate operating time of electrophoretic filter).

three filter volumes. The yield of detonating as resulting from electrolytic breakdown of the water was 0.3 liter/A·h. The gases were released in the form of fine bubbles and were readily entrained in the flow of water passing through the filter from bottom to top.

Requirements Imposed on the Filter

Clean-up units were passed on the bypass line of the primary reactor loop. In this case the accumulation of suspended particulates in the loop is described by the equation:

$$\frac{d(CV)}{dt} = P - Q(C - C'), \tag{6}$$

where V is the volume of the primary loop. Suppose ξ, Q, P, V constant. Then

$$C = C_0 e^{-\frac{Q\xi t}{V}} + \frac{P}{QS}\left(1 - e^{-\frac{Q\xi t}{V}}\right), \tag{7}$$

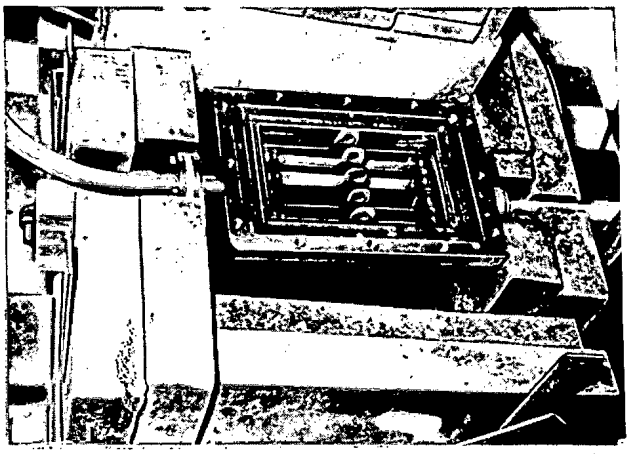

Fig. 6. Electrophoretic filter with top shield and lid removed.

where C_0 is the concentration of suspended particulates in the loop at the instant the filter goes into operation. The steady-state concentration in the loop may be found from the formula:

$$C_\infty = \frac{P}{Q\xi} . \qquad (8)$$

In our case, the visibility of the reactor declines at a concentration 2 mg/kg of suspended particulate matter, and the core cannot be seen at all when the concentration reaches 10 mg/kg. A concentration of 1 mg/kg will not interfere with inspection of the core, i.e., the initial parameter is C_∞ = 1 mg/kg, which, at P = 1.9 g/MWd, will assure the required effective water flowrate through the filter.

Filter Characteristics

Taking as point of departure the effective water flowrate specified above, we chose the following parameters for the electrophoretic filter:

Flowrate of clarified water, kg/h	250-500
Interelectrode voltage, V	110-220
Interelectrode distance, cm	1
Time of contact (at Q = 250 liter/h), min	2
Volume of interelectrode space, liters	7.5
Electrode size, mm	170 x 572
Number of anode plates	4
Number of cathode plates	5
Filter size, mm	400 x 224 x 935

The electrode membranes are fabricated as caprone fabric jackets. Plexiglas insulators are employed. The cathode plates are made of 1Kh18N9T stainless steel, while the anode plates are made of platinum-plated titanium. The thickness of the platinum coating is 3.0 μ. The strength of the platinum coating was checked by a special experiment. After passing 7.56 A · h/cm^2 (corresponding to 14,000 h of filter service), the anode surface proved to be unaffected; no platinum was found either on the cathode or in solution.

Figure 4 shows how the filter is incorporated in the reactor primary loop. It was installed with ease in the drainage channel of the pump house by surrounding it with sectioned lead biological shielding 13 cm thick. The diagram also shows the filter characteristics. The value of u based on formula (5) falls within the range (10 to 20) · 10^{-5} cm^2/sec. After 100 h of service (the usual weekly operating cycle of the reactor), an appreciably high activity accumulates in the filter at a gamma dose rate to 1000 μr/sec.

Twenty to thirty liters of water is passed through the filter from top to bottom to wash out the filter, and air is bubbled through for 5 to 10 min. After the washing the cleansing properties of the filter are completely restored. This procedure takes 15 to 20 min and is usually carried out before the reactor is started up.

Figure 5 shows the variation in the optical density of the primary-loop water while the electrophoretic filter is in service. Portions I-III of the curve show filter operation without washdown at the values: Q = 250 to 500 kg/h; U = 110 V; ξ = 0.9 to 0.5; I = 5 A. Portions IV–IX of the curve correspond to the case where the filter is washed down before each cycle of 100 h, at the values Q = 500 kg/h; U = 110 V; ξ = 1.0.

The electrophoretic filter solved the problem of water clean-up in the reactor primary loop, as we see. The filter (Fig. 6) is simply designed, compact, is easy to regenerate, requires a negligible volume of wash water, is easy to service, operates reliably, and drains only a very small amount of electric power (less than 0.5 kW, in fact). The only serious shortcoming of the filter is the liberation of about 20 liters per hour detonating gas. But this amount

is still small compared to the amount liberated by radiolysis in the core (e.g. about 800 liters/h detonating gas are released in the deaerator of the VVR-M reactor).

The authors welcome this opportunity to express their deep gratitude to Academician B. P. Konstantinov for his constant interest in the progress of the work. The authors are also indebted to V. P. Rodzevich for developing the design of the device, to V. D. Trenin and R. N. Rodionov for performing analyses, and to D. A. Yashin and B. S. Razov for their kind assistance in the work.

LITERATURE CITED

1. V. V. Goncharov et al., Second Geneva conference on the peaceful uses of atomic energy (1958).
2. Atomnaya tekhnika za rubezhom, No. 6, 19 (1963).
3. S. Hatchen and H. Rae, Nucl. Sci. and Engng., 10, 316 (1961).

ATTENUATION OF PILE RADIATIONS IN SERPENTINITE SAND

(UDC 621.039.538.4)

G. A. Vasil'ev, A. P. Veselkin, Yu. A. Egorov, G. G. Moiseev, and Yu. V. Pankrat'ev

Translated from Atomnaya Énergiya, Vol. 19, No. 4,
pp. 354-359, October, 1965
Original article submitted January 29, 1965

Results of an experimental study of the attenuation of pile radiations in serpentine sand having a bulk density of 1.62 g/cm^3 are reported. The sand investigated contains about 11.5% chemically bound water liberated at temperatures upwards of 450°C.

The attenuation of fast flux and thermal flux, attenuation of neutron and gamma dose rate, and fast-neutron spectra in serpentinite sand were measured. Relaxation lengths of fast neutrons computed from experimental data are compared to relaxation lengths of fast neutrons in boron carbide, serpentinite concrete, and iron-ore concentrate.

Serpentine rock presents some interest as a structural material used in biological shielding of nuclear reactors and consists almost entirely of serpentine. This mineral belongs to the group of hydrated magnesium silicates; its composition is given by the chemical formula $Mg_6[Si_4O_{10}][OH]_8$. The oxide ratio (wt.%) are: MgO 43; SiO_2 44.1; H_2O 12.9. The usual impurities present are FeO, Fe_2O_3, and NiO. The specific weight of serpentine is 2.5 to 2.7 g/cm^3.

Serpentinite blocks are widespread in the USSR in the Ural mountains, in the northern Caucasus, in the Transcaucasian districts, in Siberia, and in Kazakhstan. Serpentinite deposits are usually accompanied by asbestos deposits. At the present time the world's largest asbestos deposit at Bazhenovo is being worked; other important deposits in the Soviet Union are found in the Kazakh SSR and in the Tuva autonomous district. At mills in the Bazhenovo deposit site the yield of commercial asbestos per ton of processed ore is 80 kg [1]; the remaining mass consists of serpentinite for the most part. It has been reported [2] that veins of pure serpentinite containing no asbestos have been discovered in a quarry located in the central strip of the Bazhenovo deposit. According to a statement by the present authors, mining of monolithic blocks incurs no additional costs and may be carried out in parallel with the working of the asbestos deposits. In many places the serpentinite shows only insignificant cracking, so that monolithic blocks ≈ 1 cubic meter or more in volume can be quarried.

Serpentinite contains bound water in addition to magnesium, iron, and silicon; the bound water is released only when the serpentinite is heated to temperatures upwards of 450°C [3], so that serpentinite can be properly regarded as a high-temperature material suitable for use in the biological shielding of nuclear reactors. The concentration of hydrogen nuclei in serpentinite is about 1.5 wt.%, which is entirely adequate to attenuate intermediate neutron flux and fast flux identically.

Serpentinite may be used as aggregate in shielding, or may be used as fill in blocks sawed whole. The specific weight of monolithic serpentinite is about 2.6 tons per cubic meter; the thermal conductivity is 2.16 to 2.56 kcal/m · h · deg C [4]. Serpentinite shows excellent retention of the sawed edge, so that shapes of high dimensional accuracy can be fashioned from the material with a compressive strength ranging from 400 to 600 kg/cm^2.

The results of an experimental study of the shielding properties of serpentinite concrete are described in the literature [5]. Data on the attenuation of pile radiations in serpentinite fill are not found in the literature.

Increased interest in ore and rock of possible use in the biological shielding of nuclear reactors has been noted in recent years. The shielding properties of standard iron-ore enriched concentrate containing ≈60 wt.% Fe, ≈30 wt.% O, and trace amounts of Si, Mg, Ca, Al, and other elements have been studied in [6]. Experiments at the BR-5 reactor

TABLE 1. Oxide Content in Serpentinite

Oxides	SiO_2	MgO	$FeO + Fe_2O_3$	Al_2O_3	CaO	SO_3	H_2O	Miscellaneous
Content, wt.%	38,83	37,39	8,47	1,60	1,12	0,18	11,48	0,93

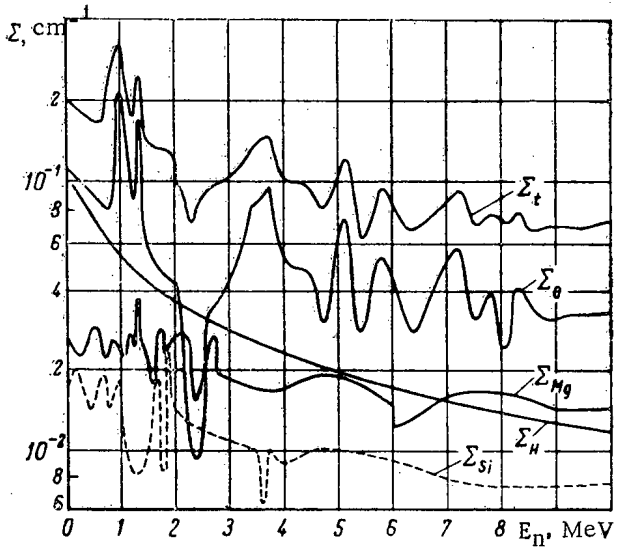

Fig. 1. Macroscopic interaction cross sections of neutrons for serpentinite (Σ_t) and its constituents.

have demonstrated that the neutron relaxation length in this material ranges from 14 to 25 cm (at γ = 2.6 tons per cubic meter) depending in neutron energy. Since iron-ore concentrate contains no hydrogen, the relaxation length of thermal and epithermal neutrons is much higher: 20-21 cm (using copper and indium indicators). When roughly 3 wt.% water is introduced into the concentrate, the relaxation length decreases to 11-13.3 cm, depending on neutron energy. As the authors of [6] noted, however, the water component in iron-ore shielding is unstable at elevated temperatures.

In an earlier article [7], data were reported on the attenuation of pile radiations from the ASTR reactor in sand, clay, and other abundant materials. The relaxation lengths of fast neutrons, which we evaluated from published results of Hurst dosimeter measurements at material thickness from 0 to 152 cm are: 18.1 cm for dry sand (γ = 1.71 g/cm^3), 11.2 cm for wet sand (γ = 2.02 g/cm^3; 8.1 wt.% water). The relaxation length computed from the fast flux attenuation function for clay seems to us a bit low. It should be about 17 cm for clay having a bulk density of 1.35 g/cm^3.

A study of the shielding properties of serpentinite was performed on a water-cooled water-moderated research reactor. Serpentinite from the Bazhenovo deposit in the form of a fine sand fraction of 0-2 mm mesh with asbestos fiber inclusions was used in the study. The chemical composition is listed in Table 1. Boxes of serpentinite sand were placed in a stepped recess in the reactor shielding right up against the core tank (boxes were 680 by 680 by 300 mm or 940 by 400 mm). The maximum thickness of a serpentinite layer was about 180 cm. When the serpentinite was charged into the boxes no tamping or vibratory compaction, was attempted, nor were asbestos fibers removed. The bulk density of the serpentinite was 1.62 ton per cubic meter.

Measurements were conducted in "semi-infinite" and in "barrier" geometry. In the first case indicators and sensors were placed in thin-walled duralumin tubes installed in the boxes. Attenuation functions of fast flux and intermediate flux were studied by determining induced activity in this geometry, and scintillation dosimeters were employed to determine the gamma-ray dose rate [8]. Al (n, α); Al (n, p); P (n, p); In (n, n') threshold indicators were placed in boron–cadmium filters. Attenuation of thermal flux and epithermal flux measured using dysprosium (Dy^{164}) indicators with or without cadmium.

In barrier geometry, the energy distributions of fast neutrons passed through layers of serpentinite of different thicknesses were studied, as was the attenuation of neutron dose rate. Fast-neutron spectra were measured with a single-crystal spectrometer separating pulses due to neutrons or to gamma photons by setting up a space charge across the last dynodes of a photomultiplier tube [10]. Measurements were carried out behind serpentinite layers of thickness 0, 30, 60, 90, 100, and 140 cm.

Attenuation of Fast Flux

The macroscopic removal cross section of fast neutrons was computed to obtain a preliminary estimate of the shielding properties of serpentinite sand having a bulk density $\approx$ 1.62 tons per cubic meter and the chemical composition indicated in Table 1, and was found to be 0.0602 cm^{-1} (Table 2). The principal contribution to the fast neutron removal cross section of serpentinite is that of oxygen (~45%) and hydrogen (~21%). In Fig. 1 we see the neutron energy dependence of the total cross section for serpentinite and its basic constituents. The irregularities (peaks and valleys) in the behavior of the total cross section are ascribable mostly to the neutron energy dependence of the total cross section of oxygen.

TABLE 2. Concentration of Nuclei of Elements Included in the Composition of Serpentinite, and Effective Removal Cross Sections of Fast Neutrons (γ = 1.62 g/cm^3)

Element	Microscopic sections, barns [13]	Concentration of nuclei per cm^3 serpentinite · 10^{22} nuclei / cm^3	Macroscopic removal cross section, cm^{-1}
Hydrogen	1	1.25	0.0125
Magnesium	1.22	0.905	0.010
Silicon	1.26	0.626	0.0079
Oxygen	0.92	2.996	0.0272
Iron	1.9	0.10	0.0019
Aluminum	1.31	0.030	0.0004
Calcium	1.58	0.019	0.0003

TABLE 3. Relaxation Lengths of Fast Neutrons in Various Shielding Materials

Material	γ_3, ton/cm^3	Effective threshold detector, MeV			
		1.5	3	5	7
Serpentinite sand	1.62	15.2	15.7	17	17.7
Boron carbide	1.3*	—	15.7	—	—
Serpentinite concrete	2.2	10.9	10.9	11.2	11.6
Iron-ore concentrate	2.6	—	14.6	—	15.0
Iron-ore concentrate with 3 wt.% water	2.6	12.5†	12.8	—	13.3
Monolithic serpentinite	2.6	9.5	9.8	10.6	11.0

*Higher density of boron carbide fill is practically unattainable.

† Measured with Th^{232} fission chamber, $E_{eff} \approx 2$ MeV [6].

Graphs of the fast flux attenuation function for four energy groups measured by threshold indicators appear in Fig. 2. According to the data reported in [11], the effective energy thresholds of the indicators Al(n, α), Al(n, p), and P(n, p) are 7, 5, and 3 MeV, respectively. The effective energy threshold for the indium indicator may be assigned the value ~1.5 MeV. The curves graphed in Fig. 2 were plotted with due consideration of the fast flux geometric attenuation factor along the axis of the recess (in the shielding). We realize from the diagram that the attenuation of the flux of fast neutrons in the indicated energy groups proceeds exponentially, and the relaxation length of the neutrons in each group remains constant within the range of thicknesses measured.

The relaxation lengths of fast neutrons belonging to different energy groups were computed from the data for indicator measurements, in Table 3 for attenuation in serpentinite (as sand or as monolithic block). The table lists similar data for boron carbide [9], serpentinite concrete [5], and iron-ore concentrate [6], to aid in comparison. The error in the determination of the relaxation length of fast neutrons in serpentinite remains within 4%. Relaxation lengths for monolithic serpentinite were computed under the assumption they varied in inverse proportion to the density of the material. A comparison of the data listed in Table 3 makes it clear that the relaxation length of fast neutrons in serpentinite sand (γ = 1.62 ton/m^3) is the same as in boron carbide (γ = 1.3 ton/m^3). The shielding properties of serpentinite monolithic blocks are substantially superior against fast flux to the shielding properties of iron-ore concentrate pellets and only very slightly superior to those of serpentinite concrete.

Spectra of Fast Neutrons Transmitted Through Serpentinite Layers of Different Thicknesses

The energy distributions of fast neutrons passed through serpentinite layers of thicknesses 0, 30, 60, 100 and 140 cm are shown in Fig. 3. A layer of lead 10 cm thick was placed constantly ahead of the core to lower the

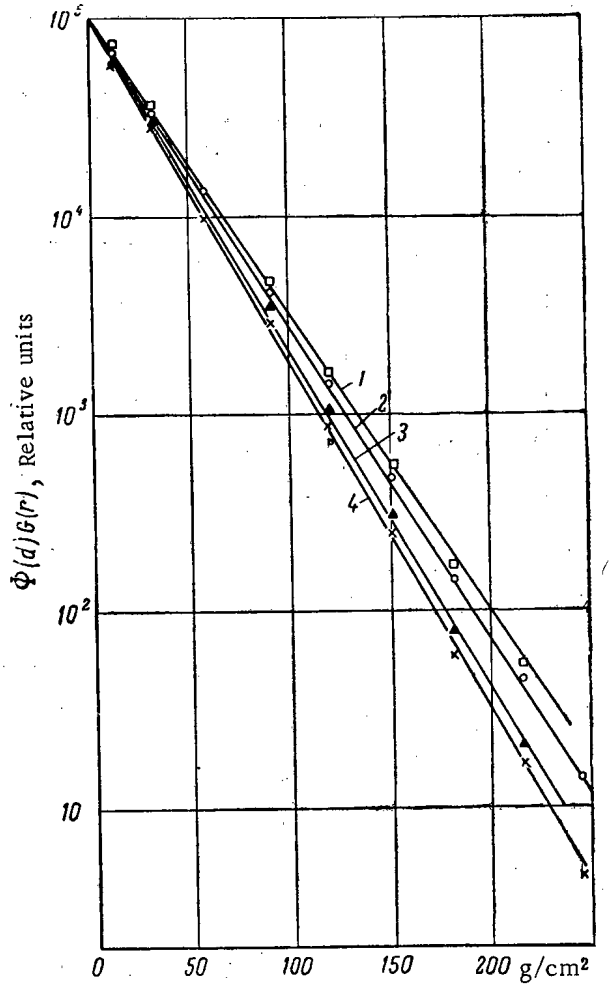

Fig. 2. Fast flux attenutation in serpentinite fill, as measured by the indicators: 1) Al(n, α); 2) Al(n, p); 3) P(n, p); 4) In (n,n').

TABLE 4. Relaxation Lengths of Neutron Energy Groups in Serpentinite Sand, Computed from Spectral Measurements

E_n, MeV	0,9—1,5	1,5—2,5	2,5—4	4—10
λ, cm	14,9	15,2	14,9	15,7
E_n, MeV	1,5—12	3—12	5—12	7—12
λ, cm	15,3	15,7	16,3	17

γ-ray background during the measurements. We see from Fig. 3 that the spectra of fast neutrons vary primarily in the 3 to 8 MeV energy region. The dip in the spectrum in the 3-5 MeV region is evidently due to the peak in the oxygen total cross section at neutron energy 3.8 MeV. A certain build-up of neutrons is observed in the 5-8 MeV range.

Spectral measurement data were used in computing the relaxation lengths of neutrons belonging to distinct energy groups (Table 4). Errors in measurements of the relaxation lengths were within 3-5%.

Comparison of the data in Tables 3 and 4 shows that the relaxation lengths of neutrons of energies above 1.5, 3.5, and 6 MeV obtained from indicator measurements and as a result of processing of the spectra are in excellent agreement (especially for the first two groups). The relaxation lengths of fast neutrons belonging to these energy groups may be used in many-group shielding calculations.

Attenuation of Thermal Flux and Epithermal Flux

Figure 4 shows the attenuation functions of thermal flux and epithermal flux (geometric attenuation taken into account) as well as the cadmium ratio. The diagram shows a certain build-up of thermal and epithermal neutrons

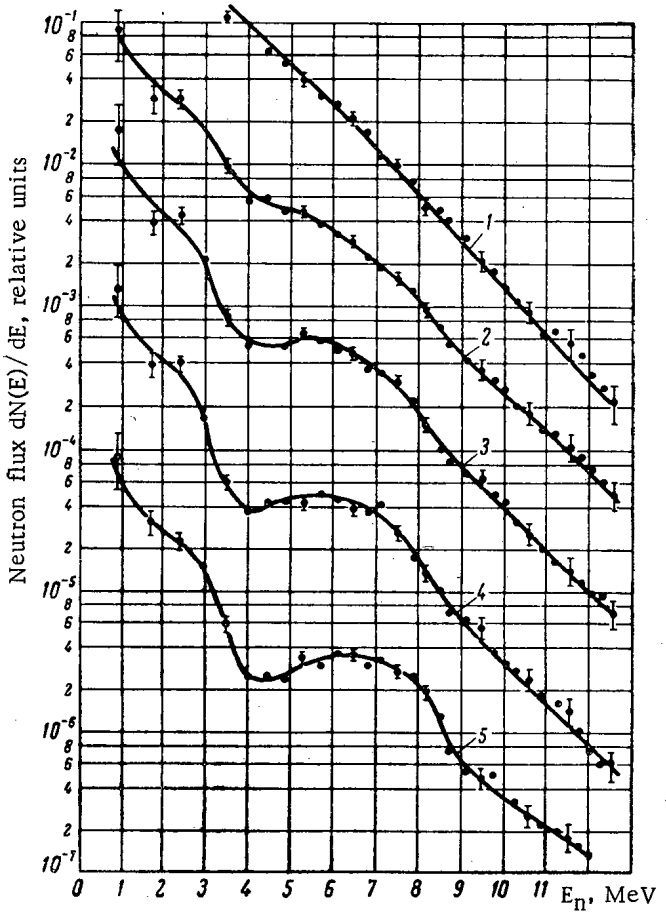

Fig. 3. Energy distributions of fast neutrons after traversal of serpentinite layers of different thickness, cm: 1) 0, 2) 30; 3) 60; 4) 100; 5) 140.

at narrow serpentinite thicknesses. Starting with a thickness of ~30 g/cm^2, the attenuation slopes exponentially with constant relaxation length over the range of thicknesses measured. The relaxation length of thermal and epithermal neutrons is 15.2 cm. Neutrons of greater than 1.5 MeV energy have the same relaxation length.

The relaxation length obtained for thermal and epithermal neutrons in serpentinite sand is far below the relaxation length of thermal and epithermal neutrons in iron-ore concentrate (20-21 cm). This is explained by the presence of considerable amounts of water in the serpentinite (thus a slower build-up of moderated neutrons).

Attenuation of Neutron Dose Rate

The attenuation of total dose rate in barrier geometry is measured by an isodose neutron detector and a general-purpose RUS-5 scintillation radiometer. The RUS-5 device was also employed to measure the attenuation of the dose rate of intermediate neutrons (in the 0.4 eV-0.5 MeV range). The curve giving the attenuation of dose rate for neutrons of greater than 0.5 MeV energy was plotted by comparing the results of total dose rate measurements and intermediate neutron dose as obtained by the RUS-5 radiometer. Fast neutron measurements by the counter enabled us to evaluate attenuation of the dose rate of neutrons of greater than 2 MeV energy in serpentinite.

Figure 5 shows (in absolute units) the attenuation in serpentinite of the total dose rate, of the dose rate for fast neutrons, and of the dose rate for intermediate-spectrum neutrons. The slope of the dose attenuation curves is the same and does not vary over the range of serpentinite thicknesses measured. The relaxation length of the dose computed from the attenuation curves is 15.2 cm. Attenuation of the total and partial neutron doses is determined by the attenuation of neutron flux such that $E_n > 1.5$ MeV. Figure 5 shows that the ratio of total neutron dose such that $E > 2$ MeV is two, and remains unchanged over the range of serpentinite thicknesses measured.

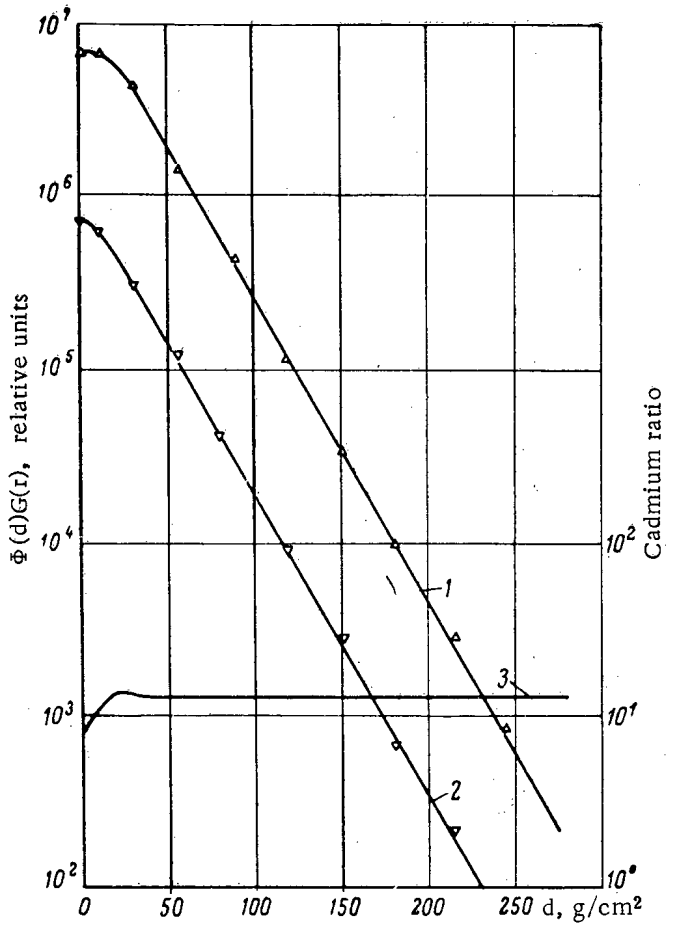

Fig. 4. Attenuation of thermal flux (1) and epithermal flux (2), and cadmium ratio (3) in serpentinite fill.

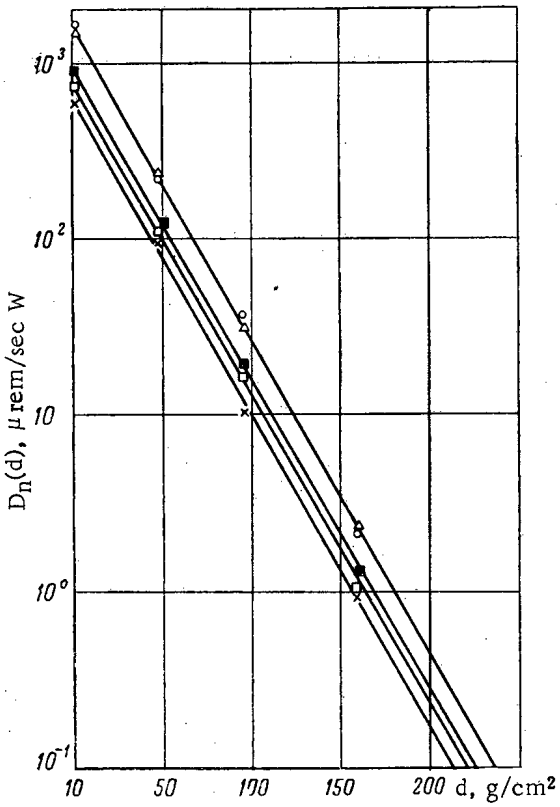

Fig. 5. Attenuation of neutron dose rate after neutrons have traversed several layers of serpentinite: ○—total dose (isodose detector [14]); Δ—total dose (RUS-5); ■—fast neutron dose (RUS-5); □—fast neutron dose (E_n > 2 MeV); ×—intermediate neutron dose (RUS-5).

Attenuation of γ-Radiation in Serpentinite

A scintillation dosimeter was employed to measure the attenuation of γ-ray dose rate in serpentinite. The relaxation length of the dose was about 22 cm for a serpentinite layer 270 g/cm² thick. This value agrees with the relaxation length of the γ-ray dose in serpentinite concrete with a reported density of 1.62 g/cm³, for which $\lambda_\gamma \approx 20$ cm [5] (we note a 10% discrepancy).

SUMMARY

The experimental results show that serpentinite sand fill is not at all inferior to boron carbide in its shielding properties; the bulk density of the latter does not exceed 1.3 ton/m³ even after careful compacting. Furthermore, the cost of one [metric] ton of serpentinite is less than 3 rubles.

Serpentinite sand used as fast-neutron shielding is inferior to iron-ore concentrate; but monolithic serpentinite has far shorter relaxation lengths at the same density as the iron-ore concentrate. The presence of approximately 11 wt.% bound water in the serpentinite accounts for the high shielding effectiveness against intermediate neutrons (even at temperatures to 450°C); the relaxation length of intermediate neutrons is far shorter in serpentinite than it is in iron-ore concentrate.

The shielding properties of serpentinite fill may be improved by adding iron shot. The iron-water mixture must not contain less than 0.3 wt.% hydrogen to achieve identical attenuation of fast flux and intermediate flux. This hydrogen concentration will be attained in a mixture consisting of 25 wt.% serpentinite and 75 wt.% iron. In a mixture so constituted the relaxation length of the total neutron dose will be about 8.5-9 cm (at a mixture bulk density of 4.5-5 g/cm³). A mixture of that bulk density may be achieved by careful sorting and grading of the components.

The authors express their indebtedness to the reactor staff and to others who cooperated in the experiment.

LITERATURE CITED

1. Industrial requirements for the quality of mineral raw materials. Asbestos. No. 5 [in Russian], Moscow State geol. and industr. press (1959).
2. N. S. Krutsko and Yu. S. Solov'ev, Trudy Gorno-geol. inst., No. 56, 149 (1961).
3. Hungerford et al., Atomnaya tekhnika za rubezhom, No. 10, 20 (1960).
4. V. N. Kabranova, Physical properties of rocks [in Russian], Moscow State fuel industry press (1962).
5. G. A. Vasil'ev et al., Atomnaya énergiya, 18, 121 (1965).
6. V. K. Daruga et al., Atomnaya énergiya, 17, 63 (1964).
7. D. M. Wheller and L. H. Bostick, Military field expedient shielding experiment. Comair Nuclear Research and Development Laboratory, October 18 (1960), DA-44-192-ENC-13.
8. V. N. Avaev et al., Advances in reactor shielding physics. Collection [in Russian], Moscow State atom press (1963), p. 260.
9. D. L. Broder et al., Advances in reactor shielding physics. Collection [in Russian], Moscow State atom press (1963), p. 60.
10. V. N. Avaev et al., Atomnaya énergiya, 15, 20 (1963).
11. B. I. Sinitsyn and S. G. Tsypin, Atomnaya énergiya, 14, 306 (1962).
12. I. B. Keirim-Markus et al., Atomnaya énergiya, 15, 336 (1963).
13. Reactor Handbook. Ed. C. Tipton, New York (1960), Vol. 1, p. 1027.
14. Kh. D. Androsenko and G. I. Smirenkin, Pribory i tekhn. eksper., No. 5, 64 (1962).

All abbreviations of periodicals in the above bibliography are letter-by-letter transliterations of the abbreviations as given in the original Russian journal. *Some or all of this periodical literature may well be available in English translation.* A complete list of the cover-to-cover English translations appears at the back of this issue.

THEORY OF CASCADES FOR SEPERATING MULTI-COMPONENT ISOTOPE MIXTURES

(UDC 621.039.31)

R. Ya. Kucherov and V. P. Minenko

Translated from Atomnaya Énergiya, Vol. 19, No. 4,
pp. 360-367, October, 1965
Original article submitted March 10, 1965

The article discusses a stationary process for the separation of multi-component isotope mixtures in cascades of arbitrary profile. It includes a theoretical investigation of the extreme cases in which the relative rate of isotope exchange has values of zero and infinity. A solution is obtained for a system of transport equations for a rectangular stepped cascade, and a calculation procedure for such cascades is worked out.

The development of nuclear technology today has brought an increased interest in the problem of separating multi-component isotope mixtures. This problem arises in the production of pure isotopes of elements which have more than two stable isotopes and in many cases in which binary isotopes are separated in the form of chemical compounds.

References [1-4] tell of experimental investigations concerned with the separation of multi-component isotope mixtures in cascades. However, the theory of this process has not been sufficiently developed. The authors know of only two theoretical studies [5, 6]: the first deals with a column in which there is no removal of the product, and the second with the development of a theory for an ideal cascade.

The purpose of the present study is to solve a system of transport equations in the stationary case for cascades of arbitrary profile* which include input and removal of the product, as well as to work out a calculation procedure for practical cascades. When isotopes are separated in the form of chemical compounds, the basic process in the cascade may be accompanied by isotope exchange between the molecules of the components, with the result that the number of molecules of an individual component does not remain the same. The effect of this process on the separation depends on its relative rate. In the present study we consider the two extreme cases—zero and infinite relative rates of isotope exchange—to which most of the practical problems of isotope separation can be reduced.

1. Relative Rate of Isotope Exchange

In the separation of multi-component mixtures consisting of nonmonatomic molecules the process in each stage upsets the equilibrium distribution of isotopes among the components. This leads to a process tending to the reestablishment of equilibrium through isotope exchange.

For the sake of simplicity, we shall consider the distribution of a substance consisting of molecules of the type XY. We shall assume that the elements X and Y are different. The components of a mixture, in accordance with the isotopic composition of their molecules X^mY^n, will be denoted by the indices mn. Let the element X have q_1 isotopes and let the element Y have q_2 isotopes. We shall denote the number of components in the mixture by $q_1q_2 = k$. The mole-fraction concentrations of the components are $[X^mY^n] = N_{mn}$. The mole fractions of the corresponding isotopes will be denoted by x_m and y_n.

Suppose that at time $t = 0$ this mixture, filling some volume, has concentrations $N_{mn}(0)$ which are different from the equilibrium concentrations. The decrease in the number of molecules of the component mn per unit volume resulting from isotope exchange in time dt may be written as

*By "profile" we shall mean the distribution L(s) of the flow rate of the mixture of isotopes along the cascade, where s is the longitudinal coordinate.

$$d_1\varrho_{mn} = -\varrho_{mn} \sum_{i\neq n,\ j\neq m} \gamma_{ji}^{mn} \varrho_{ij}\, dt, \tag{1.1}$$

where γ_{ij}^{mn} are kinetic coefficients independent of concentration. Similarly, the increase in the number of molecules is:

$$d_2\varrho_{mn} = \sum_{i\neq n,\ j\neq m} \gamma_{jn}^{mi} \varrho_{mi}\varrho_{jn}\, dt. \tag{1.2}$$

If we assume the coefficients γ to be equal for all components, after some simple transformations, we obtain the differential equation

$$\frac{1}{\gamma}\cdot\frac{d\varrho_{mn}}{dt} = -\varrho_{mn}\sum_{i,j}\varrho_{ij} + \sum_i \varrho_{mi}\sum_j \varrho_{jn}. \tag{1.3}$$

From the conditions that the number of atoms of the isotopes must remain constant, it follows that $\sum_i \varrho_{mi}$, $\sum_i \varrho_{jn}$ and $\sum_{i,j}\varrho_{ij} = \varrho$ are independent of time. Consequently, after integrating and changing to mole-fraction concentrations, we find

$$N_{mn}(t) - x_m y_n = [N_{mn}(0) - x_m y_n]\exp(-\gamma\varrho t). \tag{1.4}$$

Let t_0 be the length of time the mixture remains in the given volume. From (1.4), writing

$$\beta = \exp(-\gamma\varrho t_0), \tag{1.5}$$

we obtain

$$N_{mn}(t_0) = \beta N_{mn}(0) + (1-\beta)\, x_m y_n. \tag{1.6}$$

Let us now consider the separating cascade. To simplify our discussion, we shall consider a cascade scheme in which isotope exchange takes place in exchangers situated at the outlets of the separating stages. This scheme enables us to write the transport equations correctly in a first approximation using ε. The residence time of the mixture in the exchanger is $t_0 = h/L$, where h is the exchanger holdup (if the exchange takes place directly in the separating stage, h is the holdup of the stage in the corresponding phase. From this it follows that

$$\beta = \exp\left(-\gamma\varrho\frac{h}{L}\right). \tag{1.7}$$

As can be seen from formula (1.6), the effect of the exchange on the separation may be evaluated by means of the expression:

$$\frac{1-\beta}{\beta} = \frac{N_{mn}(0) - N_{mn}(t_0)}{N_{mn}(t_0) - x_m y_n}, \tag{1.8}$$

which we shall herein after call the relative exchange rate v.

It follows from formula (1.8) that in the extreme case when $v = \infty$, we have $N_{mn}(t_0) = x_m y_n$, and when $v = 0$, we have $N_{mn}(t_0) = N_{mn}(0)$. It will be shown below that even when $v \sim 1$, the isotope exchange may have a considerable influence on the separation. Conversely, in the case when $v \ll 1$, the exchange may be neglected. When $v = 0$, the number of molecules of each component remains constant.

2. Derivation of the Transport Equations for the Case of Zero Exchange Rate

Let us consider a separating cascade with an arbitrary profile. At some points of the cascade the mixture is fed in or removed. We shall assume that the cascade consists of a finite number of segments each of which has a continuous profile. At the points of discontinuity of L(s), as well as at the input and output points, there is a discontinuity of the cascade parameters. The part of a cascade included between two adjacent points of discontinuity of the parameters will be called a section. Let B denote the total number of sections in a cascade and let b be the

index number of an individual section. Each section consists of σ^b separating stages connected in series. The serial number of a stage will be denoted by s (for stages within the same section we shall omit the index b).

In a separating section the total flow L and the concentrations of the components N_m are given by the equations

$$L = L' + L''; \tag{2.1}$$

$$LN_m = L'N'_m + L''N''_m \quad (m = 1, \ldots, k), \tag{2.2}$$

where L', and L" are the flows leaving the stages at the beginning and at the end of the section, respectively; N'_m and N''_m are the concentrations of component m in the corresponding flows. We introduce the relative coefficient of separation

$$\alpha_{mn} = \frac{N'_m}{N''_m} \cdot \frac{N''_n}{N'_n} \quad (1 \leqslant m,\ n \leqslant k). \tag{2.3}$$

In the general case the coefficients of separation depend on the concentrations of the components; however, this dependence is so weak that the values α_{mn} may be regarded as constant. In general the isotopes satisfy the inequality

$$|\alpha_{mn} - 1| \ll 1. \tag{2.4}$$

Using this fact, we introduce the small parameter

$$\varepsilon = \frac{1}{k} \sqrt{\sum_{m,\,n} (\alpha_{mn} - 1)^2}. \tag{2.5}$$

In the remainder of this discussion we shall neglect of a smaller order of magnitude. From Eqs. (2.1) and (2.2) we readily obtain

$$\delta'' N_m = \frac{\Theta}{1 - \Theta} \delta' N_m, \tag{2.6}$$

where $\delta' N_m = N'_m - N_m$; $\delta'' N_m = N_m - N''_m$ and $\Theta = L'/L$. If we assume that $|\Theta(s) - 0.5| \sim \varepsilon$, then $|\delta' N_m - \delta'' N_m| / 2 \sim \varepsilon |\delta N_m|$, where $\delta N_m = \delta' N_m + \delta'' N_m = N'_m - N''_m$.

Let us estimate the quantity δN_m. From the identity

$$\sum_{n=1}^{k} N_n = 1 \tag{2.7}$$

it follows that

$$\sum_n \delta' N_n = \sum_n \delta'' N_n = 0. \tag{2.8}$$

Using the definition (2.3), we readily find

$$N''_n (N'_m - N''_m) = N''_m (\alpha_{mn} N'_n - N''_n). \tag{2.9}$$

Summing (2.9) over n and using (2.7) and (2.8), we find

$$N'_m - N''_m = N''_m \sum_{n=1}^{k} (\alpha_{mn} - 1) N'_n,$$

i.e., the order of magnitude of $|\delta N_m|$ is no greater than εN_m.

We shall call $\varepsilon_{mn} = \ln \alpha_{mn}$ the relative coefficient of enrichment. Let us rewrite (2.3) in the form

$$\varepsilon_{mn} = \ln \frac{N'_m}{N''_m} - \ln \frac{N'_n}{N''_n}. \tag{2.10}$$

From this it can be seen that the relative coefficients of enrichment are additive and antisymmetric:

$$\left.\begin{aligned} \varepsilon_{mn} &= \varepsilon_{mr} + \varepsilon_{rn}, \\ \varepsilon_{nm} &= -\varepsilon_{mn}. \end{aligned}\right\} \tag{2.11}$$

Consider an expression of the type $\ln (N'/N'') = \ln (N'/N) - \ln (N''/N)$. Expanding $\ln (N'/N'') = [1 + \delta' N/N)] - \ln [1 - (\delta' N/N]$ into a Taylor's series in $\frac{\delta' N}{N} \approx \varepsilon$ and $\frac{\delta'' N}{N} \approx \varepsilon$, we find $\ln \frac{N'}{N''} = \frac{\delta N}{N}$. to within terms of the order of ε^2 inclusive. Thus, (2,10) may be written in the form:

$$\varepsilon_{mn} = \frac{\delta N_m}{N_m} - \frac{\delta N_n}{N_n} \tag{2.12}$$

or

$$N_n \delta N_m = N_m \varepsilon_{mn} N_n + N_m \delta N_n. \tag{2.13}$$

In (2.13) we sum over n and obtain

$$\delta N_m = N_m \sum_{n=1}^{k} \varepsilon_{mn} N_n. \tag{2.14}$$

From this, using the equations $\delta N_m = \delta' N_m + \delta'' N_n$, and (2.6), we find

$$N'_m - N_m = (1 - \Theta) N_m \sum_{n=1}^{k} \varepsilon_{mn} N_n. \tag{2.15}$$

It should be noted that these relations may also be derived from an analysis of the thermodynamics of the process.

Let us take a hypothetical cross section of the cascade between stages s−1 and s, which belong to section b. The law of conservation of matter is written in the form

$$L'(s-1) + \sum_{r=b}^{B} F^r = L''(s) + \sum_{r=b}^{B} P^r; \tag{2.16}$$

$$L'(s-1) N'_m(s-1) + \sum_{r=b}^{B} F^r \tilde{N}_m(\sigma^r) = L''(s) N''_m(s) + \sum_{r=b}^{B} P^r N_m(\sigma^r). \tag{2.17}$$

Here P^r and F^r are the output and input flows, respectively, at the end of section r; $N_m(\sigma^r)$ is the concentration of component m at the corresponding removal point; $\tilde{N}_m(\sigma^r)$ is the concentration in the corresponding input flow. Passing from difference equations to differential equations and making some simple transformations, we obtain a system of transport equations in section b for a k-component isotope mixture:

$$\frac{dN_m(s)}{ds} = N_m(s) \sum_{n=1}^{k} \varepsilon_{mn} N_n(s) - \frac{2}{L^b(s)} \sum_{r=b}^{B} \times \{P^r [N_m(\sigma^r) - N_m(s)] - F^r [\tilde{N}_m(\sigma^r) - N_m(s)]\}. \tag{2.18}$$

In this system only (k − 1) equations are independent, since the identity (2.7) is its first integral. When k = 2, the system (2.18) becomes the well-known transport equation for a binary mixture.

Setting L(s) = const and B = 1, we obtain the system of transport equations given earlier in [5] for thermal diffusion.

3. The Extreme Case of an Infinite Exchange Rate

Writing the concentrations at the outlets of a stage or the inlets of the exchangers as $\overline{N}'_{mn}$ and $\overline{N}''_{mn}$, respectively, we can rewrite Eqs. (2.15) in the form

$$\overline{N}'_{mn} - N_{mn} = (1-\Theta) N_{mn} \sum_{i,j} \varepsilon_{ij}^{mn} N_{ij}. \tag{3.1}$$

The relative coefficient of enrichment are determined from the equation of the separating stage

$$\alpha_{ij}^{mn} = \frac{\overline{N}'_{mn}}{\overline{N}''_{mn}} \cdot \frac{\overline{N}''_{ij}}{\overline{N}'_{ij}} \tag{3.2}$$

by means of the formula

$$\varepsilon_{ij}^{mn} = \ln \alpha_{ij}^{mn}. \tag{3.3}$$

It is evident that the values ε_{ij}^{mn} are additive and antisymmetric.

By the definition of mole-fraction concentrations, we have

$$x_m = \sum_{n=1}^{q_2} N_{mn}, \quad y_n = \sum_{m=1}^{q_1} N_{mn}. \tag{3.4}$$

Since in an exchanger (unlike the case of a separating stage) the isotope concentrations in the mixture do not change, we find from Eqs. (3.1) and (3.4) that the concentrations x'_m and x''_m at the outlets of the exchangers satisfy the equations

$$\left.\begin{aligned} x'_m - x_m &= (1-\Theta) \sum_{n,\, i,\, j} \varepsilon_{ij}^{mn} N_{mn} N_{ij}, \\ x_m - x''_m &= \frac{\Theta}{1-\Theta} (x'_m - x_m). \end{aligned}\right\} \tag{3.5}$$

Writing the law of conservation of matter for the isotopes X^m and passing to differential equations, we obtain the system of transport equations

$$\begin{aligned} \frac{dx_m(s)}{ds} = {} & \sum_{n,\, i,\, j} \varepsilon_{ij}^{mn} N_{mn}(s)\, N_{ij}(s) - \frac{2}{L^b(s)} \sum_{r=b}^{B} \\ & \times \{P^r [x_m(\sigma^r) - x_m(s)] - F^r [\tilde{x}_m(\sigma^r) - x_m(s)]\}. \end{aligned} \tag{3.6}$$

In the extreme case of an infinite rate of exchange (see Section 1)

$$N_{mn}(s) = x_m(s)\, y_n(s). \tag{3.7}$$

If we make the substitution $\varepsilon_{ij}^{mn} = \varepsilon_{mj}^{mn} + \varepsilon_{ij}^{mj}$ in (3.6) and utilize (3.7), noting the identity for $\sum_{n,\, i,\, j} \varepsilon_{mj}^{mn} N_{mn} N_{ij}$, we find

$$\frac{dx_m}{ds} = x_m \sum_{ij} \varepsilon_{ij}^{mj} x_i y_j - \frac{2}{L^b} \sum_{r} \times \{P^r [x_m(\sigma^r) - x_m] - F^r [\tilde{x}_m(\sigma^r) - x_m]\}. \tag{3.8}$$

In a similar manner, we can write the transport equations for the isotopes of element Y.

The system of transport equations, consisting of (3.8) and the equations for the isotopes of the element Y, enables us to carry out the complete calculation for the cascade. It should be noted that the equations of this system contain only coefficients of relative enrichment whose unwritten indices are identical. We may expect that the

dependence of the coefficients of enrichment on the identical indices will become apparent in the second-order terms. This is easily proved in the case when the coefficients of separation depend only on the mass numbers. As a result, we can divide the system of transport equations into two independent systems of the form

$$\frac{dx_m(s)}{ds} = x_m(s)\sum_{i=1}^{q_1}\varepsilon_i^m x_i(s) - \frac{2}{L^b(s)}\sum_{r=b}^{B}\times\{P^r[x_m(\sigma^r)-x_m(s)]-F^r[\widetilde{x}_m(\sigma^r)-x_m(s)]\}. \tag{3.9}$$

Here the coefficients ε_i^m are obtained from ε_{ij}^{m} by fixing the identical indices j. It is readily seen that the values ε_i^m are additive and antisymmetric.

Thus, in the case of an infinite rate of exchange the transport equations for the isotopes completely coincide with the transport equations for the components of a mixture with a zero rate of exchange.

Let us estimate the effect of the isotope exchange on the separation. Taking account of the equation

$$dN_{mn} = x_m dy_n + y_n dx_m,$$

we find

$$\frac{dN_{mn}}{ds} = N_{mn}\sum_{ij}(\varepsilon_{ij}^{mj}+\varepsilon_{ij}^{in})N_{ij} - \frac{2}{L^b}\sum_{r}\times\{P^r[x_m y_n\sigma^r)+y_n x_m(\sigma^r)-2N_{mn}]$$
$$-F^r[x_m\widetilde{y}_n(\sigma^r)+y_n x_m(\sigma^r)-2N_{mn}]\}. \tag{3.10}$$

From a comparison of (3.10) and (2.18) it follows that in total-reflux operation the effect of the isotope exchange is manifested as a second-order effect, since we generally have $|\varepsilon_{ij}^{mj}+\varepsilon_{ij}^{in}-\varepsilon_{ij}^{mn}|\sim\varepsilon^2$, whereas when there is removal, it is a first-order effect.

It is readily shown that in the cases when the kinetic coefficients γ are considered identical for all components of the mixture, the transport equations for mixtures consisting of arbitrary molecules may be represented in the form of independent systems of the type (3.9).

4. Solutions of the System of Transport Equations

Since the written forms of the transport equations in the extreme cases of high and low rates of isotope exchange are identical we shall concern ourselves with solving the system (2.18). Let us write

$$2\sum_{r=b}^{B}[P^r N_m(\sigma^r)-F^2\widetilde{N}_m(\sigma^r)] = g_m^b. \tag{4.1}$$

Using (2.7), we obtain

$$2\sum_{r=b}^{B}(P^r-F^r) = \sum_{m=1}^{k} g_m^b. \tag{4.2}$$

If we use this notation, the system (2.18) becomes

$$L^b(s)\frac{dN_m(s)}{ds} = L^b(s)N_m(s)\sum_{n=1}^{k}\varepsilon_{mn}N_n(s) - g_m^b + N_m(s)\sum_{n=1}^{k} g_n^b. \tag{4.3}$$

From the equation for component m we successively subtract the equations for the remaining components, so that we obtain (k − 1) equations of the type

$$\frac{d\ln N_m(s)}{ds} - \frac{d\ln N_n(s)}{ds} = \varepsilon_{mn} - \frac{g_m^b}{L^b(s)N_m(s)} + \frac{g_n^b}{L^b(s)N_n(s)}. \tag{4.4}$$

Equations (4.4) and the identity (2.7) together form a complete system for determining the concentrations of the components. It is readily shown that the systems of differential Eqs. (4.3) and (4.4) are equivalent if the condition (2.7) is satisfied.

In the simplest case, when the cascade operates without removal ($g_m^b = 0$), the system (4.4) is readily integrable, and the solution is of the form

$$N_m(s) = \frac{N_m(0)}{\sum_{n=1}^{k} N_n(0) \exp \varepsilon_{nm} s}. \tag{4.5}$$

Thus, the distribution of concentrations of components in such operation is independent of the shape of the cascade.

In order to find a solution in the general case, let us consider an individual section. We shall temporarily omit the index b and introduce a numbering system for the stages within the section, $0 \leq s \leq \sigma$. If we write

$$L(s) N_m(s) = x_m(s), \tag{4.6}$$

then

$$\sum_{m=1}^{k} x_m(s) = L(s) \tag{4.7}$$

and Eqs. (4.4) become

$$\frac{d \ln x_m}{ds} - \frac{d \ln x_n}{ds} = \varepsilon_{mn} - \frac{g_m}{x_m} + \frac{g_n}{x_n}. \tag{4.8}$$

Making the substitution

$$\frac{d \ln x_m}{ds} = \frac{g_m}{x_m} = \frac{d \ln \bar{x}_m}{ds}, \tag{4.9}$$

we reduce Eqs. (4.8) to the form

$$\frac{d}{ds} \ln \frac{\bar{x}_m}{\bar{x}_n} = \varepsilon_{mn}. \tag{4.10}$$

As a result, we obtain

$$\frac{\bar{x}_m(s)}{\bar{x}_m(0)} = \frac{\bar{x}_n(s)}{\bar{x}_n(0)} \exp \varepsilon_{mn} s. \tag{4.11}$$

The solution of the linear differential Eq. (4.9) with the boundary condition $x_m(0) = x_{m0}$ is of the form

$$x_m(s) = \frac{\bar{x}_m(s)}{\bar{x}_m(0)} \left\{ x_{m0} - g_m \int_0^s \frac{\bar{x}_m(0)}{\bar{x}_m(t)} dt \right\}. \tag{4.12}$$

We introduce the notation

$$\varphi_m(s) = \frac{\bar{x}_m(0)}{\bar{x}_m(s)}, \tag{4.13}$$

by means of which we shall write Eqs. (4.12) and (4.11), respectively, as

$$x_m(s) \varphi_m(s) = x_{m0} - g_m \int_0^s \varphi_m(t) dt; \tag{4.14}$$

$$\varphi_m(s) = \varphi_n(s) \exp \varepsilon_{nm} s. \tag{4.15}$$

In (4.14) we sum over m, and using (4.7) and (4.15), we find

$$\varphi_n(s) + \frac{1}{L(s)} \int_0^s \varphi_n(t) \sum_{m=1}^{k} g_m \exp \varepsilon_{mn}(s-t) \cdot dt = \frac{1}{L(s)} \sum_{m=1}^{k} x_{m0} \exp \varepsilon_{mn} s. \tag{4.16}$$

Thus, the system (2.18) has been reduced to (4.16), a Volteva integral equation with a degenerate kernel, and k−1 algebraic relations for the functions $\varphi_m(s)$. For a given form of L(s) the Eq. (4.16) has a unique solution, which may be constructed, for example, by the method of successive approximation. After this, using formulas (4.14) and (4.6), we find the concentrations of the components of the mixture (within the given section).

Let us consider the case which is of greatest practical interest: a rectangular stepped cascade. Within one section we have L(s) = const, and Eq. (4.6) may be written as

$$\varphi_n(s) + \int_0^s \varphi_n(t) \sum_{m=1}^{k} c_m \exp \varepsilon_{mn}(s-t)\, dt = \sum_{m=1}^{k} N_{m0} \exp \varepsilon_{mn} s, \tag{4.17}$$

where

$$c_m = \frac{g_m}{L}. \tag{4.18}$$

The integral Eq. (4.17) is solved by the Laplace transform method. It should be noted that the kernel and the free term of the equation are analytic functions in the entire open plane of the complex argument z. Consequently $\varphi_n(z)$ can be analytically continued for all $|z| < \infty$, and we shall denote the continuation for all real values of the argument z = s by $\psi_n(s)$.

Applying the Laplace transform to $\psi_n(s)$, we find

$$F_n(q) \left\{ 1 + \sum_{m=1}^{k} \frac{c_m}{q - \varepsilon_{mn}} \right\} = \sum_{m=1}^{k} \frac{N_{m0}}{q - \varepsilon_{mn}}, \tag{4.19}$$

where

$$F_n(q) = \int_0^\infty \exp(-qs)\, \psi_n(s)\, ds. \tag{4.20}$$

By the inversion formula we have

$$\psi_n(s) = \frac{1}{2\pi i} \int_{q_0 - i\infty}^{q_0 + i\infty} \exp(qs)\, F_n(q)\, dq. \tag{4.21}$$

As can be seen from formula (4.19), when $q \to \infty$, the function $F_n(q)$ approaches 0 like q^{-1}. Consequently, in (4.21) we integrate along a contour closed at the left, and, applying the residue theorem, we obtain

$$\psi_n(s) = \sum \operatorname{res} [F_n(q) \exp qs] \quad (0 \leqslant s < \infty). \tag{4.22}$$

Since $\varphi_n(s)$ is identical with $\psi_n(s)$ in the interval $0 \leq s \leq \delta$, we can substitute into (4.22) the value of $F_n(q)$ from (4.19) and obtain

$$\varphi_n(s) = \sum \operatorname{res} \left[\frac{\sum_{m=1}^{k} N_{m0}(q - \varepsilon_{mn})^{-1}}{1 + \sum_{m=1}^{k} c_m (q - \varepsilon_{mn})^{-1}} \exp qs \right]. \tag{4.23}$$

In particular, for a cascade with no removal ($c_m = 0$; $m = 1, \ldots, k$), we have

$$\varphi_n(s) = \sum_{m=1}^{k} N_{m0} \exp \varepsilon_{mn} s,$$

which leads to the formula (4.5) for the distribution of concentrations in such a cascade.

Rewriting (4.23) in the form

$$\varphi_n(s) = \sum \text{res} \times \left[\frac{\sum_m N_{m0} \prod_{j \neq m} (q - \varepsilon_{jn})}{\prod_m (q - \varepsilon_{mn}) + \sum_m c_m \prod_{j \neq m} (q - \varepsilon_{jn})} \exp qs \right],$$

we find that the number of poles is k, since all the poles are determined by the zeros of the denominator. The latter are found from an algebraic equation of degree k:

$$1 + \sum_{m=1}^{k} \frac{c_m}{q - \varepsilon_{mn}} = 0. \tag{4.24}$$

Since the components are different, the roots of Eq. (4.24) are simple roots in the general case. If the mixture contains two components with very similar properties, for which $|\varepsilon_{mn}| \sim \varepsilon^{\beta}$, where $B > 1$, we may assume that this mixture consists of one component whose concentration is $N_m(s) + N_n(s)$. An analysis of the roots for the case $k = 2$ shows that they are always real. It can be shown that the roots of Eq. (4.24) are real for any number of components.

If we denote the roots of (4.24) by q_{nj}, we can write

$$\varphi_n(s) = -\sum_{j=1}^{k} \left\{ \sum_{m=1}^{k} \frac{N_{m0}}{q_{nj} - \varepsilon_{mn}} \times \left[\sum_{m=1}^{k} \frac{c_m}{(q_{nj} - \varepsilon_{mn})^2} \right]^{-1} \right\} \exp q_{nj} s. \tag{4.25}$$

Now we introduce the index of the section B, and write (4.25) in the form

$$\varphi_n(s) = \sum_{j=1}^{k} a_{nj}^{b} \exp q_{nj}^{b} s, \tag{4.26}$$

where a_{nj}^{b} denotes the quantity in curly brackets in (4.25). Multiplying (4.26) by exp ε_{nm}s and taking account of (4.15), we find that a_{nj}^{b} is independent of n and

$$q_{nj}^{b} = q_{mj}^{b} + \varepsilon_{mn}. \tag{4.27}$$

The last formula may also be obtained easily from Eq. (4.24). Thus,

$$\varphi_n^{b}(s) = \sum_{j=1}^{k} a_j^{b} \exp q_{nj}^{b} s. \tag{4.28}$$

Here

$$a_j^{b} = -\sum_{m=1}^{k} \frac{N_{m0}^{b}}{q_{mj}^{b}} \left[\sum_{m=1}^{k} \frac{c_m^{b}}{(q_{mj}^{b})^2} \right]^{-1}, \tag{4.29}$$

where N_{m0}^{b} is the concentration of component m at the beginning of section b. We substitute (4.28) into (4.12). Taking account of (4.6) and (4.18), after integrating, we obtain

$$N_m(s) = \frac{\left(N^b_{m0} + c^b_m \sum_{j=1}^{k} \frac{a^b_j}{q^b_{mj}}\right) - c^b_m \sum_{j=1}^{k} \frac{a^b_j}{q^b_{mj}} \exp q^b_{mj} s \quad \sum_{j=1} a^b_j \exp q^b_{mj} s}{k} \qquad (4.30)$$

Now let us consider Eq. (4.24). For a cascade with no removal this equation is homogeneous and has a zero root $q_{nn} = 0$. In the general case $c^b_n \neq 0$ for every root, since the cascade does not yield an infinite degree of separation. Consequently, Eq. (4.24), which is inhomogeneous in the general case, does not have any zero roots, and formula (4.28) is the sum of a finite number of exponential terms. Since a finite number of exponents do not form a complete system of functions, it follows from the integral Eq. (4.17), written in the form

$$\varphi^b_n(s) = \sum_{m=1}^{k} \left(N^b_{m0} - c^b_m \int_0^s dt \times \varphi^b_n(t) \exp \varepsilon_{nm} t\right) \exp \varepsilon_{nm} s,$$

that the value of the primitive function at the lower limit of integration s = 0 for all m = 1, . . . , k is equal to $-N^b_{m0}/c^b_m$. Carrying out the integration, we obtain

$$c^b_m \sum_{j=1}^{k} \frac{a^b_j}{q^b_{mj}} + N^b_{m0} = 0; \qquad (4.31)$$

$$N_m(s) = -c^b_m \sum_{j=1}^{k} \frac{a^b_j}{q^b_{mj}} \exp q^b_{mj} s \times \left(\sum_{j=1}^{k} a^b_j \exp q^b_{mj} s\right)^{-1}. \qquad (4.32)$$

Setting s = 0 in (4.32) and taking account of (4.31), we find

$$\sum_{j=1}^{k} a^b_j = 1. \qquad (4.33)$$

As can be seen from (4.29), $a^b_j = a_j(c^b_1, \ldots, c^b_k)$. It is readily shown that

$$\lim a^b_j = N^b_{j0}, \quad (c^b_1, \ldots, c^b_k) \to 0. \qquad (4.34)$$

5. Calculation of Rectangular Stepped Cascades

Let us carry out the calculation for a cascade with the given parameters ε_{mn}, L^b, P^b, F^b, σ^b, B, $\tilde{N}_m(\sigma^b)$. Consider the results shown in section 4. We assume that the quantities c^b_m are known. Using the algebraic Eq. (4.24) and the relations (4.27), we find all the roots q^b_{mn}. From the system of Eqs. (4.32) with $s = \sigma^b$, taking account of Eq. (4.33), we find the coefficient a^b_j. Then, using the relations (4.31), we find N^b_{m0} and, consequently, $c^{b=1}_m$. It is therefore desirable to use the following method for the calculation of the cascade.

Let the concentrations at one end of the cascade be specified in an arbitrary manner. By the method indicated, we find the concentrations at all the points of the cascade at which material is removed. Varying the concentrations at the end of the cascade, we can see to it that the system satisfies the conditions

$$\sum_{b=1}^{B} P^b N_m(\sigma^b) = \sum_{b=1}^{B} F^b \tilde{N}_m(\sigma^b), \qquad (5.1)$$

which correspond to the law of conservation of matter for the cascade as a whole. In the calculation of specific problems of isotope separation it has been found that the number of such intervals required for obtaining a result with satisfactory accuracy is proportional to k − 1. This becomes almost obvious if we write the system (4.3) in the form:

$$L^b(s)\frac{d\ln N_m(s)}{ds}=L^b(s)\sum_{n=1}^{k}\varepsilon_{mn}N_n(s)-\frac{g_m^b}{N_m(s)}+\sum_{n=1}^{k}g_n^b.$$

Furthermore, in practical calculations we must first of all use a correct numbering system for the roots of Eq. (4.24). Let us write

$$1+\sum_{m=1}^{k}\frac{c_{mt}}{q-\varepsilon_{mn}}=0, \tag{5.2}$$

where t varies from 0 to 1. When t = 0, we have $q_{nm}=\varepsilon_{mn}$. For small values of t ($c_{mt}\ll\varepsilon$; m = 1, . . ., k), by expanding into a MacLaurin's series, we find $q_{mn}\approx\varepsilon_{mn}-c_{mt}$ (there are no zero roots). From this it follows that as t increases, the signs of the roots do not change and the order in which the roots are arranged remains the same, since otherwise at least one of the elements of the q_{mn} matrix would have to pass through 0. Thus,

$$\frac{q_{ni}-q_{nj}}{\varepsilon_{ij}}>0. \tag{5.3}$$

Taking account of Eq. (4.27), we can write formulas (4.32), as

$$N_m(s)=-c_m^b\sum_j\frac{a_j^b}{q_{mj}^b}\exp q_{nj}^b s\times\left(\sum_j a_j^{\nu}\exp q_{nj}^b s\right)^{-1}. \tag{5.4}$$

We introduce

$$x_j^b(s)=a_j^b\exp q_{nj}^b s. \tag{5.5}$$

As a result, (5.4) becomes

$$N_m(s)=-c_m^b\sum_j\frac{x_j^b(s)}{q_{mj}^b}\left(\sum_j x_j^b(s)\right)^{-1}. \tag{5.6}$$

If we express all the values $x_j^b(\sigma^b)$ by one of them [the system (5.6) is homogeneous], by using (5.5) and (5.33), we obtain the coefficients a_j^b. The value of N_{m0}^b is determined from the formulas (4.31). After satisfying the conditions (5.1), we find $N_m(s)$ from (5.6).

In conclusion, it should be mentioned that this method was used on the Ural-1 electronic computer for calculating a cascade for the separation of oxygen isotopes by low-temperature distillation of nitric oxide.

The authors thank I. G. Gverdtsiteli and Yu. V. Nikolaev for their comments on the results of this work.

LITERATURE CITED

1. K. Clusius, Helv. chim. acta, 44, 1349 (1961).
2. K. Clusius and K. Schleich, Helv. chim. acta, 45, 1702 (1962).
3. K. Clusius and E. Varde, Helv. chim. acta, 45, 2273 (1962).
4. K. Clusius and E. Varde, Helv. chim. acta, 46, 2146 (1963).
5. E. Schumacher and K. Clusius, Helv. chim. acta, 36, 949 (1953).
6. A. de la Garza, G. Garrett, and I. Murphy, Chem. Eng. Sci., 15, 188 (1961).

A STUDY OF THE DOSE-RATE FIELD IN AN IRRADIATOR WITH γ-RAY SOURCE CONSISTING OF SPENT REACTOR FUEL ELEMENTS

(UDC 541.15)

V. E. Drozdov, I. M. Zakharova, and S. P. Dobrovol'skii

Translated from Atomnaya Énergiya, Vol. 19, No. 4,
pp. 367-371, October, 1965
Original article submitted November 17, 1964; revised March 12, 1965

Experiments were performed to determine the distribution of activity along a fuel element from the RFT reactor. It was shown that the distribution of activity is satisfactorily described by a cosine function, and that the formulas used to compute the dose rate field of an irradiator with uniformly distributed activity along the radiation source are inapplicable to radiators consisting of fuel elements (the disagreement was 23% for the RFT and 32% for the First Atomic Power Station). Better agreement was obtained between experimental data and values computed by our formulas.

An experimental and theoretical study was made of the dose rate field from a single fuel element and from a hollow, cylindrical irradiator made up of eighteen RFT fuel elements. Working formulas were obtained for computing the dose rate field from spent fuel elements. In computing the dose rate field inside a hollow, cylindrical irradiator made of fuel elements of finite diameter, it was shown that the activity can be considered to be distributed according to a cosine law over the surface of an infinitely thin cylinder with a radius equal to the arithmetic mean of the minimum and maximum radii of the irradiator.

In recent years, radiation equipment has been built in which the γ-radiation from spent reactor fuel elements was used [1, 2]. For physical computations involving radiochemical devices, it is necessary to know the dose rate field from an irradiator made of spent fuel elements.

It is well known that the activity of fuel elements is not distributed uniformly along their length [3, 4]; it falls monotonically from the center to the end of a fuel element. For example, the nonuniformity in activity distribution (in what follows, we will understand by nonuniformity the ratio of specific γ-activity at the center of a fuel element to the specific activity at its end, i.e., $\eta = m_c/m_k$) for fuel elements from the First Atomic Power Station is approximately four [3].

The first experiments on the measurement of dose rate fields in an irradiator made of spent fuel elements showed that the dose values computed by standard formulas for sources with uniformly distributed activity differed considerably from the experimental data.

Calculation and Experimental Determination of Activity Distribution Along a Fuel Element

The distribution of activity along a fuel element corresponds to the distribution of neutron flux along the height of a reactor (keeping in mind reactors with vertically arranged fuel elements). As is well known, this distribution is described rather well by a cosine function of the form

$$m(x) = m_0 \cos px, \tag{1}$$

where x is the running coordinate; $p = \frac{\pi}{2(L + \Delta L)}$; L is half the fuel element length; ΔL is the effective reflector extrapolation length from the core face. From normalization conditions, $m_0 = \frac{M_p}{2 \sin pL}$, where M is the total absolute activity of the fuel element.

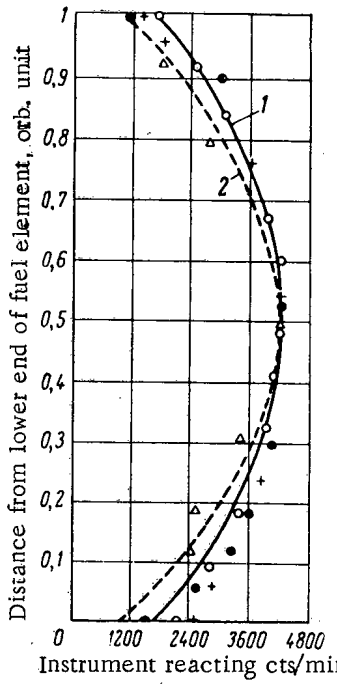

Fig. 1. Distribution of activity along RFT fuel elements: 1) calculation (2L = 102 cm); ○, ●, +) experimental data for three fuel elements. First Atomic Power Station: 2) calculation (2L = 175 cm); △) experimental data [3]. Maximum activities of the fuel elements superimposed.

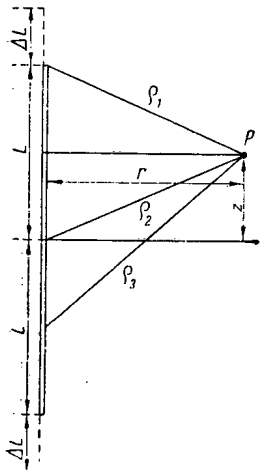

Fig. 2. Diagram for calculating the dose rate from a cosine-law, linear source.

The value of the effective reflector extrapolation length ΔL is determined by the point where the analytical continuation of the asymptotic solution (or simply, of the solution) goes to zero. For existing reactors, it is usually known sufficiently exactly (from experimental data or from reactor design calculations). Thus, the effective extrapolation length is 6-8 cm for uranium-water lattices with H_2O reflectors over a wide range of core configurations [5, 6]. For reactors of the X-10 type with natural uranium and graphite moderator, the value of the effective extrapolation length is the diffusion length in the graphite reflector, i.e., 50-60 cm [7].

A calculated curve for the activity distribution along a fuel element from the First Atomic Power Station, where the effective extrapolation length is 20 cm, is shown in Fig. 1 (curve 2). Experimental points taken from [3] are plotted on the same figure, and lie reasonably close to the computed curve. In cases where there is no reliable data on the value of ΔL for a given reactor, it is convenient to measure the distribution of γ-activity along a fuel element. We performed such measurements on fuel elements from the RFT reactor.

In the lower part of the shielding of a shipping container for the transportation of fuel elements, a hole 4 mm in diameter and 250 mm long was drilled assuring very good collimation of a γ-ray beam. An SBT-9 end-window counter connected to the measuring circuit of a standard TISS dosimetry instrument was aligned with the hole. By means of a hand winch, one of the spent fuel elements was lifted into the container from the storage vault, and the γ-radiation from individual sections of the fuel element was recorded by the instruments. A locking mechanism on the winch assured discrete displacements of the fuel element before the collimator in steps of 5 cm. In order to reduce the contribution of radiation scattered through the vault shielding to a minimum, the counter was shielded by lead.

During the measurements, the maximum counting rate for the most active fuel element reached ~7000 cts/min, which was within the limits of the normal technical capabilities of the circuit. The average error of relative measurements was ±5%.

The results of measurements made on three fuel elements are shown in Fig. 1. All the data are normalized to a single activity. Here again, for purposes of comparison, the theoretical distribution is drawn for the activity along a fuel element from the RFT reactor with the effective extrapolation length assumed to be 20 cm. It is clear from the figure that the experimental points are in rather good agreement with the theoretical curves (the error does not exceed 10%). The large deviations at the ends of the curves apparently result from different values of the extrapolation length at the upper and lower faces of the reflector. This depends both on structural features and on physical reasons, temperature effects in particular.

Despite the existing disagreement of theoretical curves and experimental points for the ends of the fuel elements, the ratio of the average activity along the length of the fuel element to the activity at the end differs inconsequentially; for the theoretical activity distribution along the fuel element it is 1.25 and for the experimental, 1.22.

Calculation of Dose Rate Field From a Single, Spent Fuel Element

We determine the dose rate from a fuel element in the form of a linear source with cosine-law distribution of activity along its length at an arbitrary point located a distance r from the fuel element and a distance z from its center (Fig. 2). From the figure, the dose rate at an arbitrary point is

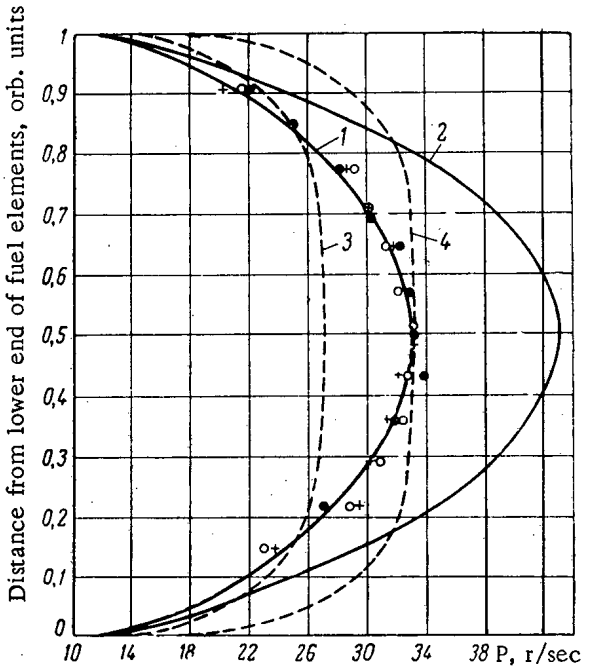

Fig. 3. Dose rate field from an RFT fuel element with an activity of 5000 g-equiv Ra and from a First Atomic Power Station fuel element with an activity of 6700 g-equiv Ra at r = 8 cm: 1, 2) calculated curves for the case of cosine activity distribution along the fuel element; 3,4) calculated curves for uniform distribution of activity along the fuel element; O, ●, +) experimental points for RFT fuel elements.

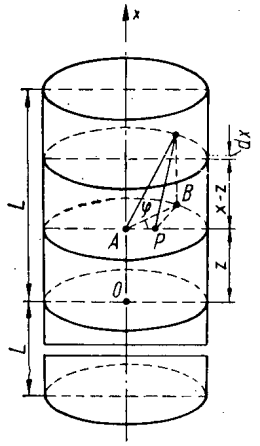

Fig. 4. Diagram for calculating the dose rate field inside a hollow, cylindrical irradiator with cosine distribution of activity in height.

$$P = K_\gamma m_0 \int_{-L}^{L} \frac{\cos px}{(z-x)^2 + r^2}\, dx. \tag{2}$$

The integral in (2) is not expressed in elementary functions, and therefore it is impossible to tabulate it.

However, this difficulty can be avoided if an activity distribution function along the fuel element is selected which is close to cos px. The function

$$f(px) = 1 - \frac{p^2x^2}{\gamma}. \tag{3}$$

is such a function.

The value of γ is selected on the basis of the conditions: f(px) = 1 when x = 0; f (px) = cos px when x = ± L. Furthermore, from equation (3), we find

$$\gamma = \frac{p^2L^2}{1-\cos pL}.$$

With such a choice for γ, Eq. (3) agrees exactly with the cosine distribution at x = 0 and x = ± L. At values L < x < 0 and 0 > x > L, the discrepancy is a few percent.

After substitution of the function f(px) for cos px in expression (2), integration, and elementary transformations, we obtain

$$P = K_\gamma m_0 \left[\left(\frac{1}{r} - \frac{p^2z^2}{\gamma r} + \frac{p^2 r}{\gamma} \right) \operatorname{arctg} \frac{L-z}{r} + \operatorname{arc\,tg} \frac{L+z}{r} - \frac{2p^2L}{\gamma} + \frac{p^2z}{\gamma} \ln \frac{(L+z)^2+r^2}{(L-z)^2+r^2} \right]. \tag{4}$$

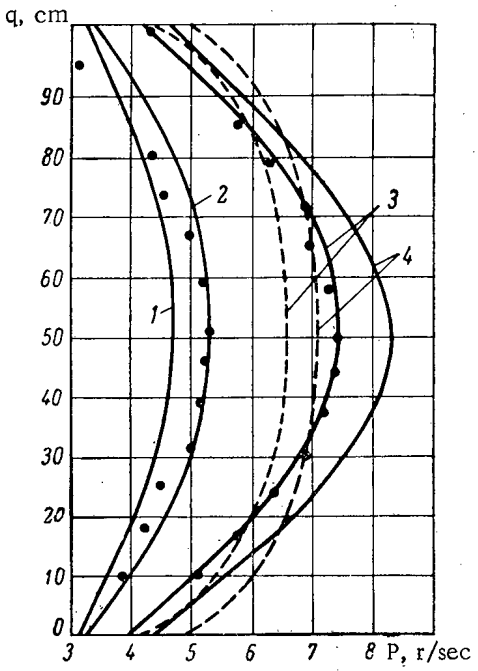

Fig. 5. Dose rate field for the internal region of a cylindrical irradiator with an activity of 6000 g-equiv Ra composed of 18 fuel elements at various distances b from the axis: 1) 0; 2) 13 cm; 3) 33 cm; 4) 41 cm; – – – – –) uniform distribution of activity along the fuel element; ●) experimental values.

This expression is considerably simplified at z = 0 (at the central cross section of the fuel element) and at z = L (at the end of the fuel element).

Using formula (4), dose rate fields were computed for a First Atomic Power Station fuel element and for an RFT fuel element. Because it is impossible to consider an RFT fuel element to be infinitely thin (its diameter is 66 mm), corrections taken from [8] for a nonabsorbing tube were introduced. The results of the dose rate field calculations for First Atomic Power Station and RFT fuel elements are given in Fig. 3. Also plotted in the figure are experimental points for three fuel elements obtained by the ferrosulfate method and reduced to the same activity of 5000 g-equiv Ra. These points are in good agreement with the calculated curve, which took into account the finite geometry [8]. The disagreement does not exceed 7%, which is consistent with the experimental error of ±3%. Also shown in Fig. 3 for purposes of comparison are dose rate values for an arbitrary fuel element with activity uniformly distributed along its length and with the same total activity (curves 3 and 4).

Calculation of Dose Rate Field for a Hollow, Cylindrical Irradiator Made of Spent Fuel Elements

In γ-ray equipment intended for the irradiation of objects, the irradiators most often are in the form of hollow cylinders consisting of several sources arranged along the cylinder walls.

It is impossible to use the computational formulas given in [8-10] for irradiators consisting of fuel elements having a cosine distribution of activity with irradiator height. The irradiator studied consisted of eighteen fuel elements from the RFT reactor. The diameter of the irradiator was 90 cm (between fuel element axes), and the height was 102 cm.

The absolute activity of each fuel element was determined by the method of chemical dosimetry with an accuracy of ± 3%.

The measurements of the irradiator dose rate field were also performed using chemical dosimetry techniques. The dosimetry stands were located in a steel radiochemical apparatus at various distances from the irradiator axis. During dosimetry, the vessel was rotated at 3 rpm; the fuel elements remained stationary. The apparatus consisted of two concentric cylinders: an outer one with a diameter of 690 mm and 5 mm wall thickness; an inner one with 210 mm diameter and 8 mm wall thickness. The height of the vessel was 120 cm.

To calculate the dose rate field, the origin of the coordinate system was chosen to be in the central transverse cross section of an irradiator having a height 2L (Fig. 4). The distribution of specific activity with irradiator height was found from the expression

$$\sigma(x) = \sigma_0 \cos px, \tag{5}$$

where

$$\sigma_0 = \frac{M_0 D}{4\pi R \sin pL};$$

M is the total activity of the irradiator in g-equiv Ra. The activity was considered to be distributed over the surface of an infinitely thin cylinder of radius R and height 2L.

Replacing cos px by its approximate value, as in the case of a single fuel element, we obtain an expression for the dose rate at an arbitrary point inside the hollow cylinder at a distance z from the central plane and at a distance r from the axis

$$P = K_\gamma \sigma_0 R \int_{-L}^{+L} \int_0^\pi \times \frac{\left(1 - \frac{p^2 x^2}{\gamma}\right) dx\, d\varphi}{R^2 + b^2 - 2Rb\cos\varphi + (z-x)^2}. \tag{6}$$

After integration and some algebraic transformations, we obtain:

$$\begin{aligned} P = 2\pi K_\gamma \sigma_0 R \Bigg\{ & \left(\frac{1}{b+R} - \frac{p^2 z^2}{\gamma(b+r)}\right)\Big(F(\varphi, k) - F(\varphi', k)\Big) \\ & + \frac{p^2 z}{\gamma} \ln \frac{(z+L)^2 + (R^2+b^2) + \sqrt{(z+L)^4 + 2(R^2+b^2)(z+L)^2 + (R^2-b^2)^2}}{(z-L)^2 + (R^2+b^2) + \sqrt{(z-L)^4 + 2(R^2+b^2)(z-L)^2 + (R^2-b^2)^2}} \\ & + \frac{p^2 (R-b)^2}{\gamma(R+b)(1-k^2)} \left[\operatorname{tg}\varphi' \sqrt{1 - k^2 \sin^2\varphi'} - \operatorname{tg}\varphi \sqrt{1 - k^2 \sin^2\varphi}\right] + E(\varphi, k) - E(\varphi', k) \Bigg\}, \end{aligned} \tag{7}$$

where $F(\varphi, k)$, $E(\varphi, k)$ are elliptic integrals of the first and second kind, respectively;

$$\varphi = \operatorname{arctg} \frac{z+L}{R-b}; \quad \varphi' = \operatorname{arctg} \frac{z-L}{R-b}.$$

Expression (7) is considerably simplified when z = 0 and z = L.

Calculated results and experimental data for the dose rate from a cylinderical irradiator are presented in Figs. 5 and 6 (q is the distance from the bottom of the irradiator).

It should be noted that the distribution of the dose rate field from fuel elements varies little with time (see Fig. 6) because the self-absorption coefficient, which depends on the γ-ray spectrum, remains practically constant at large values of storage time.

The computed curves, including corrections for each value of b, were in agreement with the experimental points. Corrections were made to the calculated curves for the finite geometry of the irradiator, for absorption of γ-radiation in the walls of the outer cylinder, and for shielding of part of the fuel elements by the inner cylinder of the apparatus. It is clear from Fig. 5 that the experimental points for b = 33 cm fall nicely along the calculated curve. In this case, the correction for finite geometry amounts to 8%. The calculated and experimental data for b = 13 cm are in good agreement at the center, but there is a discrepancy of 8-16% at the top of the irradiator. This disagreement can be explained by the fact that γ-ray absorption in the walls of the inner cylinder is more effective at b = 13 cm and by the presence of several absorbing structural features in the upper portion. At b = 41 cm, which corresponds to the maximum diameter of the irradiator, the correction for finite geometry is ~16% according to the data in [8]. In [9], the correction for finite geometry at the axis of the irradiator, where b = 0, is <1%.

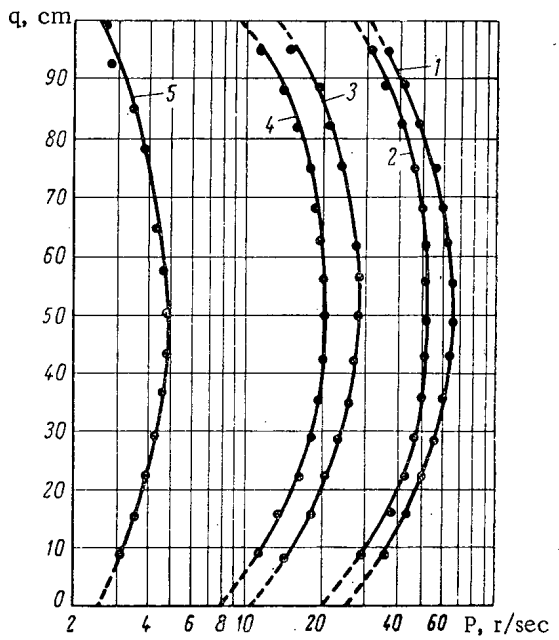

Fig. 6. Experimental values of the dose rate from a cylindrical irradiator consisting of 18 RFT fuel elements for various values of the storage time t_s, days: 1) 159; 2) 169; 3) 257; 4) 283; 5) 512.

Values of the dose rate field are also given in Fig. 5 for an arbitrary irradiator in which the activity is uniformly distributed over the surface. Values of the dose rate at the central cross section of the actual irradiator in comparison with the arbitrary irradiator are 17% less at b = 41 cm and 12% less at b = 33 cm.

For practical calculations of the dose rate field of an irradiator made of fuel elements 66 mm in diameter, the irradiator can be considered to be infinitely thin [9].

For more accurate calculations, it is necessary to introduce a correction for the finite geometry of the irradiator [8-10].

The authors take this opportunity to express their gratitute to Yu. S. Ryabukhin for assistance and valuable suggestions, to A. G. Vasil'ev and V. P. Trusova for carrying out the dosimetry, and to M. E. Eroshov for help in performing the experiments.

LITERATURE CITED

1. V. I. Sinitsyn, Radiation Equipment and its Use, A Review of Foreign Technology [in Russian], Moscow TsITEI (1961).
2. V. L. Karpov et al., Atomnaya Énergiya, 8, No. 5, 446 (1960).
3. A. P. Smirnov-Averin, et al., Atomnaya Énergiya, 8, No. 5, 446 (1960).
4. V. V. Gonsharov, et al., in Transactions of the Second International Conference on the Peaceful Use of Atomic Energy [in Russian], Dokl. sovetskikh uchenykh, Vol. 2, Moscow, Atomizdat (1959), p. 243.
5. Nuclear Reactors, USAEC Reports [in Russian], Vol. 1, Moscow, Izd-vo inostr. lit. (1956).
6. G. I. Marchuk, Ed., Reactor Critical Masses [in Russian], Moscow, Gosatomozdat (1961).
7. N. Kaplan and J. Chernick, in Proceedings of the International Conference on the Peaceful Use of Atomic Energy (Geneva, 1955).
8. B. Price, et al., Radiation Shielding [Translated from the English],Moscow, Izd-vo inostr. lit. (1959).
9. A. Kh. Breger et al., Problemy fizicheskoi khimii, No. 2, Mowcow, Goskhimizdat (1959), p. 132.
10. N. G. Gusev et al., Shielding Against Radiation from Extended Sources [in Russian], Moscow, Atomizdat (1961).

All abbreviations of periodicals in the above bibliography are letter-by-letter transliterations of the abbreviations as given in the original Russian journal. *Some or all of this periodical literature may well be available in English translation.* A complete list of the cover-to-cover English translations appears at the back of this issue.

EFFECT OF TEMPERATURE AND NEUTRON IRRADIATION ON THE PLASTIC DEFORMATION OF α-URANIUM SINGLE CRYSTALS

(UDC 621.039.553)

F. P. Butra, Z. F. Evkina, O. L. Fufaeva, I. A. Korobeinikov, and L. M. Lebedev

Translated from Atomnaya Énergiya, Vol. 19, No. 4, pp. 372-380, October, 1965
Original article submitted February 22, 1965

The plastic deformation of α-uranium single crystals was studied for various crystallographic orientations and temperatures. Explanations are given for the form of the strain curves in terms of the principal systems of plastic deformation. The single crystals were irradiated by neutrons in a reactor at temperatures up to 100°C with integral fluxes up to $5.5 \cdot 10^{17}$ neutrons/cm^2 and a flux of $4 \cdot 10^{20}$ neutrons/cm^2. The irradiation increased the critical shearing stress by factors of 3 to 5 for slip in the (010) plane and reduced the relative elongation and the region of "easy slip." On annealing single crystals irradiated by fluxes up to $5.5 \cdot 10^{17}$ neutrons/cm^2 the mechanical characteristics were restored.

Compressive and tensile tests carried out on single crystals and coarse-grained samples have shown that, depending on the crystallographic direction of the external force, α-uranium undergoes deformation by way of slip, twinning, or the formation of strain or fault bands [1-6]. In compressive tests at −196°C the authors of [4] found a considerable increase in the resistance to slip in the (010) plane. Tensile tests in [7] carried out on imperfect single crystals at −196°C showed the same systems of plastic deformation as at room temperature, except for the strain bands. The elongation at the point of rupture never exceeded 2% in these experiments. Strain and compression diagrams were not given in [1-7].

Neutron irradiation of polycrystalline α-uranium increases the electrical resistance [8, 9]. Irradiation by fluxes approaching 10^{20} neutrons/cm^2 leads to complete loss of ductility (elongation falls to zero [10]).

The effect of neutron irradiation on the radiation growth of α-uranium single crystals was considered earlier [11], whereas hitherto there has been no information on the plastic deformation of irradiation α-uranium single crystals.

In this paper we present strain diagrams and data on the plastic deformation of nonirradiated α-uranium single crystals tensile-tested at temperatures from 20 to −196°C. Irradiated single crystals and single crystals annealed after irradiation were deformed at room temperature.

EXPERIMENTAL METHOD

Single crystals were prepared from uranium purified electrolytically to 99.99%. The ingots were rolled in a copper sheath at 600°C to form plates 0.6 to 0.8 mm thick; these were brought to 0.5 to 0.4 mm in the cold state. Samples for tensile tests were prepared from 100 × 5 × (0.4-0.5) mm plates by stamping. The working length was 9 mm and breadth 1.5 mm. In these samples the single crystals were grown by the β → α phase-recrystallization method [6].

The single crystals were subjected to tensile tests on a laboratory apparatus giving a strain rate of 3 mm/h and also on an MM-150V machine. For straining the samples at low temperatures a system in the form of a metal tank separated into two sections by a partition was used. One section (containing the sample) was filled with ethyl alcohol for test temperatures down to −110°C, with isopentane from −130 to −160°C, and with liquid nitrogen at −196°C. Liquid nitrogen was poured into the other section. The alcohol and isopentane were cooled through the partition and

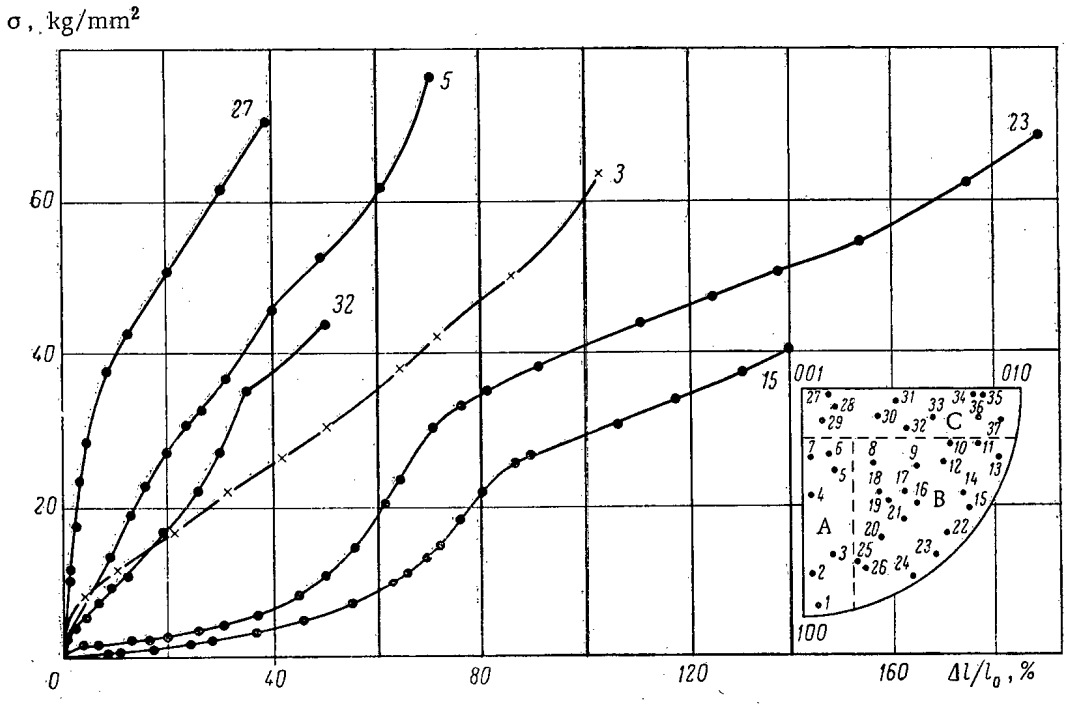

Fig. 1. Orientation dependence of stress-strain curves and orientation of strain axes for single crystals deformed at room temperature.

by copper plates passing from one section into the other. The required sample temperature was set up by duly proportioning the liquid nitrogen in the second section. The temperature was measured by a thermocouple sealed to the upper head of the sample at a point which remained in the cooling liquid during the whole experiment.

The single crystals obtained by the $\beta \rightarrow \alpha$ transformation were irradiated in a reactor in hermetically-sealed aluminum capsules at temperatures not exceeding 100°C. The samples irradiated by fluxes up to $1.6 \cdot 10^{16}$ neutrons/cm^2 were strained with local lead shielding on a laboratory apparatus. The single crystals irradiated with fluxes of $2.5 \cdot 10^{16}$ neutrons/cm^2 and upward were tested on an MM-150V machine with remote control and automatic photorecording of the strain diagram. Unfortunately this machine would not give an elongation exceeding 70%.

The plastic-deformation systems were determined from microphotographs and back-reflection Laue photographs. The stress-strain curves were constructed point by point with the true stress along the axis of ordinates.

RESULTS OF EXPERIMENTS

1. Nonirradiated Single Crystals

Deformations at room temperature. Figure 1 shows the orientation of the strain axes for all the single crystals, together with typical strain curves in stress-strain coordinates.

It was established in [12] that single crystals belonging to region A (see Fig. 1) begin deforming by twinning $\{130\} - (\bar{3}10)$ with subsequent slip (010) – [100] in the twinned parts. As the angle between the [100] and the strain axis increases, slip in the (010) plane becomes more and more difficult in the twinned parts owing to the unfavorable orientation (curves 3, 5).

Single crystals corresponding to region B undergo substantial elongation under the influence of small stresses; the strain curves show considerable sections with little hardening (curves 15, 23). With the onset of intense $\{130\}$ twinning the material hardens sharply and there is a rapid rise in the strain curves.

In single crystals of region C plastic deformation begins at large stresses by twinning in several planes [for example, (172), (176), (112)] with the formation of strain and fault bands. If in the formation of strain or fault bands parts of the crystal rotate into a position favorable for slip along the (010) plane, strain extends to considerable elongations. Sharp boundaries cannot be drawn between regions A, B, and C.

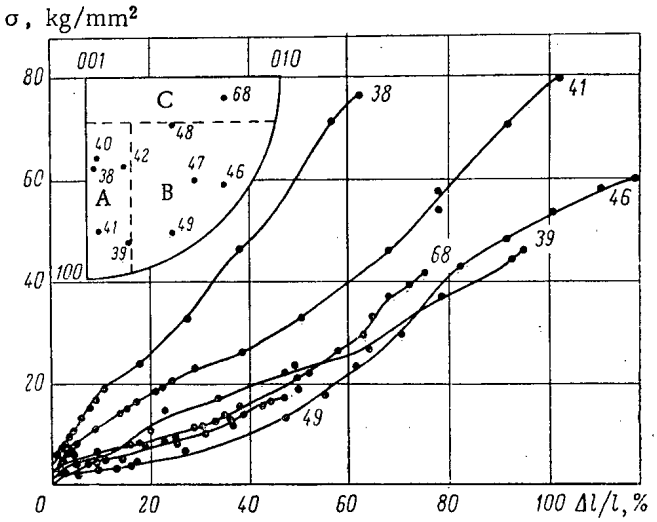

Fig. 2. Orientation dependence of the stress-strain curves and orientation of the strain axes for single crystals deformed at temperatures from −80 to −105°C.

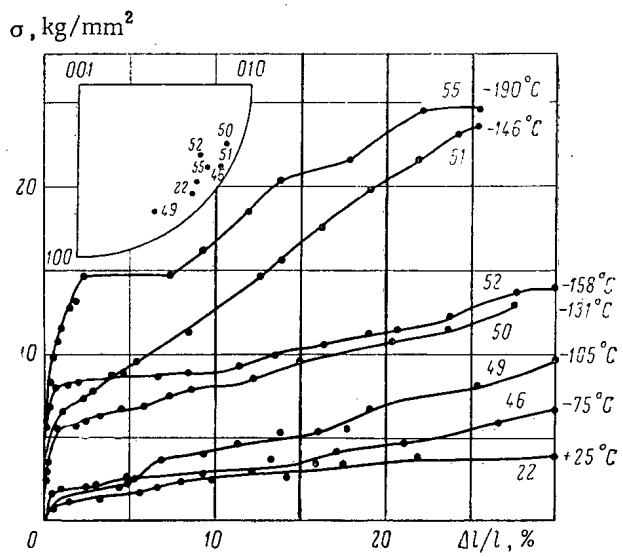

Fig. 3. Effect of temperature on the stress-strain curves of single crystals with neighboring strain-axis.

In single crystals which begin their plastic deformation by way of slip in the system (010) − [100], there is a certain critical shearing stress S for this system:

$$S = \sigma_0 \sin \chi_0 \cdot \cos \lambda_0,$$

where σ_0 is the yield stress, $\sin \chi_0 \cdot \cos \gamma_0$ is an orientation factor or connecting the direction of the strain axis with the slip plane and the direction of slip in this [13]. The quantity S depends on the perfection of the structure; in single crystals obtained by recrystallization in the α-phase it equals 0.280 ± 0.03 kg/mm², while in the single crystals obtained by the $\beta \rightarrow \alpha$ transformation, with block disorientation up to 2 or 3°, S reaches 0.5 to 1.0 kg/mm².

Deformation at low temperatures. Reducing the temperature to −100° does not introduce any substantial changes into the form of the strain curves (Fig. 2). Metallographic and x-ray data show that the systems of deformation at these temperatures are the same as at room temperature. On further reducing the temperature, the resistance to slip (010) − [100] rises sharply, and this is responsible for the behavior of the strain curves in Fig. 3 and 4. At −196°C the elongation of the single crystals depends sharply on the crystallographic orientation of the strain axes (see Fig. 4); in regions A and B the elongation reaches 25 to 35%, but in region C never more than 2%. At this temperature the resistance to twinning rises slightly in agreement with the results of [4]. The single crystals sharply distinguished by elongation also differ in respect of their rupture surfaces (Fig. 5). Single crystals of region C fail by rupturing in a plane close to the plane of active twinning (172), as noted in [7]. The rupture surfaces of single crystals with substantial elongations have a stepped-lamellar structure (see Fig. 5a) and hence cannot be given any definite indices. Large elongations at −196°C are only found for those single crystals which undergo deformation by means of a combination of two systems: slip (010) − [100] and twinning $\{130\} - (\overline{310})$. In this case the local overstresses arising on twinning relax as a result of slip in the (010) plane, and the short and dense (130) twins obstruct the development of cracks in the slip plane [14]. In the sample in which deformation begins with twinning (172), it would require a stress exceeding the ultimate tensile strength of the single crystal to effect slip in the (010) plane.

The result of tensile tests at various temperatures on single crystals which deform initially by slip in the (010) plane enable us to draw a graph relating the average critical shearing stress to temperature for the (010) − [100] slip system (Fig. 6).

2. Irradiated Single Crystals

x-Ray diffraction and metallographic examination showed that irradiation by fluxes up to $1.6 \cdot 10^{16}$ neutrons/cm² made no difference to the systems of plastic deformation. In irradiated single crystals, however, the onset of strain took place less homogeneously than that in samples. The lines on the sample surface appearing as a result of the emergence of slip bands became rarer and coarser.

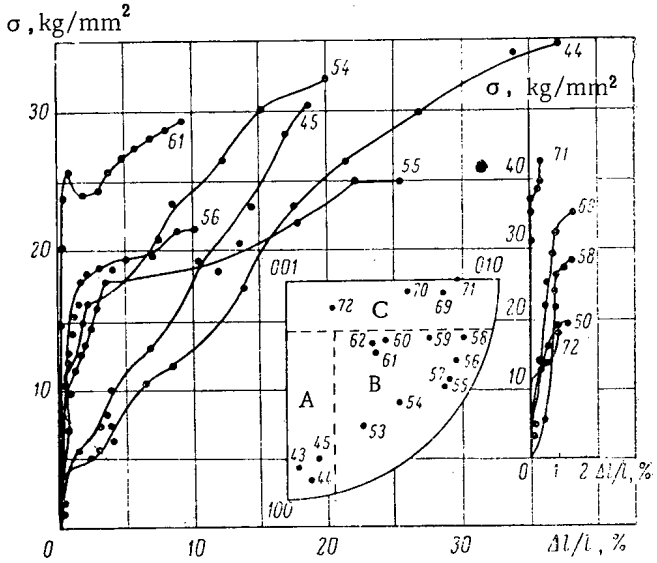

Fig. 4. Orientation dependence of stress-strain curves and orientation of strain axes of single crystals deformed at −196°C.

Fig. 5. Microphotographs of the rupture surfaces of single crystals deformed at −196°C (×70): a) sample 54; b) sample 69.

In the irradiated single crystals the deformation of which started with slip in the (010) − [100] system, the yield stress rose rapidly for small fluxes and tended to saturation at fluxes close to 10^{17} neutrons/cm^2. Figure 7 shows the initial parts of the stress-strain curves for single crystals greatly elongated by slip as a result of favorable orientation of the strain axes for deformation in the (010) − [100] system. On the strain curves of the irradiated single crystals there are also sections corresponding to easy slip, although these are smaller than on the strain curves of the nonirradiated crystals. On the machine-recorded strain curves of the irradiated single crystals there are clear "yield teeth"; on the strain curves of nonirradiated single crystals these are either absent or very weak (Fig. 8). The form of the machine-recorded strain curves for nonirradiated single crystals and for single crystals irradiated with fluxes of $2.6 \cdot 10^{16}$ to $5.5 \cdot 10^{17}$ neutrons/cm^2 indicates that the same strain systems act for this degree of irradiation.

For the principal slip system (010) − [100] the critical shearing stress S was determined as a function of neutron flux (Fig. 9). For fluxes up to $2.5 \cdot 10^{16}$ neutrons/cm^2, S rises rapidly and approaches saturation for fluxes of approximately 10^{17} neutrons/cm^2. For copper, saturation is reached at a flux of around $2 \cdot 10^{18}$ neutrons/cm^2 [15].

The change in the critical shearing stress in single crystals with increasing neutron flux is similar to the change in the electrical resistance of irradiated single crystals of α-uranium [8, 9]. Hence the saturation S may also be explained by the passage of the whole material through a thermal-peak state, when dynamic equilibrium sets in at the irradiation temperature between generated and annihilated radiation defects.

The curve of Fig. 9 is approximately described by the expression

$$S = S_0 + A\,(1 - e^{-vN}),$$

where S_0 is the critical shearing stress for the nonirradiated crystal, A is the maximum increment in critical shearing stress under irradiation, v is the volume of the thermal peak, and N is the number of fissions per unit volume, proportional to the value of the neutron flux. It is shown in [8] that the volume of the thermal peak in an alloy of uranium with 9% molybdenum, determined from diffusion data, equals $2.38 \cdot 10^{-17}$ cm^3, but according to the data on annealing in the homogeneous phase the thermal-peak volume is $6.28 \cdot 10^{17}$ cm^3. Measurements of the electrical resistance of irradiated natural uranium [9] showed that the volume of the thermal peak was $2 \cdot 10^{-16}$ cm^3. According to our own data, the value of this quantity determined from the change in the critical shearing stress is $5.6 \cdot 10^{-16}$ cm^3.

For single crystals in which the initial deformation takes place by slip in the (010) plane, the elongation after irradiation with a flux of $4 \cdot 10^{20}$ neutrons/cm^2 reached 40% (Fig. 10). It should be noted that the samples were strained nonuniformly along their length, so that the true relative elongation was still greater. Other single crystals irradiated under the same conditions were subjected to bending tests; they withstood fifteen 90° to-and-fro bendings before failure. Thus single crystals of α-uranium, irradiated by large neutrons fluxes still have greater ductility.

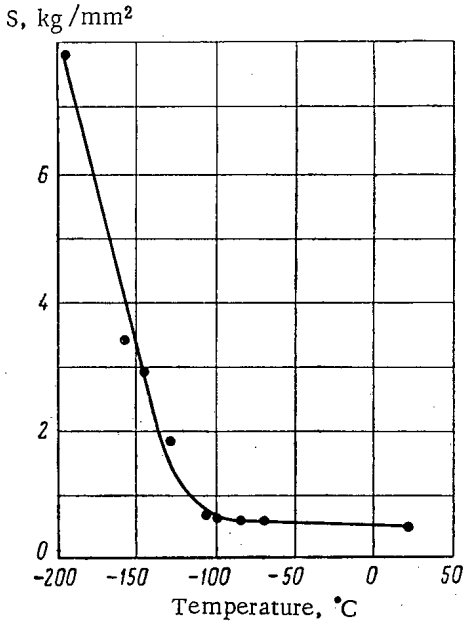

Fig. 6. Critical shearing stress as a function of temperature for slip system (010) – [100].

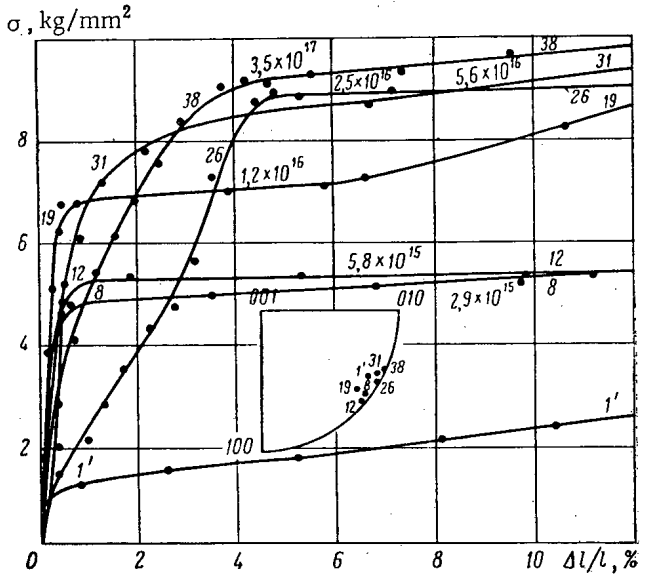

Fig. 7. Initials sections of stress-strain curves for single crystals irradiated with different fluxes (neutrons/cm²) (1' is a nonirradiated single crystal).

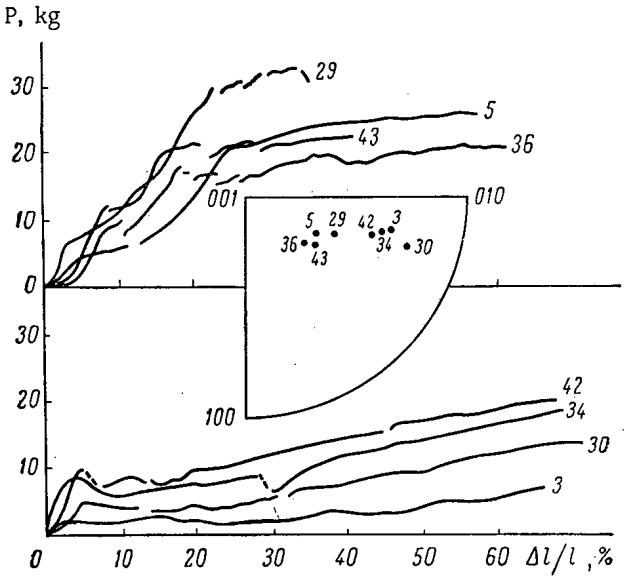

Fig. 8. Strain curves of two groups of single crystals irradiated with different fluxes (in neutrons/cm²):.29 and 30: $2.5 \cdot 10^{16}$; 34 and 36: $5 \cdot 10^{16}$; 42 and 43: $3.5 \cdot 10^{17}$; 3 and 5: nonirradiated single crystals.

Effect of annealing after irradiation. In order to elucidate the stability of the lattice damage caused by irradiation and its effects on the mechanical properties of the single crystals, experiments on the annealing of irradiated samples were made at various temperatures.

Single crystals irradiated at 60°C by fluxes of $1.6 \cdot 10^{16}$ and $5.5 \cdot 10^{17}$ neutrons/cm² were annealed for 2 h at 200, 300, and 450°C. All the single crystals had similar orientations of the strain axes, corresponding to the onset of deformation by slip in the (010) plane. The results appear in Figs. 11 and 12 and in the table.

After irradiation the ductility of the single crystals (large elongation to failure) remained, but the yield stress rose on account of the increased critical shearing S in the (010) plane. Annealing at 200°C has little effect on the form of the strain curves, although S changes considerably, especially for samples irradiated with a flux of $5.5 \cdot 10^{17}$ neutrons/cm² (Fig. 13). Annealing at 450°C after irradiation with a flux of $1.6 \cdot 10^{16}$ neutrons/cm² brings the single crystals to a state close to the original (i.e., before irradiation). Figure 11 shows the strain curve of a nonirradiated crystal for comparison. The radiation damage of single crystals irradiated by a flux of $5.5 \cdot 10^{17}$ neutrons/cm² is greater, so that in these the relation between S and annealing temperature (see Fig. 13) is sharper, and it would appear that for these samples a 2-h anneal at 450°C is insufficient for complete softening.

For small degrees of deformation, the polished surfaces of the single crystals show clear lines due to slip bands. In nonirradiated crystals these are fine and uniformly distributed over the surface. After irradiation the slip bands become coarse and the intervals between them differ considerably (Fig. 14). Annealing at 200°C has little effect on the thickness and distribution of the slip bands on the sample surface. Annealing at 450°C leads to a sharp

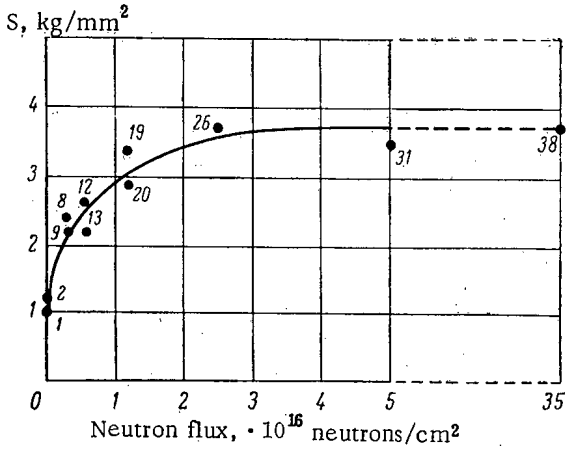

Fig. 9. Critical shearing stress as a function of neutrons flux for the slip system (010)—[100].

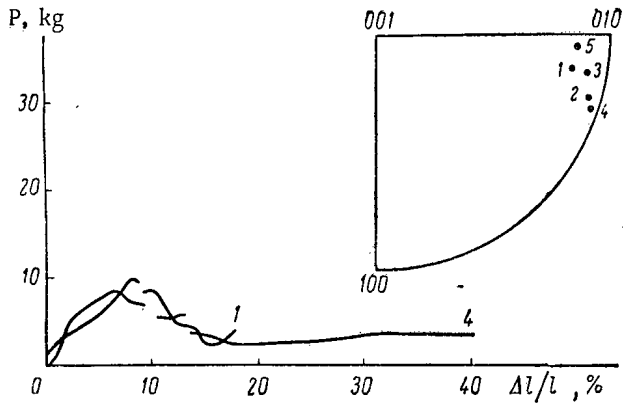

Fig. 10. Strain curves and orientation of the strain axes for single crystals irradiated with $4 \cdot 10^{20}$ neutrons/cm².

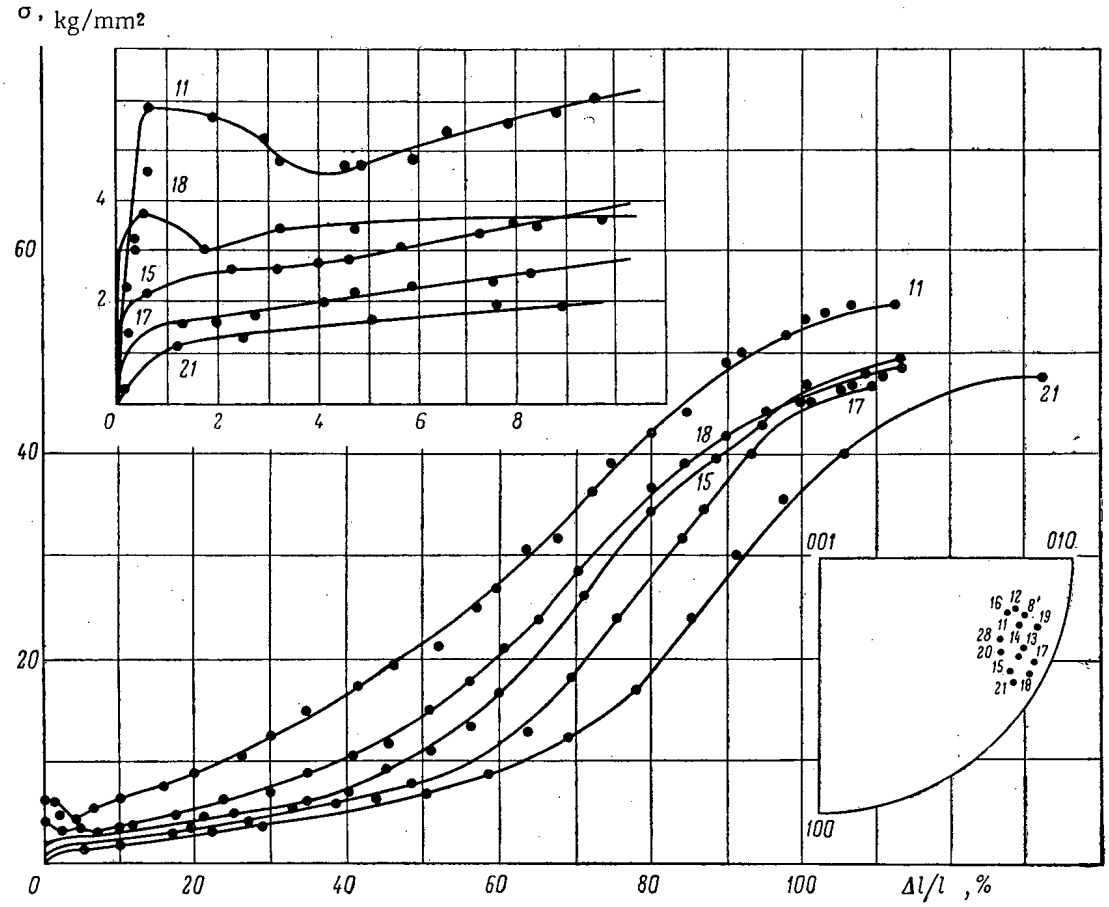

Fig. 11. Orientation of strain axes and stress-strain curves of single crystals irradiated by a flux of $1.6 \cdot 10^{16}$ neutrons/cm² and annealed for 2 h at various temperatures, °C: 18 : 200; 15 : 300; 17 : 450; 11 : without annealing; 21 : nonirradiated single crystal.

change: The thickness of the lines associated with the slip bands and their distribution over the surface become the same as in the nonirradiated single crystal. Thus two-hour annealing α-uranium single crystals at 450°C after irradiation with a flux of $1.6 \cdot 10^{16}$ neutrons/cm² eliminates the radiation defects in the crystal lattice which impede plastic deformation by slip.

Yield Stress and Relative Elongation of Single Crystals, Both Nonirradiated and Irradiated with Subsequent Annealing; Deformation by Extension at Room Temperature

Flux, neutrons/cm	Annealing temp., °C	No. of sample	Yield stress, kg/mm²	Rel. elongation, %	Flux neutrons/cm²	Annealing temp., °C	No. of sample	Yield stress, kg/mm²	Rel. elongation, %
—	—	21	1,2	188	$1,6\cdot10^{16}$	300	15	2,5	113
—	—	8′	1,65	106	$1,6\cdot10^{16}$	300	19	3,6	132
—	—	54′	4,1	>71	$1,6\cdot10^{16}$	300	28	3,0	114
$1,6\cdot10^{16}$	—	11	5,8	113	$5,5\cdot10^{17}$	300	3	13,5	>71
$1,6\cdot10^{16}$	—	14	5,0	113	$5,5\cdot10^{17}$	300	5	9,2	>71
$5,5\cdot10^{17}$	—	7	21,3	>71	$5,5\cdot10^{17}$	300	9	11,2	>71
$5,5\cdot10^{17}$	—	8	22,1	>71	$1,6\cdot10^{16}$	450	13	1,2	109
$1,6\cdot10^{16}$	200	18	3,7	106	$1,6\cdot10^{16}$	450	16	2,2	120
$1,6\cdot10^{16}$	200	20	4,2	120	$1,6\cdot10^{16}$	450	17	1,4	110
$1,6\cdot10^{16}$	200	22	6,6	118	$5,5\cdot10^{17}$	450	1	6,2	>71
$5,5\cdot10^{17}$	200	4	11,6	>71	$5,5\cdot10^{17}$	450	2	4,8	>71
$5,5\cdot10^{17}$	200	6	15,9	>71	—	—	—	—	—
$5,5\cdot10^{17}$	200	10	13,2	>71	—	—	—	—	—

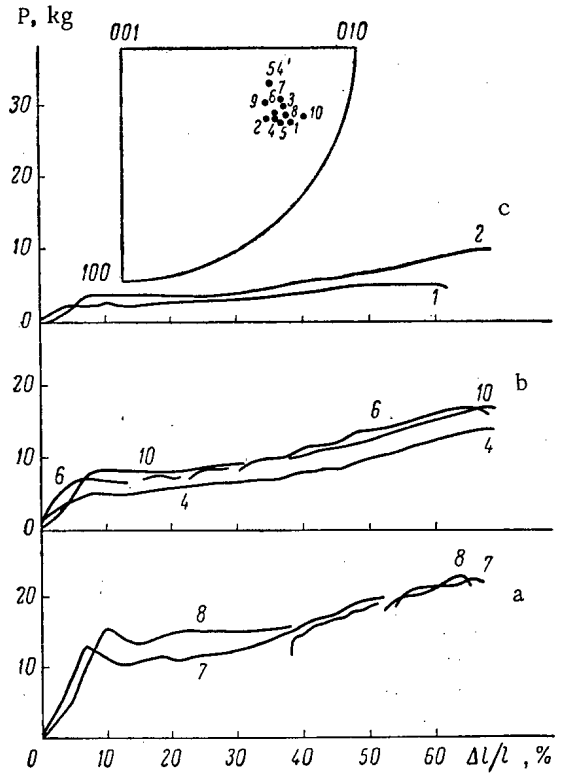

Fig. 12. Orientation of strain axes and strain curves of single crystals annealed for 2 h after irradiation with a flux of $5.5 \cdot 10^{17}$ neutrons/cm²: a) without annealing; b) annealing at 200°C; c) annealing at 450°C.

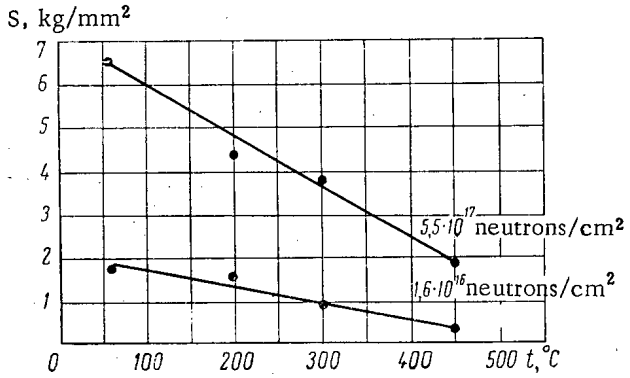

Fig. 13. Effect of the annealing temperature of the irradiated single crystals on the critical shearing stress of the (010) − [100] system.

DISCUSSION OF RESULTS AND SUMMARY

The study of strain in single crystals of α-uranium from +20 to −196°C has shown that the plastic deformation of both perfect single crystals obtained by recrystallization in the α-region and imperfect ones obtained by the β→α transformation takes place by way of the same slip and twinning systems. The perfection of the structure, however, affects such mechanical characteristics as the critical shearing stress for slip. In samples with block disorientations of 2 to 3° the value of S for the (010) − [100] system at room temperature equals 0.6 ± kg/mm².

Our experiments have shown that for appropriate orientation of the strain axes the single crystals undergo slip deformation in the (010) − [100] system with little hardening up to comparatively large elongations (40%). This kind of deformation is called easy slip. Slip in the (010) plane also occurs at −196°C (see Fig. 3 and 4); however, the 10 to 12-times increase in the critical shearing stress for certain orientations of the strain axes impedes the relaxation of local overstresses on twinning, and this leads to rupture of the samples for slight elongations.

Fig. 14. Microphotographs of the surface of single crystals after slight deformations (× 120): a) nonirradiated single crystals; b) single crystal irradiated with a flux of $1.6 \cdot 10^{16}$ neutrons/cm^2; c) single crystal annealed at 450°C for 2 h after irradiation.

Slip is the simplest form of plastic deformation, and the most sensitive to disruption of the crystal lattice. Hence the effect of neutron irradiation on plastic deformation appears most markedly in single crystals whose strain axis orientation corresponds to the onset of deformation by slip in the system (010) – [100]. The rise in the yield stress and the appearance of "yield teeth" in such samples characterizes radiation hardening.

It is suggested in [16, 17] that, as a result of fast-neutron irradiation, "impoverished zones" with high vacancy concentrations are formed in metals. The radiation hardening is explained by a dispersed distribution of the impoverished zones and their interaction with dislocations. Electron-microscope study of uranium irradiated by a flux of thermal neutrons (10^{17} neutrons/cm^2) [18] showed damage in the form of a series of fine spots having definite crystallographic orientations and also in the form of dislocation loops.

We are not quite sure of the nature of the radiation defects in the irradiated α-uranium single crystals, but it may well be that radiation damage to the lattice after irradiation by fluxes up to $5.5 \cdot 10^{17}$ neutrons/cm^2 fixes the dislocation sources and thus impedes deformation by way of slip. At first, when the radiation dose is still small, damage to the lattice increases rapidly, but as the total flux rises the part played by radiation annealing becomes more important, until dynamic equilibrium sets in between the defects being formed and those being annihilated; this leads to saturation of the critical shearing stress associated with slip. After irradiation by large fluxes ($4 \cdot 10^{20}$ neutrons/cm^2, burnup 0.16%) the single crystals still have considerable ductility, the elongation reaching 40% for slip in the (010) plane.

Radiation defects are sensitive to annealing. Annealing single crystals irradiated by fluxes up to $5.5 \cdot 10^{17}$ neutrons/cm^2 leads to a softening process. After two-hour annealing at 200°C the critical shearing stress of the (010) – [100] system changes little, but after annealing at 450°C it falls and approaches the value for nonirradiated samples. At 450°C the mobility of the atoms is quite considerable, and this leads to the resorption of the complexes of radiation defects restraining the multiplication and motion of dislocations.

LITERATURE CITED

1. R. Cahn, Acta metallurgica, 1. 49 (1953).
2. L. Lloyd and H. Chiswik, Trans. AIME, 203, 1209 (1955).
3. P. Lacombe, D. Calais, and N. Simenel, J. Nucl. Materials, 4, 325 (1959).
4. R. Teeg and R. Ogilve, J. Nucl. Materials, 3, 81 (1961).
5. L. Lloyd et al., J. Nucl. Materials, 4, 231 (1961).
6. P. Lacombe and D. Calais, In the book, "Transactions of the Second International Conference for the Peaceful Uses of Atomic Energy," Collection of papers by foreign scientists [Russian translation], Vol. 6, Moscow, Atomizdat (1959), p. 126.
7. A. Lemogne and P. Lacombe, J. Nucl. Materials, 2, 203 (1959).
8. S. T. Konobeevskii et al., "Atomnaya Énergiya," 4, 34 (1958).
9. G. Quere and F. Nakache, J. Nucl. Materials, 2, 203 (1959).
10. S. Billington and J. Crawford, Radiation Damage Solids, New York (1961).
11. In the Book "Transactions of the International Conference on the Peaceful Uses of Atomic Energy, Geneva (1955), Metallurgy of Nuclear Energy and Effect of Irradiation on Materials " [in Russian], Moscow, Metallurgizdat (1956), p. 642.
12. F. P. Butra, E. F. Evkina, and O. P. Fufaeva, "Fizika metallov i metallovedenie," 15, 873 (1963).
13. E. Shmidt and V. Boas, Ductility of Crystals (Especially Metals) [in Russian], Moscow, GONTI (1938).
15. V. I. Rozhanskii, "Dokl. AN SSSR," 123, 648 (1958).
16. A. Seeger, Radiation Damage Solids, Vol. 1, Vienna IAEA (1962), p. 101.
17. J. Diehl et al., Phys. Letters, 4, 236 (1963).
18. E. Ruede and S. Amelinckx, J. Nucl. Materials, 9, 116 (1963).

ABSTRACTS

DISSOCIATION OF FAST IONS OF MOLECULAR HYDROGEN AND CHARGE EXCHANGE OF FAST PROTONS IN A LITHIUM ARC

(UDC 621.039.6)

G. F. Bogdanov, A. N. Karkhov, and Yu. A. Kucheryaev

Translated from Atomnaya Énergiya, Vol. 19, No. 4,
p. 381, October, 1965
Original article submitted May 26, 1965

The dissociation of fast H_2^+ ions in a high-vacuum lithium arc is used to accumulate high-temperature plasma in the DSKh-2 apparatus [1]. Similar experiments were performed with the "Ogra" equipment in 1963 [2]. To select optimum accumulation conditions, we need to know the principal parameters of the arc, namely its density and electron temperature, the cross-section for the formation of protons by the dissociation of fast H_2^+ ions on Li^+ ions, and the effective cross-section for charge exchange by fast protons in the lithium arc. Our article described the measurement of all these quantities except the electron temperature. The electron density was measured with a radio-interferometer working at 8 mm wavelength. To separate the products of the elementary processes occurring during single passage of a beam of H_2^+ or H_1^+ ions of energies 40-160 keV through the lithium arc, we used the magnetic field of "Orga."

To record fast neutral atoms from dissociation and charge exchange, we used a thin nickel foil. The yield of protons from the foil in the above energy range was measured in two different ways.

It was found that the density of the arc increases with the amount of lithium vapor fed to the anode, but is almost independent of the voltage applied to the arc. During the cross-section measurements, the density of the arc was varied in the range $(0.5\text{-}4) \cdot 10^{12}$ cm^{-3}.

The cross-section for proton formation by dissociation of H_2^+ ions with energy 160 keV on Li^+ ions is $\sim 1.0 \cdot 10^{-15}$ cm^2, about 1.5 protons being formed for each molecular ion lost. When the energy of the H_2^+ ions is decreased to 40 keV, the cross-section for proton formation remains unchanged, but the cross-section for formation of fast neutral atoms of hydrogen increases by a factor of ~2.5. The dissociation cross-section is independent of the condition of the arc.

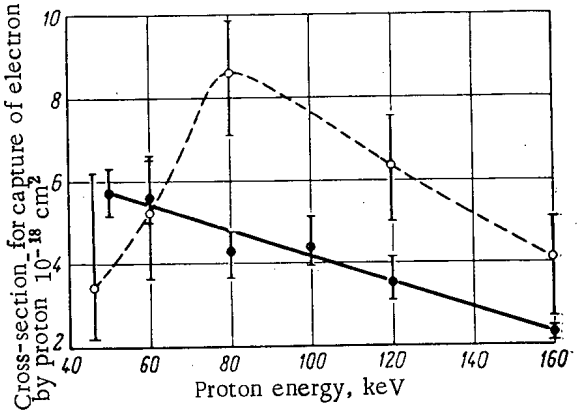

Cross-section of capture of electron by proton in the arc, plotted versus proton energy: ○ – 0.04 mg/cm^2 foil; ● – 0.2 mg/cm^2 foil.

The study of charge exchange by fast protons in the lithium arc is complicated by a number of interfering factors (charge exchange with the residual gas in the "Ogra" chamber, scattering of protons by the beam receiver, and presence in the proton beam of H_2^+ ions with energies equal to half of those of the protons). The diagram shows the effective cross-section for charge exchange in the lithium arc, plotted versus the proton energy. The solid curve was measured with a 0.2 mg/cm^2 foil. The dashed curve, which was measured with a 0.04 mg/cm^2 foil, illustrates the influence of H^+ ions present in the proton beam. The charge-exchange cross-section was not found to vary with the arc conditions outside the scatter limits (shown as vertical lines on the graph).

To check the method, separate measurements were made of the dissociation cross-section of fast H_2^+ ions and of the charge-exchange cross-section of fast protons in nitrogen.

The measured values of the cross-section for formation and loss of protons yield an explanation in general terms of the results of experiments on hot plasma accumulation in the "Ogra" apparatus with lithium arc.

LITERATURE CITED

1. Thermonuclear Division Semiannual Progress Report. ORNL-3564 (1963), p. 16; ORNL-3652 (1964), p. 28.
2. N. N. Semashko, Report to Symposium on Magnetic Traps (Paris, 1963) [in Russian], L. A. Artsimovich, Report No. 297 presented by the USSR to the Third International Conference on the Peaceful Uses of Atomic Energy, Geneva (1964).

AGES AND MIGRATION AREAS OF NEUTRONS FROM POLYENERGETIC SOURCES IN ORGANIC AND METAL-HYDROGEN-CONTAINING COMPOUNDS

(UDC 621.039.532)

D. A. Kozhevnikov

Translated from Atomnaya Énergiya, Vol. 19, No. 4,
p. 382, October, 1965
Original article submitted February 23, 1965. Note submitted May 24, 1965

For physical calculations on nuclear reactors and shielding, we need to know the ages and migration areas of fission-spectrum neutrons in moderators; such data have been found experimentally only with ampoule sources, while theoretical calculations are difficult because of our lack of knowledge of neutrons characteristics and the difficulty of allowing for certain specific effects (heterogeneity). The energy spectra of neutrons from ampoule sources are quite different from the fission spectrum, so that the experimental curves cannot be used without some corrections. In our paper, we solve the problem of determining the age and migration areas of neutrons from a polyenergetic source by means of the experimental values of these parameters for neutrons from sources with different spectra (in the same media).

The age $\tau^*_A(\varepsilon)$ of neutrons with energy ε from a polyenergetic source with spectrum A is equal to

$$\tau^*_A(\varepsilon) = [\tau^*_B(\varepsilon) - \tau^0_B(\varepsilon)]\, K^{AB} + \tau^0_A(\varepsilon),$$

where $\tau^*_B(\varepsilon)$ is the age of neutrons from a polyenergetic source with spectrum B; $\tau^0_A(\varepsilon)$ and $\tau^0_B(\varepsilon)$ are the monoenergetic ages for the lower limits of spectra A and B, respectively; and K^{AB} is the modulus of spectrum A relative to spectrum B, equal to

$$K^{AB} = \frac{\langle \varepsilon_0 \rangle_A}{\langle \varepsilon_0 \rangle_B}, \quad \langle \varepsilon_0 \rangle_{A,B} = \int_{(\varepsilon_0)} g_{A,B}(\varepsilon_0)\, \varepsilon_0\, d\varepsilon_0,$$

where $g(\varepsilon_0)$ is the weight function of the spectrum. The monoenergetic ages $\tau^0_{A,B}(\varepsilon)$ can be calculated accurately, because inelastic scattering and diffraction of neutrons do not occur at energies $\varepsilon \leq \varepsilon_0^{\min}$. Furthermore, in this energy range the scattering cross-sections for neutrons of the nuclei of many elements are either constant or vary only slightly with the neutron energies. The migration area of thermal neutrons is calculated similarly to the age:

$$M^2_A = (M^2_B - M^2_{0B})\, K^{AB} + M^2_{0A}.$$

Our article gives the ages of indium neutrons in various moderators (H_2O, D_2O, $C_{12}H_{10}$, $C_{15}H_{16}$, $C_{12}H_{10}O_{0.735}$, CH_2, C^{12}, Be^9, BeO) for the sources U^{235}, Po – Be, Ra – Be, Pu – Be, Po – B. The table gives the quantitative characteristics of the energy spectra of these sources ($\langle \varepsilon_0 \rangle$ = mean energy, $D[\varepsilon_0]$ = spectral dispersion).

Characteristics of Energy Spectra of Various Sources

Source	$\langle \varepsilon_0 \rangle$, MeV	$D[\varepsilon_0]$, MeV^2
U^{235}	2,03	2,50
Po—Be	4,35	5,70
Ra—Be	3,63	8,17
Po—B	3,07	1,00
Pu—Be	4,07	6,92

In determining the age and migration areas of neutrons in heterogeneous metal-water mixtures by the method described above, we are confronted with the problem of estimating theerrors caused by ignoring the heterogeneity in calculating $\tau^0_{A,B}(\varepsilon)$. It is shown that the maximum error in τ^* and M^2 for the fission spectrum is less than half of the error in τ^0 and M^2_0. Graphs are given of the calculated ages of indium neutrons from the fission spectrum in

zirconium-water, bismuth-water, iron-water and aluminum-water mixtures, plotted versus the volume ratio of metal to water for various degrees of heterogeneity. For some mixtures, in addition to the experimental results obtained with ampoule types sources, we give results of measurements of the fission spectrum; these agree with the theory. The ages and migration areas of fission-spectrum neutrons in complex media can thus be calculated from laboratory measurements with ampoule type sources, without the need for experiments with reactors or critical assemblies.

REDUCING CAPTURE γ-RADIATION AND RADIATIVE HEAT EMISSION IN A REACTOR VESSEL BY BLOCKING AND BORONIZING THE THERMAL SHIELD

(UDC 539.121.73 : 539.122)

E. N Goryanina, K. K. Popkov, S. M. Rubanov, and S. A. Tsvetkova

Translated from Atomnaya Énergiya, Vol. 19, No. 4,
p. 383, October, 1965
Original article submitted May 22, 1964; revised June 15, 1965

This paper is a theoretical study of the effects of boronizing the iron-water thermal shield of a water-moderated water-cooled reactor, and also of various types of blocking of the reactor vessel, on radiative heat emission, and on the γ-ray dose due to radiative capture of neutrons in the thermal shield and reactor vessel.

The authors study iron-water thermal shields with homogeneous and heterogeneous compositions, with iron concentration ~70 vol.%.

The spatio-energetic distributions of the neutron fluxes were calculated with an M-20 computer, in plane geometry, with the semi-grouped scheme suggested in [1].

The homogeneous type of thermal shielding was an iron-water mixture of thickness 25 cm. An estimate was made of the compositions, varying with thickness of the thermal shielding layer, to which was added boron. In the heterogeneous types, the thermal shielding was boronized by successive replacement of the steel screens by screens of boron steel (0.5 and 1 wt. % boron); the thermal shielding was 28 cm thick.

The paper also discusses compositions in which the boron concentration in the thermal shielding screen nearest to the reactor vessel was varied. To study the efficiency of blocking the outer surface of the vessel, the blocking materials used were boron steel (with up to 5 wt. % boron), boron carbide, lead and lead boride. Layers of various thicknesses were used: for boron steel, lead and lead boride they were up to 10 cm, for boron carbide up to 3 cm. Compositions were also studied in which various boron concentrations were used in the primary shielding water. The methods of calculation used were those given in [2, 3, 4].

The paper shows (1) that addition of boron to the thermal shielding screens reduces radiative thermal emission in the reactor vessel, (2) that it is not desirable to use boron steel screens with > 2% boron in the thermal shielding, and (3) that the use of boron-containing materials and lead for blocking the outer surface of the reactor vessel can markedly reduce the capture γ-ray fluxes from the thermal shielding and vessel (by a factor of three to five).

The most effective material is lead; however, increase of blocking layer thickness d_b leads to increased yield of capture γ-radiation from lead, and this becomes predominant at $d_b > 6$ cm. Lead boride is free from this defect, and its use shows some promise.

LITERATURE CITED

1. D. L. Broder et al., Atomnaya Énergiya, 12, 129 (1962).
2. D. L. Broder and K. K. Popkov, Atomnaya Énergiya, 15, 370 (1963).
3. L. P. Bokacheva et al., Inzh.-fiz. zh., VI, 47 (1963).
4. D. L. Broder, K. K. Popkov, and S. M. Rubanov, Biological Shielding of Marine Reactors [in Russian], Leningrad Sudostroenie (1964).

METHOD FOR CALCULATING THE FUEL DEPLETION IN A CYLINDRICAL REACTOR WITH A MOBILE COMPENSATING SYSTEM

(UDC 621.039.51)

G. V. Mukhina, A. N. Protsenko, and N. M. Trukhachev

Translated from Atomnaya Énergiya, Vol. 19, No. 4,
pp. 383-384, October, 1965
Original article submitted May 26, 1965

The changes in reactivity and the run duration of a reactor basically depend on the distribution of neutron fluxes, which vary during the depletion process. Most of the planned and operating reactors are maintained in the critical state by means of a compensating system (CS) of control elements which are arranged in a certain manner in the core. Figure 1 shows one of the possible CS positions in themost general case. Here, the core without CS has $3 \times 3 = 9$ zones. The introduction of compensating elements in this case resulted in two new zones: ABCD and BEFC. The boundaries AE, EF, FD, and DA are mobile. As the CS shifts, certain zones may disappear, and others may appear. In certain cases there may be 15 zones.

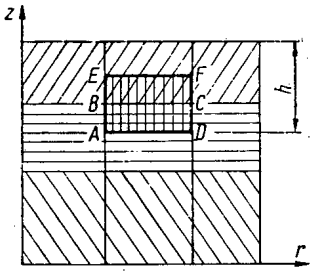

Fig. 1. One of the possible CS positions in the reactor.

The presence of a CS, the position of which changes during the depletion process, may cause considerable distortions of the neutron fluxes and, in the final analysis, greatly influence the run duration. The present article describes a method for the numerical solution of the nonlinear two-dimensional (the coefficients of the given equation implicitly depend on the solution) quasisteady-state (the coefficients of the given "steady-state" equation implicitly depend on time) problem of determining the neutron distribution and the critical parameter.

The system of basic reactor equations in the multigroup diffusion approximation is considered. "Matching" conditions are assigned at the internal boundaries of the zones, and the logarithmic derivatives of the neutron flux are assigned at the reactor's external boundary [1, 2]. The

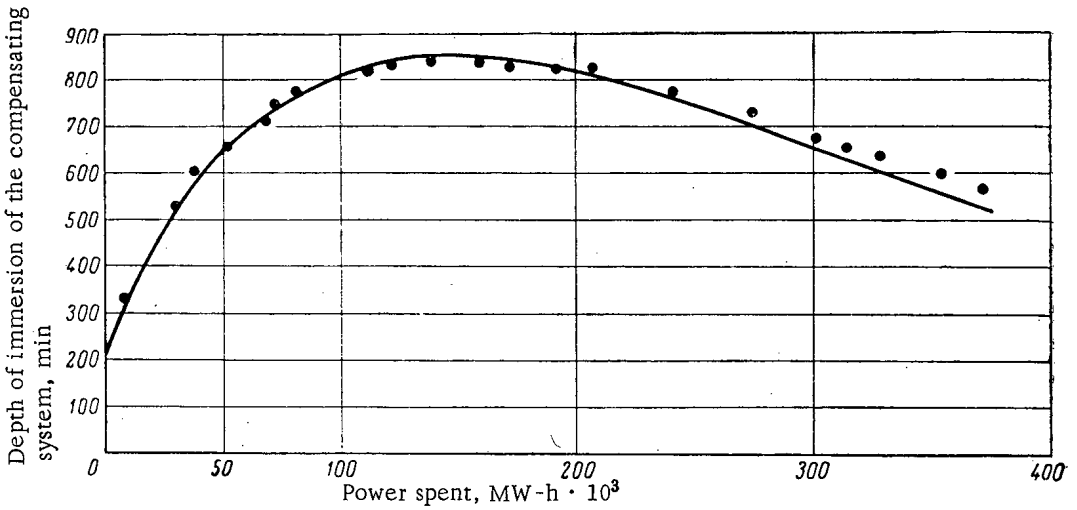

Fig. 2. CS position in dependence on the depletion of fuel in the reactor of the atomic icebreaker. "Lenin."

numerical solution of such a problem is rendered complicated by the fact that the coefficients entering the equations and the boundary conditions depend on the coordinates and the time, while the method for calculating these coefficients and the depletion equation are rather cumbersome for most reactors. Therefore, we used a method for determining all the parameters which made it possible to reduce the computer time by a factor of several tens. These parameters are represented by polynomials, the argument of which is a quantity proportional to the integral heat release:

$$\Phi_f(r, z, t) = \Phi_f^+(r, z, t) + \Phi_f^-(r, z, t),$$

where

$$\Phi_f^{\pm} = \int_{t_1}^{t_2} \Phi(r, z, t) \sum_f^{\pm}(r, z, t)\, dt.$$

Here $t_2 - t_1$ is the time interval during which CS is present (absent) at a certain given point of the core; Φ is the thermal neutron flux, normalized with respect to power.

The two-dimensional boundary problem was solved by using the grid method; the "continuous count" method was used for solving the finite-difference equations [3].

Figure 2 shows the results obtained in calculating the variation of the CS position during the depletion process for the atomic icebreaker Lenin (solid curve). The points refer to experimental data [4]. The agreement between the theoretical and experimental results is entirely satisfactory.

LITERATURE CITED

1. A. D. Galanin, Theory of Thermal Nuclear Reactors [in Russian], Moscow, Atomizdat (1959).
2. G. I. Marchuk, Methods for Calculating Nuclear Reactors [in Russian], Moscow, Gosatomizdat (1961).
3. A. N. Tikhonov and A. A. Samarskii, Dokl. AN SSSR, 108, 393 (1956).
4. I. I. Afrikantov et al., Report No. 313, submitted by the USSR at the Third International Conference on the Peaceful Uses of Atomic Energy, Geneva (1964).

CHOICE OF THE BOUNDARY CONDITIONS IN USING THE METHOD OF SPHERICAL HARMONICS

(UDC 621.039.51.12)

V S. Shulepin

Translated from Atomnaya Énergiya, Vol. 19, No. 4,
p. 385, October, 1965
Original article submitted April 20, 1965. Abstract submitted June 21, 1965

This article is devoted to the application of the variational principles presented in [1, 2] for determining the conditions at the boundary between two media in solving the single-velocity kinetic equation in the P_n-approximation of the method of spherical harmonics. In seeking the conditions at the boundary between two media, the use of the variational method [1] provides one half of the number of boundary conditions that is required for solving the kinetic equation in the even or the odd P_n-approximation. The necessary number of boundary conditions can be obtained by using the variational principles [2]. The present article describes the use of the method [1] for determining the conditions at the boundary between two media on the basis of variational principles [2].

The boundary conditions found as a result of using the variational principles are in complete agreement with the corresponding conditions given in [3]. However, the variational boundary conditions cannot be considered as the best. For instance, in the case of the P_2-approximation, numerical calculations show that the conditions of continuity of unidirectional neutron fluxes at the boundary between two media are better than the variational boundary conditions. The expansion of the solution of the kinetic equation $\varphi(z, \mu)$ in a series with respect to Legendre polynomials in the P_2-approximation is given by

$$\varphi(z, \mu) = \frac{1}{2}[\varphi_0(z) + 3\varphi_1(z) P_1(\mu) + 5\varphi_2(z) P_2(\mu)], \quad (1)$$

where z is the space coordinate (two-dimensional geometry), μ is the cosine of the angle between the direction in which the neutrons move and the z axis, and μ are Legendre polynomials. When the solution is written in the form given by (1), the condition for the continuity of unidirectional fluxes is equivalent to the condition for the continuity of

$$\varphi_1 \text{ and } \varphi_0 + \frac{5}{4}\varphi_2, \quad (2)$$

while the variational conditions imply the conditions for the continuity of φ_1 and $\varphi_0 + 2\varphi_2$.

The results of numerical calculations (in the single-velocity approximation) of the cell loss factor and the critical core dimension in reactors with reflectors indicate that the accuracy of calculations based on conditions (2) is close to the accuracy of the P_3-approximation.

LITERATURE CITED

1. V. S. Vladimirov, Vychislitel'naya Matematika, No. 7, 93 (1961).
2. G. Pomraning and M. Clark, Nucl. Sci. Engng, 16, 155 (1963).
3. G. Ya. Rumyantsev, Atomnaya Énergiya, 10, 26 (1961).

LETTERS TO THE EDITOR

LEAKAGE OF PARTICLES FROM THE ACCUMULATOR CAUSED BY AMPLITUDE AND FREQUENCY INSTABILITY OF THE COMPENSATING FIELD

(UDC 621.384.60)

A. S. Bakai

Translated from Atomnaya Énergiya, Vol. 19, No. 4,
pp. 386-388, October, 1965
Original article submitted January 16, 1965

The total number of particles N(t) in the accumulator is determined by the number of particles n(t) injected per unit time and the mean lifetime τ of a particle in the accumulator:

$$N(t)=e^{-\lambda t}\left[N_0+\int_0^t n(s)\,e^{\lambda s}\,ds\right],$$

where $\lambda = 1/\tau$.

For a constant injection intensity n(t) = n, the accumulation of the necessary number of particles N is completed during the time

$$t=-\frac{1}{\lambda}\ln\left(\frac{\lambda N-n}{n}\right),$$

while the maximum number of particles stored is $N_{max} = n/\lambda$. After the end of injection, the accumulated current decreases, obeying the $e^{-\lambda t}$ law.

The value of the particle leakage λ from the accumulator can be written as a sum of several terms:

$$\lambda=\sum\lambda_i,$$

each of which characterizes the magnitude of leakage caused by a certain specific factor. Generally, the λ_i values are not independent; however, the effect of any single factor on the lifetime of a particle in the accumulator can be characterized by the corresponding leakage value λ_i in the absence of all the other factors.

The magnitude of the particle leakage from the accumulator caused by collisions with the residual gas atoms and the quantum character of radiation was calculated in [1, 2]. We shall calculate here the amount of leakage due to the instability of the amplitude and frequency of the potential difference applied to the dees, which compensates the radiation loss of the particle energy. A similar problem was stated in Blackman's report [3], but, as far as we know, its solution has not been published.

We shall consider that the amplitude V and the frequency ν of the compensating field are random functions, while

$$\left.\begin{aligned}&\langle V\rangle=V_0;\quad\langle\nu\rangle=\nu_0;\\&\left\langle\left(\frac{\Delta V}{V_0}\right)^2\right\rangle=\varepsilon_1^2;\quad\left\langle\left(\frac{\Delta\nu}{\nu_0}\right)^2\right\rangle=\varepsilon_2^2,\end{aligned}\right\}\qquad(1)$$

where

$$\Delta V=V-V_0;\quad\Delta\nu=\nu-\nu_0.$$

We shall assume that the disturbances $\Delta\nu$ and ΔV constitute fast random processes, while their spectral densities lie at frequencies which greatly exceed the frequency of synchrotron oscillations, but are much lower than the particle revolution frequency. Then, the equations of radial and phase motion of an electron in the accumulator, averaged with respect to a certain number of revolutions, can be written thus [1]:

$$\left.\begin{aligned}\dot{A} &= -\left(\Gamma_1+\frac{\Delta V}{V_0}\,\Omega_0^2\,\mathrm{ctg}\,\varphi_s\right)A;\\ \dot{\varepsilon} &= -2\Gamma\varepsilon-\eta\Omega_0^2\left(1+\frac{\Delta V}{V_0}\right)+\frac{\Delta V}{V_0}\,\Omega_0^2\,\mathrm{ctg}\,\varphi_s;\\ \dot{\eta} &= \varepsilon+q\,\frac{\Delta\nu}{\nu_0},\end{aligned}\right\} \qquad (2)$$

where A is the amplitude of radial oscillations;

$$\varepsilon=q\alpha\,\frac{E-E_s}{E_s};$$

η is the phase shift of the compensating field; q is the frequency multiplicity; α is the expansion coefficient of the orbit;

$$\Omega_0^2=\frac{eV_0\sin\varphi_s}{2\pi E_s}$$

is the square of the frequency of phase oscillations; and Γ_1 and Γ are the damping decrements.

The stable motion of particles corresponds to trajectories in a certain limited region of the phase space; the particles leave the accumulator when the trajectories reach the boundary of this region. The region boundary can be assigned by the equations:

$$A=\pm A_0;\ \Omega_0^2\eta^2+\varepsilon^2=u_0^2. \qquad (3)$$

The amplitude of radial oscillations decreases in time as $\sim e^{-\Gamma_1 t}$, while the random character of changes in the particle energy inside the dee leads only to insignificant changes in the rate of decrease. On the average, the amplitude of phase oscillations decreases as $e^{-\Gamma t}$; however, the diffusion of the particle trajectory in the phase space occurs due to the random character of the right-hand sides in (2). As a result of this diffusion, the trajectory reaches the boundary of region (3), and the particle leaves the accumulator.* If the mean value of the random impulse is small ($\varepsilon^2_{1,2} \ll \Gamma$), the particle dwells almost all the time in a small region of the phase space in the neighborhood of the point

$$A=\eta=\varepsilon=0$$

while, if it leaves this region, it is highly probable that it will return to it. For determining the lifetime of a particle, it is sufficient to determine the steady-state distribution of particles in the stability region of the phase space for the assigned intensity of injection into this region.

It should be noted that the steady-state distribution depends only on the over-all number of injected particles, since, no matter at what point of the phase space a particle was injected, it is highly probable that it will be found in the vicinity of the $A = \eta = \varepsilon = 0$ point shortly after injection.

The distribution density $\Phi(A, \eta, \varepsilon)$ of particles in the phase space is determined by the Fokker–Planck–Kolmogorov equation. This equation can be conveniently written by using the variables

$$u=(\Omega_0^2\gamma^2+\varepsilon^2)^{1/2};\quad v=\mathrm{arc\ tg}\,\frac{\varepsilon}{\Omega_0\eta}.$$

*The method for determining the mean lifetime of the systems described by equations of the type (2) and (3) has been described in detail in [2]. The fundamentals of this method are briefly set forth in the present article.

Since it is clear from the physical point of view that the distribution density does not depend on the phase v, the averaging can be performed with respect to v. Then, the Fokker–Planck–Kolmogorov equation, averaged with respect to the variable v, will assume the following form:

$$\frac{\partial \Phi}{\partial t} = \frac{\partial}{\partial A}\left[\alpha_1 A^2 \frac{\partial \Phi}{\partial A} + \Gamma_1 A \Phi\right] + \frac{\partial}{\partial u}\left[(\beta + \beta_1 u^2)\frac{\partial \Phi}{\partial u} + \frac{1}{u}(\Gamma u^2 - \beta)\Phi\right] + g(u, A), \tag{4}$$

while

(4')

where

$$\Phi(\pm A_0, u) = \Phi(A, u_0) = 0,\ \alpha_1 = \frac{\Omega_0^4}{4}\operatorname{ctg}^2\varphi_s\varepsilon_1^2;$$

$$\beta = \alpha_1 + \frac{1}{4}\Omega_0^2 q^2 \varepsilon_2^2;\ \beta_1 = \frac{1}{8}\Omega_0^2\varepsilon_1^2;$$

and g(u, A) is the injection density, averaged with respect to the variable.

Since the steady-state distribution density is independent of the form of g(u, A), the density equation can be written thus:

$$\frac{\partial}{\partial A}\left[\alpha_1 A^2 \frac{\partial \Phi}{\partial A} + \Gamma_1 A_1 \Phi\right] + \frac{\partial}{\partial u}\left[(\beta + \beta_1 u^2)\frac{\partial \Phi}{\partial u} \times (\Gamma u^2 - \beta)\Phi\right] + \lambda\Phi = 0, \tag{5}$$

where

$$\lambda = \frac{\int_{-A_0}^{A_0}\int_0^{u_0} g(u, A)\, du\, dA}{\int_{-A_0}^{A_0}\int_0^{u_0} \Phi(A, u)\, du\, dA}.$$

Thus, the problem has been reduced to the determination of the eigenfunction and the eigenvalue of the operator (5), (4'). The positive function of this operator is unique, and it corresponds to the smallest eigenvalue. It should be noted that the variables in Eq. (5) can be separated, while the smallness of the leakage λ makes it possible to seek the solution of this equation as an expansion with respect to powers of λ [2].

The solution of Eq. (5) with the boundary conditions 4', which determines the steady-state distribution of particles in the phase space, is given by

$$\Phi(A, u) = \delta(A)\frac{u}{\left(1 + \frac{\beta_1}{\beta}u^2\right)^{\frac{\Gamma+\beta_1}{2\beta_1}}} \times \left\{1 + \frac{\lambda}{2(\Gamma - \beta_1)}\int_0^{u^2}\left[1 - \left(1 + \frac{\beta_1}{\beta}v\right)^{\frac{\Gamma-\beta_1}{2\beta_1}}\right]\frac{dv}{v}\right\}, \tag{6}$$

while the leakage value is

$$\lambda = \frac{2(\Gamma - \beta_1)}{\int_0^{u_0^2}\left[\left(1 + \frac{\beta_1}{\beta}v\right)^{\frac{\Gamma-\beta_1}{2\beta_1}} - 1\right]\frac{dv}{v}}. \tag{7}$$

The approximate expressions for λ can readily be obtained from Eq. (7), noting that $\Gamma \gg \beta_1$. Thus, for instance, for $\beta_1 u_0^2/\beta \ll 1$,

$$\lambda \approx \frac{(\Gamma-\beta_1)^2 u_0^2}{\beta} e^{\frac{-\Gamma-\beta_1}{2\beta} u_0^2}, \tag{8}$$

while, for $\frac{\beta_1 u_0^2}{\beta} \approx 1$,

$$\lambda \approx \frac{\Gamma^2}{\beta_1}\left(1+\frac{\beta_1}{\beta}u_0^2\right)^{-\frac{\Gamma+\beta_1}{2\beta}}. \tag{9}$$

As was to be expected, in the case of instability of the compensating field's amplitude and frequency, the leakage of particles from the accumulator occurs only as a consequence of the buildup of phase oscillations.

The root-mean-square deviations of the particle parameters from their equilibrium values, calculated by means of distribution (6), are determined by the expressions:

$$\langle \varepsilon^2 \rangle = \frac{2\beta}{\Gamma}; \quad \langle \eta^2 \rangle = \frac{2\beta}{\Omega^2\Gamma}; \quad \langle \varrho^2 \rangle = \frac{2\beta}{q^2\Gamma}, \tag{10}$$

where

$$\varrho = \frac{R-R_s}{R_s}.$$

The dependence of the leakage value on energy can readily be established. For this, we note that

$$\Gamma \sim \frac{\gamma^3}{R} \sim \gamma^2; \quad u_0^2 \sim \Omega_0^2 \sim \gamma^2.$$

Here $\gamma = E/m_0c^2$, where m_0 is the rest mass of a particle. Assuming that the root-mean-square deviations ε_1^2 and ε_2^2 are fixed, we shall consider two cases.

1. $\varepsilon_1^2 \neq 0$, $\varepsilon_0^2 - 0$. From expressions (7)-(8), we have

$$\lambda \sim \gamma^2 e^{-c_1 \gamma}. \tag{11}$$

2. $\varepsilon_1^2 = 0$, $\varepsilon_2^2 \neq 0$. In this case,

$$\lambda \sim \gamma^2 e^{-c_2 \gamma^2}, \tag{12}$$

while

$$c_1, \; c_2 \gg 1.$$

The expressions obtained make it possible to determine the degree of accuracy with which the amplitude and frequency of the compensating field must be maintained for the limitation imposed on the leakage value.* As an example, we shall consider an electron-positron accumulator with strong focusing that is characterized by the following parameters:

$$E_s = 2{,}2 \cdot 10^9 \text{ eV}; \; \Gamma = 2.3 \cdot 10^{-5};$$
$$\Omega_0^2 = 6 \cdot 10^{-7}; \quad q = 4; \quad \cos\varphi_s = \frac{1}{\sqrt{2}}. \tag{13}$$

Consider that the amplitude V and the frequency ν assume with an equal probability any of the values in the following intervals:

*An allowance for the nonlinearity of synchrotron oscillations may necessitate some corrections in the expressions obtained.

$$V_0-\Delta V \leqslant V \leqslant V_0+\Delta V;$$
$$\nu_0-\Delta\nu \leqslant \nu \leqslant \nu_0+\Delta\nu,$$

then,

$$\varepsilon_1^2=\frac{1}{3}\left(\frac{\Delta V}{V_0}\right)^2; \quad \varepsilon_2^2=\frac{1}{3}\left(\frac{\Delta\nu}{\nu_0}\right)^2.$$

A mean particle lifetime of the order of hundreds of hours can be secured if

$$\frac{\Delta V}{V_0}\approx 1; \quad \frac{\Delta\nu}{\nu_0}\approx 10^{-4}.$$

The author is grateful to G. Ya. Lyubarskii for his continued interest and useful advice.

LITERATURE CITED

1. A. A. Kolomenskii and A. N. Lebedev, Theory of Cyclic Accelerators [in Russian], Moscow, Fizmatgiz (1962).
2. A. S. Bakai, G. Ya. Lyubarskii, and V. V. Rozhkov, ZhTF, 35, No. 9 (1965).
3. N. M. Blackman, in the book: Transactions of the First International Congress of the International Federation of Automatic Control [in Russian], Vol. 1, Moscow, Izd. AN SSSR, p. 181.

LIMITATIONS OF THE DENSITIES OF INTERACTING CURRENTS IN OPPOSED ULTRARELATIVISTIC BEAMS

(UDC 533.9)

M. I. Kheifets and V. D. Shapiro

Translated from Atomnaya Énergiya, Vol. 19, No. 4,
pp. 388-389, October, 1965
Original article submitted February 18, 1965

In most papers that have been published until now, the stability of interacting relativisitic beams in accumulators was considered only in the single-particle approximation [1-3], while collective instabilities, which are possible in such devices, were neglected. Only the electrostatic instabilities of self-focusing beams, which are of no importance in the ultrarelativistic case, were investigated in [4].

The present article is concerned with an investigation of the collective instabilities in a system of two opposed relativistic beams. This problem is of interest in connection with the fact that instabilities of this type may be considerable in accumulator devices.

We shall consider a system of two beams with the densities n_1 and n_2 which move at the relativistic velocities v_1 and v_2 along the y axis.

We shall assume that the density nonuniformities that arise in beams as a result of the electrostatic interaction of charges are small due to the compensation of the repulsion forces by the proper magnetic fields of the beams. Then, in the hydrodynamic approximation, the tensor of the dielectric constant in the beams is given by

$$\left.\begin{aligned} \varepsilon_{xx}=\varepsilon_{zz}=1-\frac{\Omega_1^2+\Omega_2^2}{\omega^2};\\ \varepsilon_{yy}=1-\frac{\omega^2\gamma^2+k_z^2c^2}{\omega^2}\left[\frac{\Omega_1^2}{(\omega-k_yv_1)^2}+\frac{\Omega_2^2}{(\omega-k_yv_2)^2};\right]\\ \varepsilon_{zy}=-\frac{k_zc}{\omega^2}\left(\frac{\Omega_1^2}{\omega-k_yv_1}-\frac{\Omega_2^2}{\omega-k_yv^2}\right);\\ \varepsilon_{xy}=\varepsilon_{yx}=\varepsilon_{xz}=\varepsilon_{zx}=0, \end{aligned}\right\} \quad (1)$$

where $\Omega_i^2=\frac{4\pi n_i e_i^2}{m_i}$; $\gamma=\left(1-\frac{v^2}{c^2}\right)^{1/2}$ and k_y and k_z are the components of the wave vector.

By using the Maxwell equations and the found tensor ε_{lk}, we obtain the dispersion relationship

$$\left[1-\frac{\Omega_1^2\gamma^2}{(\omega-k_yv_1)^2}-\frac{\Omega_2^2\gamma^2}{(\omega-k_yv_2)^2}\right](\omega^2-\Omega_1^2-\Omega_2^2-k^2c^2)+\frac{k_z^2\Omega_1^2\Omega_2^2(v_1-v_2)^2}{(\omega-k_yv_1)^2(\omega-k_yv_2)^2}=0. \quad (2)$$

In the nonrelativistic case ($\gamma = 1$) for $v_2 = 0$, expression (2) is transformed into the dispersion equation given in [5].

For the waves propagating along the beam ($k_z = 0$), the dispersion equation breaks up into two equations: the equation for stable longitudinal waves and the equation for stable transverse waves. The dispersion equation for longitudinal waves describes the ordinary beam instability, the increment of which tends to zero in the relativistic case.

Considering that the thickness of beams in accumulators is small $\Delta < 0.01$ cm, while $k_z \geq \pi/\Delta$, so that the condition

$$\gamma^2 \ll \frac{k_z^2\Omega^2}{k^2(\omega^2+c^2k_y^2)} \tag{3}$$

is satisfied, and considering that the beams move toward each other at the velocities $v_1 = c$ and $v_2 = -c$, we obtain the following expression from relationship (2):

$$c^2k^2+\Omega_1^2+\Omega_2^2-\omega=\frac{4\Omega_1^2\Omega_2^2k_z^2c^2}{(\omega^2-k_y^2c^2)^2}. \tag{4}$$

After investigating graphically both sides of Eq. (4), we can satisfy ourselves that, if the condition

$$k_y^4c^2(c^2k^2+\Omega_1^2+\Omega_2^2)<4\Omega_1^2\Omega_2^2k_z^2 \tag{5}$$

is fulfilled, we obtain a solution with an increasing amplitude ($\mathrm{Im}\omega > 0$). For $\omega^2 - c^2k^2y \ll c^2k_z^2$, the solution of Eq. (4) is given by

$$\omega^2=k_y^2c^2-\frac{2\Omega_1^2\Omega_2^2k_z^2c^2}{(\Omega_1^2+c^2k_z^2)^{1/2}}. \tag{6}$$

For $k_y \to 0$, we obtain the maximum rise increment:

$$Im\omega=\frac{(2\Omega_1\Omega_2k_zc)^{1/2}}{(\Omega_1^2+c^2k_z^2)^{1/4}}. \tag{7}$$

For $\Omega_{1,2} \ll ck_z$ (a condition which holds for stored beams), we obtain

$$Im\omega=\sqrt{2\Omega_1\Omega_2};\quad \tau=(2\Omega_1\Omega_2)^{-1/2}. \tag{8}$$

By comparing the time τ with the time of interaction between bunches, we can determine the maximum density in bunches for the case where the instability is negligible due to collective interactions. In particular, for bunches with equal densities, we obtain

$$n<\frac{m_0c^2}{8\pi e^2\gamma l^2}, \tag{9}$$

where l is the bunch length.

For electron or electron-positron beams,

$$n<\frac{1.5\cdot10^{11}}{\gamma l^2}.$$

For instance, for electron beams with an energy of 100 MeV and a bunch length of 40 cm or an energy of 250 MeV and a bunch length of 60 cm, $n < 2 \cdot 10^{10}$ cm^{-3}.

The authors are deeply grateful to Ya. B. Fainberg for the discussion of the results.

LITERATURE CITED

1. F. Ammon and D. Ritson, International Conference on High Energy Accelerators, USA (1961), p. 471.
2. E. M. Moroz, ZhTF, 33, 455 (1963).
3. F. Delcroix, Compt. rend. Acad. sci. colon., 256, 2305 (1963).
4. D. Finkelstein and P. A. Sturrock, Stability of Relativistic Self-Focusing Streams. Plasma Physics. Ed. J. Drummond (1961), p. 224.
5. J. Neufeld and P. Doyle, Phys. Rev., 121, 654 (1961).

XENON OSCILLATIONS IN REACTORS

(UDC 539.125.5)

I. P. Bacherikov

Translated from Atomnaya Énergiya, Vol. 19, No. 4,
pp. 389-390, October, 1965
Original article submitted October 23, 1964; revised May 27, 1965

While in the steady state, the neutron flux at any point of a thermal reactor is in equilibrium with the concentration of Xe^{135} that is formed during the burn-up of the fuel. With a change in the power level or a redistribution of the neutron field following a shift of the control rods, the equilibrium is disturbed and transient conditions set in. These conditions end with the establishment of a new equilibrium in a reactor stable with respect to xenon oscillations. During such transitions, the criticality can be preserved due to the negative power effect of reactivity. In the case of xenon instability [1, 2], there will occur rising oscillations of the neutron distribution about a new equilibrium position or there will be a monotonic drift away from the equilibrium. Local deviations of the neutron distribution, which are unavoidable under transient conditions, may be undesirable because of temperature limitations. Therefore, it is necessary to know the magnitude of these deviations, especially if the control system is not designed to suppress them. A method for estimating these deviations is given below.

We shall introduce the following notation: $\Phi_1(r)$ is the initial equilibrium distribution of neutrons; $\Phi_2(r)$ is the neutron distribution immediately after the equilibrium has been destroyed; and $\Phi_3(r)$ is the newly established equilibrium. We shall express the neutron distribution under transient conditions in terms of the deviation from the new equilibrium distribution, i.e., $\Phi(r, t) = \Phi_3(r) + \varphi(r, t)$, and we shall expand the deviation in the series:

$$\varphi(r, t) = \sum_{j=0}^{\infty} \varphi_j(r, t) \equiv \sum_{j=0}^{\infty} A_j(t) H_j(r) \tag{1}$$

with respect to suitable eigenfunctions (space harmonics) of a steady-state system with the material parameter $B_H^2(r)$ and the same geometry as the system under consideration. These functions satisfy the normalization $\int H_j^2 dv = 1$ and the equation $\nabla^2 H_j + B_H^2 H_j + h_j^2 H_j = 0$, where h_j^2 are the eigenvalues ($h_0 = 0$).

Assume $\varphi \ll \Phi_3$ and that the harmonics H_j are chosen in such a manner that the equation $\omega_j^2 + p_j\omega_j + q_j = 0$ for the frequency of their oscillations can be obtained according to [1]. The initial deviation is $\varphi(r, 0) = \Phi_2(r) - \Phi_3(r)$. The initial derivative $\frac{d\varphi}{dt}(r, 0)$ can be found from the equation of the concentration of J^{135} (which precedes Xe^{135}), which holds under transient conditions, and the expansion of this concentration in a series similar to (1).

The expression for the j-th harmonic is given by

$$\varphi_j(r, t) = e^{U_j t}\left[(\bar{\varphi}_j' - U_j\bar{\varphi}_j)\frac{\sin v_j t}{v_j} + \bar{\varphi}_j \cos v_j t\right] H_j(r), \tag{2}$$

where

$$\omega_j = U_j \pm v_j\sqrt{-1};\ \bar{\varphi}_j' = \int \frac{d\varphi}{dt}(r, 0) H_j\, dv;\quad \bar{\varphi}_j = \int \varphi(r, 0) H_j\, dv;$$

$$(\bar{\varphi}_j' - U_j\bar{\varphi}_j) = \left(P_j - \frac{q_j}{\lambda_J} - \lambda_J\right)\int \Phi_1 H_j\, dv + \left(\lambda_J - \frac{P_j}{2}\right)\int \Phi_2 H_j\, dv + \left(\frac{q_j}{\lambda_J} - \frac{P_j}{2}\right)\int \Phi_3 H_j\, dv;$$

and λ_j is the decay constant of J^{135}.

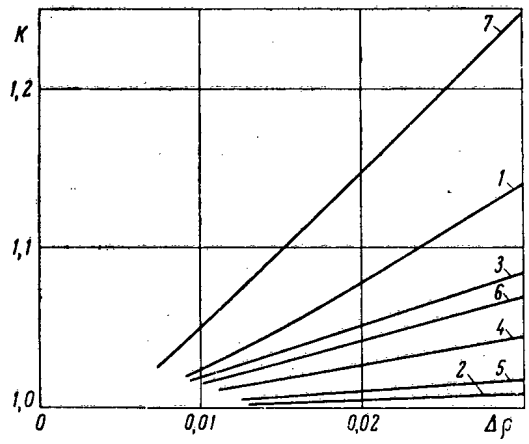

The maximum relative nonuniformity $K = (2/\pi) K_{max}$. Transition from two zones to a uniform layer: 1) Φ_1; 2) Φ_2; 3)-5) deviations for φ_{21} values equal to $^2/_3$, 1, and 2, respectively; 6) deviation for $\varphi_{21} = 1$ and $\alpha_\Phi = 0$. Transition from a uniform layer to a two-zone layer: 1) Φ_2 and Φ_3; 7) deviation for $\varphi_{21} = {}^1/_2 - 2$.

The neutron distributions Φ_1, Φ_2, and Φ_3, which satisfy the equation

$$\nabla^2\Phi + B^2(r, \Phi)\Phi = 0 \qquad (3)$$

for an arbitrarily nonuniform material parameter B^2, can be fairly simply calculated by means of expansion in a series with respect to uniform harmonics:

$$\Phi \approx A_0 \sum_{j=0}^{n} a_j F_j, \qquad (4)$$

where $a_j = A_j/A_0$; F_j satisfies the equation $\nabla^2 F_j + B_g^2 F_j + f_j^2 F_j = 0$; B_g^2 is a geometric parameter. After the substitution of (4) in (3), multiplication by F_i, and integration, we obtain a system of equations for the coefficients $a_{1,2} \ldots . n$:

$$\sum_{i=0}^{n} a_i b_{ij}^2 = a_j(1 + \lambda_j), \qquad (5)$$

where

$$j = 0, 1, \ldots, n;\ b_{ij}^2 = \frac{1}{B_g^2}\int B^2(r, \Phi) F_i F_j\, dv;\ \lambda_j = \frac{f_j^2}{B_g^2}.$$

The (n + 1)-th unknown can be the power level (the A_0 coefficient), the critical parameters B^2, or the reactor dimensions. If B^2 depends on the distribution to be determined, then, in the first approximation, the roughly estimated distribution Φ is substituted in expression (5), and the solution is found by using the method of successive approximations. For example, we calculated the deviations of the first harmonic $\sqrt{\frac{2}{H}}\sin\frac{2\pi z}{H}$ in a slab reactor divided along the middle into two zones which differed from each other by their B_0^2 values (see figure). The difference $\Delta\rho$ between the reactivities of these zones served as the argument. We used the material parameter given by

$$B^2 = B_0^2(r) + \alpha_X X(\Phi) + \alpha_\Phi \Phi(r),$$

where $X(\Phi)$ is the relative Xe^{135} contamination; $\alpha_X = -5 \cdot 10^{-4}$; $\alpha_\Phi = -2.5 \cdot 10^{-18}$; the layer thickness was H = 250 cm; the mean flux was $\Phi_2 = 4 \cdot 10^{13}$ neutrons/cm^2 sec. The ratio of the nonuniformity coefficient of the neutron distribution at maximum deviation to the nonuniformity coefficient $\pi/2$ for a uniform layer was laid off on the axis of ordinates. The curves in the figure were calculated for different ratios $\varphi_{21} = \bar{\Phi}_2/\bar{\Phi}_1$ of the new mean power level to the initial power level. These calculations show that the largest deviations of the neutron field occur during transition to the two-zone layer (curve 7).

LITERATURE CITED

1. D. Randall and D. John, Nucleonics, 16, No. 3 (1958).
2. A. Hitchcock, Stability of Nuclear Reactors [Russian translation], Moscow, Gosatomizdat (1963).

RELATION BETWEEN THERMAL CONDUCTIVITY AND OXIDE CONCENTRATIONS IN SODIUM

(621.039.534.6)

F. A. Kozlov and I. N. Antonov

Translated from Atomnaya Énergiya, Vol. 19, No. 4,
pp. 391-392, October, 1965
Original article submitted October 31, 1964

Various authors have studied heat transfer to sodium and the purification of this metal from oxides by means of cold traps. These traps collect the oxides which are precipitated at the heat exchange surface, causing unwanted thermal resistance. To get the right temperature conditions in the cold trap when oxides are accumulating in it, we need to know the value of this resistance. We can estimate this value if we know the thermal conductivity and thickness of the layer forming on the heat-exchange surface. It is obvious that as the concentration of oxides in the sodium increases, the latter's thermal conductivity must decrease.

To measure the relation between the thermal conductivity of sodium and its oxide content, we used the flat-layer method (the apparatus is shown in Fig. 1). The tube was taken from the experimental unit after it had become clogged with oxides as a result of experiments similar to those in [1].

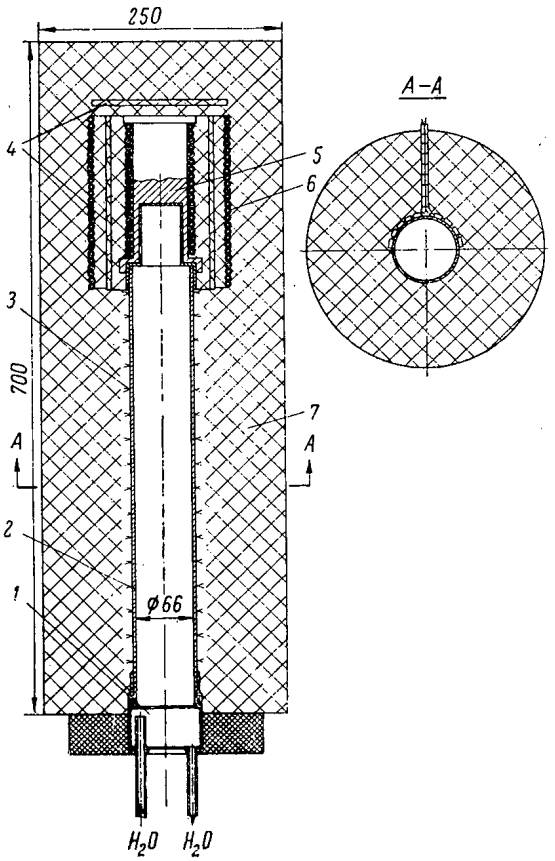

Fig. 1. Diagram of experimental unit: 1) cooler; 2) stainless steel tube; 3) thermocouples; 4) thermometers; 5) electric furnace; 6) compensation heater; 7) asbestos insulation.

In determining the thermal conductivity, the temperature distribution along the experimental unit was measured by means of chromel-copel thermocouples. The thermocouples were spaced 25 mm apart along a generator of the cylinder. The heat flow was created by an electric furnace set up on the lid of the experimental section. The power expended in the furnace was measured with a wattmeter. The bottom of the experimental section was cooled by means of running water. The heat losses of the electric furnace were compensated by means of an auxiliary thermometer and a compensating heater. Losses through the upper end of the furnace were recorded by a thermometer. Losses from the side wall of the working section were determined by calculation, for which purpose a mercury thermometer was used to measure the temperature distribution across the insulating surface and the temperature of the surrounding air. The maximum temperature of the insulating surface was 303°K. After a stationary condition had been set up and all the necessary thermal measurements made the analysis was begun. The oxygen content of the sodium was measured on specimens of length 50 mm. The error was below 20%.

Figure 2 plots the observed thermal conductivity λ versus the mean oxide concentration; all data were measured at 328°K. In processing the results, it was assumed that the temperature coefficient of the thermal conductivity is independent of the oxygen concentration and is equal to $1.23 \cdot 10^{-3}$ (deg K)$^{-1}$ [2]. As the temperature did not

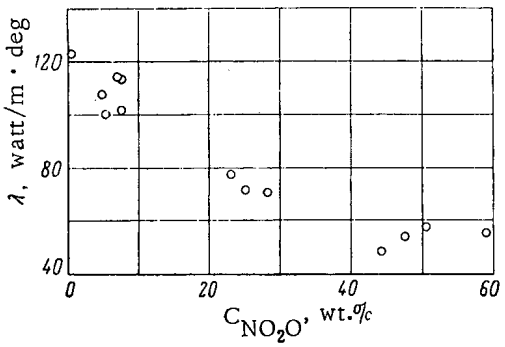

Fig. 2. Thermal conductivity of sodium versus concentration of oxides.

deviate from 328°K by more than 25°K, and the volume proportion of oxides was about 39%, this assumption should not introduce appreciable errors. The error in determining the coefficient of thermal conductivity was less than 15%. It was found that an increase of 50-60 wt.% in the oxide concentration reduces the thermal conductivity of sodium by a factor of more than 2.

In one of the samples the oxygen concentration in the sodium was 0.13 wt.% at mean temperature 328°K. The thermal conductivity of the sodium was then 123.6 watt/m · deg. According to [3, 4], the thermal conductivity of pure sodium at this temperature is 125 [3] or 121 [4] watt/m · deg. The agreement of these results shows that our experimental method was valid.

Thus the thermal conductivity of a layer of sodium and sodium oxide is less than that of pure sodium. The formation of such a layer on the heat-exchange surface may significantly affect the results of experiments on heat transfer to a liquid metal. We consider that the "thermal contact resistance" found in [5] was caused by a layer of sodium and sodium oxide, formed on the heat-exchange surface. To create a thermal contact resistance equal to those found in these experiments, it is enough to have a layer of sodium and sodium oxide with a thickness of tenths of a millimeter. In a cold trap, where oxides accumulate [6], the thickness of such a layer may be much greater than this; the thermal resistance will therefore also be large. Thus, in calculating the thermal properties of a cold trap, it is necessary to allow for the precipitation of oxides on the heat-exchange surface.

LITERATURE CITED

1. V. I. Subbotin, F. A. Kozlov, and N. N. Ivanovskii, Teplofizika vysokikh temperatur, 1, 409 (1963).
2. A. F. Alabyshev et al., Sodium and Potassium [in Russian], Moscow, Goskhimizdat (1959).
3. T. Hornbeck, Phys. Rev., 2, 217 (1913).
4. C. Bidwell, Phys. Rev., 28, 3 (1926).
5. V. I. Subbotin, M. Kh. Ibragimov, and E. V. Nomofilov, Atomnaya Énergiya, 13, 155 (1962).
6. V. I. Subbotin et al., Atomnaya Énergiya, 8, 30 (1960).

BACK-SCATTERING OF γ-RAYS FROM A SPHERICAL SURFACE

(UDC 537.531.8)

N. F. Andryushin and B. P. Bulatov

Translated from Atomnaya Énergiya, Vol. 19, No. 4,
pp. 392-393, October, 1965
Original article submitted November 23, 1964

In certain practical cases, the necessity arises for determining the dose of scattered radiation inside a closed space (e.g., a spherical cavity with a solid block of substance). Little attention has been paid to this problem. The most complete theoretical solution is that given in [1, 2]. The effect of curvature of back-scattering was studied experimentally in [3, 4].

We have experimentally studied the energy accumulation factor for reflection of γ-rays from Co^{60} and Cs^{137} by a hemispherical water surface (Fig. 1, a, b). In a cylindrical steel tank of diameter 75 cm and height 100 cm, filled with water, we placed aluminum hemispheres of various radii and wall thickness 1 mm. At the bottom of the hemisphere we placed a detector, and at its center a source of γ-rays.

The Co^{60} and Cs^{137} sources, with activity 3-250 millicuries, were of size 4 x 4 x 5 mm. The detector was a SBM-10 counter, encased in tin, aluminum and lead jackets [5, 6], and having a practically constant sensitivity to γ-energy fluxes in the range 0.08-2 MeV. To measure the accumulation factor, we also used an ionization chamber, of which the collecting electrode was the hemisphere in the water, and the high-voltage electrode a thin-walled aluminum hemisphere, fixed inside the other by Teflon spacers (the radius of the first hemisphere was 2 cm greater than that of the second). The working voltage of the chamber was 2.5 kV. During these experiments the tank was placed on glass insulators of height 3 cm.

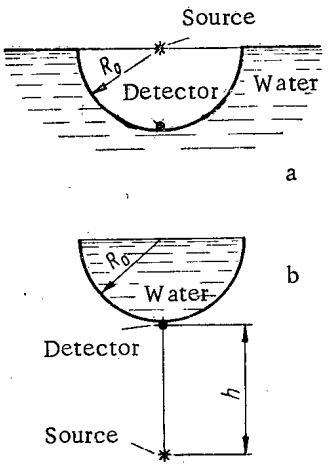

Fig. 1. Experimental layout.

In all the experiments measurements were made in the scattering medium, and then, for measurements without a scatterer, the source-detector system was placed in air. We made a correction for scattering from the thin-walled hemispheres.

B_{re} was found as the ratio of the detector readings with and without the scatterer. In each series of experiments the measurements were repeated ten times. The error in determining $[B_{re} - 1]$ was ± 10%.

In studying back-scattering from convex spherical surfaces (see Fig. 1b) filled with water, the hemispheres were suspended in air at a height of 2 m, while the source was placed in a lead collimator with an aperture angle giving full coverage of the scattering surface.

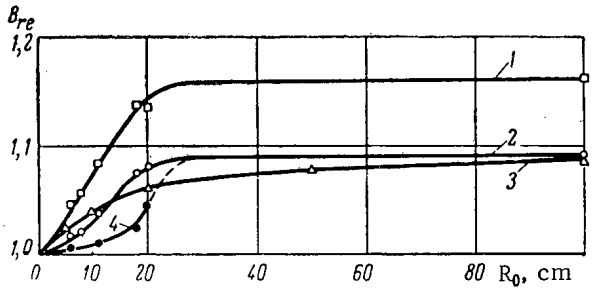

Fig. 2. B_{re} versus radius of curvature.

RESULTS

Figure 2 gives the experimental results at h = 0 (h = height of detector above surface of scatterer). Curves 1 and 2 plot the energy accumulation factor for reflection of γ-rays from Cs^{137} and Co^{60}, respectively. Accumulation

Intensity of Scattered γ-Radiation, J(h), for Various Values of h and E_γ, in Terms of the Intensity at the Point $h = R_0$

Method	Radius of spher. cavity, R_0 cm.	h	$J_{sc}(h)/J_{sc}(h = R_0)$				
			0,7 MeV	1,0 MeV	1,25 MeV	6 MeV	10 MeV
Expt.	20	R_0	1,0	—	1,0	—	—
		$0,75\,R_0$	0,6	—	0,75	—	—
		$0,5\,R_0$	0,48	—	0,61	—	—
		$0,25\,R_0$	0,42	—	0,51	—	—
		0 (Extra-polation)	0,40	—	0,45	—	—
Calc. [2]	10	0	—	0,87	—	—	—
		$0,5\,R_0$	—	0,95	—	—	—
	100	0	—	0,87	—	—	—
	500	0	—	0,78	—	0,81	0,74

factors for infinite radii of curvature were obtained by reflection from a plane water surface. Curve 3 on the same figure gives the results of calculations by the Monte Carlo method, for a spherical cavity with a solid block of concrete, at $E_\gamma = 1$ MeV [2].

The accumulation factor increases with the radius of the hemisphere, reaching limiting values equal to the accumulation factors for reflection from infinite planes [7] (1.16 and 1.087 for γ-rays from Cs^{137} and Co^{60}, respectively). The limiting values are attained for radii of ~20-30 cm, i.e., about 2 or 3 times the free path of the primary photons in water. In measurements with an ionization chamber for hemispheres of radius 20 cm and γ-rays from Co^{60}, the accumulation factor found was 1.10.

The relation between the accumulation factor and the radius can be found from the following considerations. According to [7-9], when an elementary narrow beam of γ-rays falls on the surface of a reflector, the scattered radiation can be considered as if it came from a virtual source at a depth of about 1.0-1.5 of the free path of the primary photons in the substance λ. In the case of a spherical cavity with a radius of R_0, this virtual source is a sphere of radius $(R_0 + \lambda)$, of which each point (for scatterers with Z less than 26) radiates isotropically into the half-space.

As the radius of the cavity increases, the influence of its furthest distant points decreases, owing to the increasing distance between the detector and the scattering elements, and the increased path travelled in the substance by the scattering photons. The region of the scatterer from which secondary radiation falls on the detector is therefore increasingly localized close to the detector, and in the limit becomes a circle of radius ~10 h [7]. For a scattering hemisphere, the accumulation factor varies more markedly with the radius of curvature. When $R_0 < \lambda$, the absence of the second hemisphere and the loss of scattered photons from the edges of the reflector lead to values of B_{re} about half as great as the corresponding values for a sphere, as given in [2]. When $R_0 > \lambda$, the absence of the second half of the sphere and the loss of photons become less important with increasing radius, and the experimental and theoretical curves are almost the same.

The table gives measurements of the spatial distribution of the scattered intensity of γ-radiation along the radius of a hemispherical cavity, and corresponding calculations [2] for spherical cavities in concrete. The relative scattered intensity $J_{sc}(h)/J_{sc}(h = R_0)$ for a hemisphere is about half as great as the corresponding value for a spherical cavity. As seen from the table, the spatial distribution of scattered β-radiation for primary quanta of energy $E_\gamma \leq 10$ MeV and $R_0 \leq 500$ cm is practically isotropic to within 25%.

Curve 4, Fig. 2 is the experimental curve of accumulation factor versus radius of curvature for reflection of γ-rays from Co^{60} by a convex reflector. For $R_0 < \lambda$, the curve found is sharper than in the first case; this may be explained as due to the influence of the radius of curvature and the increased quantity of scattering substance. The limiting accumulation factor is attained at about the same radii of curvature.

LITERATURE CITED

1. M. Leimdörfer, Nucl. Sci. and Engng, 17, 357 (1963).
2. M. Leimdörfer, Nucl. Sci. and Engng, 17, 352 (1963).
3. J. Putman, J. Scient. Instrum., 32, No. 10, 394 (1955).
4. B. Larsson, Private communication cited in [1].
5. B. P. Bulatov, Atomnaya Énergiya, 6, 332 (1959).
6. A. M. Panchenko, Atomnaya Énergiya, 14, 408 (1963).
7. B. P. Bulatov and O. I. Leipunskii, Atomnaya Énergiya, 7, 551 (1959).
8. M. Leimdörfer, Nucl. Sci. and Engng, 17, 345 (1963).
9. B. P. Bulatov, Atomnaya Énergiya, 5, 631 (1958).

All abbreviations of periodicals in the above bibliography are letter-by-letter transliterations of the abbreviations as given in the original Russian journal. *Some or all of this periodical literature may well be available in English translation.* A complete list of the cover-to-cover English translations appears at the back of this issue.

ANGULAR DISTRIBUTION OF THE INTENSITY OF γ - RADIATION SCATTERED BY LEAD AND WATER

(UDC 539.122 : 539.121.72)

L. M. Shirkin

Translated from Atomnaya Énergiya, Vol. 19, No. 4,
pp. 394-395, October, 1965
Original article submitted December 9, 1964

In [1, 2] it was shown experimentally that the angular distribution curve of the intensity of scattered γ-radiation varies only weakly with the range $\mu_0 x$. The sources used by these authors had energies below 1.33 MeV, while the maximum thickness of the material investigated was eight times the free path length.

We have used the Monte-Carlo method to calculate the angular distribution of the intensity of scattered γ-radiation in lead and water. We discussed a plane unidirectional source with energy 4.0 MeV and barrier geometry. The thickness of the lead barrier was 14 times the free path length, that of the water barrier 16 times the free path length (the method of calculation is described in [3]).

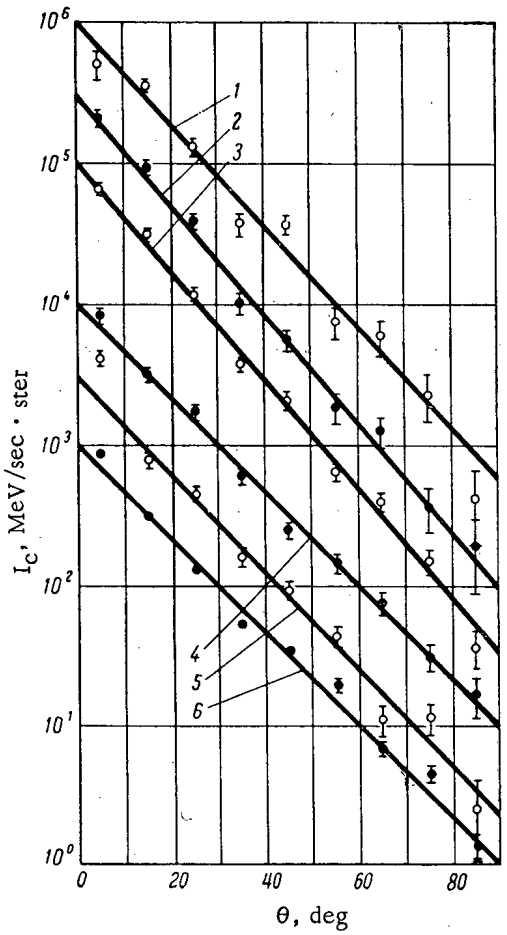

Fig. 1. Angular distribution of intensity of γ-rays scattered in lead and water. For lead: (1) $\mu_0 x \approx 3$; (2) $\mu_0 x \approx 13$; (3) averaging over whole barrier. For water: (4) $\mu_0 x \approx 3$; (5) $\mu_0 x \approx 14$; (6) averaging over whole barrier. O,●) Intensity of scattered γ-quanta in range 10^0.

To shorten the calculations, we used the splitting method [4]. In the case of lead the barrier was divided into 11 layers, in the case of water into 12. The number of γ-quanta passing through a given layer was tripled in calculating the following layer. The number of γ-quantum histories in the first lead layer was 320, that in the first water layer 450.

To improve the statistical accuracy of the results, we used the following procedure. We first constructed the angular intensity distribution of scattered γ-radiation which had passed through each of the layers obtained by splitting. By analyzing these distributions we came to the conclusion that, if the angular distribution curve shape varies with the barrier thickness at all, this variation is very slight. We therefore averaged the angular distribution over three neighboring barriers. The thickness of each successive barrier was greater than the previous one by a factor of $\mu_0 x \approx 1.2$-1.4.

Figure 1 shows the averaged angular intensity distributions of γ-radiation scattered in lead and water. The r.m.s. error for each layer was calculated from the formula

$$\sigma_i^{\Theta} \approx \sqrt{N_i (\Theta_{n+1} - \Theta_n)}\, \overline{E},$$

where $N_i (\theta_{n+1} - \theta_n)$ is the number of γ-quanta passing through the i-th layer and scattered through angles in the range $(\theta_{n+1} - \theta_n)$; $\overline{E}$ is the mean energy of the γ-quanta scattered through these angles.

Figure 1 also gives the angular intensity distributions averaged over the whole barrier. For γ-quanta with initial

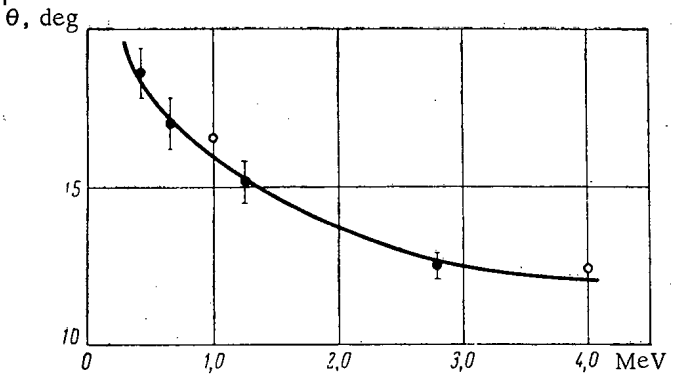

Fig. 2. Energy dependence of angular distribution constant in lead. ●) Experimental data from [5]; O) calculated by Monte-Carlo method.

energy 4.0 MeV in lead, the angular distribution constant θ_0 of the intensity was 11.2°; for water, the corresponding figure was 13.1°.

Similarly, we calculated the angular distribution constant for γ- quanta with energy 1.0 MeV, in lead. The maximum barrier thickness was 7 times the free path length. The averaged value of θ_0 was 15.4°. Figure 2 shows the energy dependence of the angular distribution constant in lead. The results confirm the conclusions reached in [2, 5], namely:

1. The angular distribution constant θ_0 varies slightly with the barrier thickness (up to $\mu_0 x \approx 15$);

2. For gamma quanta with energies $E_0 > 2$ MeV, the angular distribution constants for various materials and energies are almost the same.

LITERATURE CITED

1. Yu. A. Kazanskii, Atomnaya Énergiya, 8, 432 (1960).
2. A. V. Larichev, Atomnaya Énergiya, 11, 443 (1961).
3. L. M. Shirkin, Atomnaya Énergiya, 17, 509 (1964).
4. G. Gol'dshtein, Principles of Reactor Shielding [in Russian], Moscow Gosatomizdat (1961).
5. A. V. Larichev and V. I. Mitin, In symposium, "Problems in Radiation Dosimetry and Shielding" [in Russian], No. 2, Moscow, Gosatomizdat (1963), p. 47.

ANGULAR DISTRIBUTION OF γ-RAYS FROM A POINT SOURCE, SCATTERED IN SHIELDING

(UDC 539.122 : 539.121.72)

A. V. Larichev

Translated from Atomnaya Énergiya, Vol. 19, No. 4,
pp. 395-396, October, 1965
Original article submitted December 21, 1964

The most detailed specification of the field of scattered radiation is that given by its spectral-angle characteristics, the so-called angular energy distribution (or spectral-angular distribution). From a knowledge of the spectral-angular characteristics of scattered radiation, we can comparatively simply solve many practical problems on the radiation field behind a shielding medium, even with complex boundary conditions.

Much experimental work has recently been done on the spectral-angular characteristics of γ-rays passing through shielding media. Of the possible basic source geometries, that most fully studied in this way is the flat unidirectional source [1-5]. It is very noteworthy that there is an empirical law for the angular distribution of the intensity of scattered radiation, of the form

$$I(\theta) = ae^{-\theta/\theta_0}, \quad (1)$$

where $I(\theta)$ is the intensity per unit solid angle of radiation scattered through an angle θ; a and θ_0 are constants, characteristic for a given medium and for a given energy of the incident radiation, θ_0 being practically independent of the depth of penetration of the radiation, other things being equal.

Less attention has been paid to isotropic point sources [6-9], although the first results were published before those given above. However, the author of [8] succeeded in obtaining an empirical law for the angular distribution of I_θ, the intensity scattered per unit solid angle:

$$I_\theta = I(\theta)\, 2\pi \sin\theta\, d\theta = a' e^{-\theta/\theta_0'}, \quad (2)$$

where a' and θ_0' are constants essentially similar to a and θ_0 in (1).

In [5, 8] it was shown that a (or a') can be calculated from the energy accumulation factors B_E and the constants θ_0 (or θ_0'). As there are now plenty of data on B_E, to calculate $I(\theta)$, or I_θ from (1) and (2), we need to know how θ_0 and θ_0' vary with the atomic number Z and the energy of the incident γ-rays, E_γ. Reference [5] contains data θ_0 for lead, iron and aluminum in the energy range 0.15-2.76 MeV, while [8, 9] give data on θ_0' for a Co^{60} source in water,, iron or lead, and for an Au^{198} source in iron.

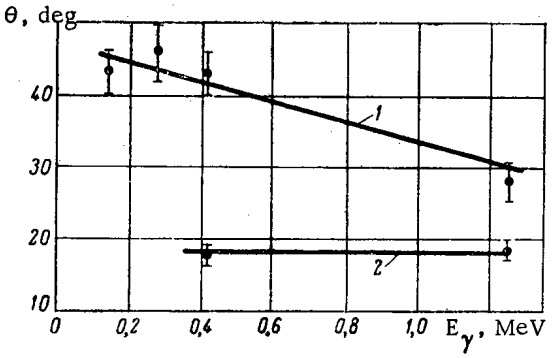

θ_0' calculated from experimental data; 1) aluminum; 2) lead.

We have attempted to supplement the data on θ_0'. Measurements of angular energy distributions were made with a scintillation spectrometer with NaI crystal by the method described in [3]. The apparent spectra were converted to true gamma ray spectra by means of the inverse matrix of the sensitivity function of the spectrometer [10]. In the range 10-70° a law of the form of (2) was found to hold for γ-rays from Ce^{141} (0.145 MeV), Hg^{203} (0.28 MeV), Au^{198} (0.411 MeV) and Co^{60} (mean energy 1.25 MeV), in aluminum, and for γ-rays from Au^{198} and Co^{60} in lead.

Within the experimental error, the values of θ_0' for γ-rays from Co^{60} agreed with those given in [9]; The figure shows the values of θ_0' calculated from our experimental data.

LITERATURE CITED

1. J. Hubbell, E. Hayward, and W. Fitus, Phys. Rev., 108, 1361 (1957).
2. E. L. Stolyarova et al., In symposium "Instruments and Methods for Radiation Analysis" [in Russian], No. 3 Moscow, Gosatomizdat (1962), p. 15.
3. A. V. Larichev and L. F. Klimanova, In symposium "Instruments and Methods for Radiation Analysis" [in Russian], No. 3, Moscow, Gosatomizdat (1962), p. 37.
4. A. V. Larichev, Topics in the Physics of Reactor Shielding [in Russian], Moscow, Gosatomizdat (1963).
5. A. V. Larichev and V. I. Mitin, In symposium "Aspects of Dosimetry and Anti-Radiation Shielding" [in Russian], No. 2, Moscow, Gosatomizdat (1963), p. 47.
6. G. Whyte, Canad. J. Phys., 33, 96 (1955).
7. Yu. A. Kazanskii and S. P. Belov, "Physics of Nuclear Fission" [in Russian], Appendix 1 to journal "Atomnaya Énergiya," Moscow, Atomizdat (1957), p. 123.
8. Yu. A. Kazanskii, Atomnaya Énergiya, 8, 432 (1960).
9. Yu. A. Kazanskii, S. P. Belov, and É. S. Matusevich, Atomnaya Énergiya, 5, 457 (1958).
10. A. V. Larichev and V. V. Laricheva, In symposium "Aspects of Dosimetry and Anti-Radiation Shielding" [in Russian], No. 1, Moscow, Gosatomizdat (1962), p. 150.

ANGULAR DISTRIBUTION OF NEUTRON DOSE CLOSE TO THE AIR – GROUND BOUNDARY

(UDC 539.125.52)

I. V. Goryachev

Translated from Atomnaya Énergiya, Vol. 19, No. 4,
pp. 396-397, October, 1965
Original article submitted January 15, 1965

Based on an analysis of computed data obtained by the Monte-Carlo method, it has been shown [1] that the angular distribution function for the neutron dose from a point, isotropic, fission source in an infinite, air medium at distances greater than a mean free path can be described by the equation:

$$F(\Omega, \Theta) = 0.033 + 0.4045e^{-0.03345\Theta}, \quad (1)$$

where $F(\Omega, \theta)$ is the fraction of the total neutron dose at a given point in space per unit solid angle coming from a direction which is characterized by the scattering angle θ measured from the line connecting source and detector. Therefore, the condition

$$2\pi \int_0^{\pi} \sin \Theta F(\Omega, \Theta)\, d\Theta = 1. \quad (2)$$

is fulfilled.

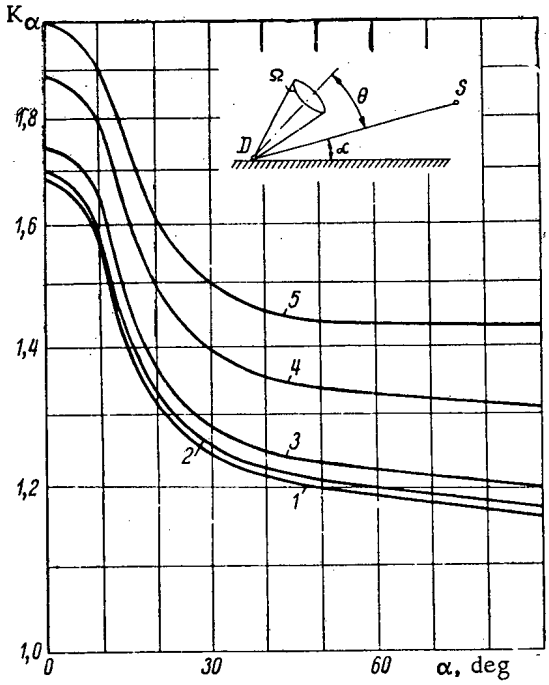

Dependence of the coefficient K_α on angle α for ground surfaces of differing composition: 1) soil (H, 1.24%; O, 52.38%; Al, 7.85%; Si, 38.53%); 2) soil (H, 1.45%; O, 55.23%; Al, 7.32%; Si, 36.02%); 3) soil (H, 2.24%; O, 57.36%; Al, 7.08%; Si, 33.32%); 4) water; 5) absolutely black surface.

This dependence is in good agreement with experimental data in [2] where a study was made of the angular distribution of neutron dose for nuclear explosions in the atmosphere. The qualitative agreement of the results in the paper mentioned indicates an identity of form for the angular distribution of neutrons from a point, isotropic, fission source in an infinite air medium and close to the air-ground interface. This conclusion was also verified theoretically and experimentally by measurements made at the TSR-II reactor which was raised above ground level. However, although the angular distribution function for neutron dose from a point, isotropic, fission source in an air medium [1], where the detector records radiation in a 4π geometry, agrees in form with the angular distribution function for neutrons near the air-ground interface, where the detector records neutrons which arrive only from the upper half-space (if neutron reflection from the ground is neglected), i.e., in 2π geometry, the numerical values of the constant term and of the factor multiplying the exponential in Eq. (1) will be different. Obviously, when the source and detector are located at the air-ground boundary, the values of the coefficients mentioned above will be twice as big as the values obtained for Eq. (1) for an infinite air medium if, in first approximation, the ground is considered an absolutely black body. For other locations of the source with

respect to detector and ground surface, characterized by the angle α between source-detector direction and the surface of the ground, these coefficients will have some intermediate values. Thus one can write

$$F(\Omega,\ \Theta,\ \alpha) = K_\alpha (0.033 + 0.4045e^{-0.03345\Theta}). \tag{3}$$

We first consider the hypothetical case of an absolutely black ground surface. Integration of Eq. (3) over the upper half-space can be carried out in the following manner:

$$2K_\alpha \left[\pi \int_0^\alpha \sin\Theta\,(0.033 + 0.4045e^{-0.03345\Theta})\,d\Theta + \int_\alpha^{\pi-\alpha} \sin\Theta \left(\pi - \arccos\frac{\operatorname{tg}\alpha}{\operatorname{tg}\Theta} \right) \times (0.033 + 0.4045e^{-0.03345\Theta})\,d\Theta \right]. \tag{4}$$

By definition of the angular distribution function, this integral must be equal to one. Hence it is easy to find values of the coefficient K_α for any angle α. Values of the coefficient K_α computed in this way for an absolutely black ground surface are shown in the figure.

The effect of the neutron albedo of the ground can be taken into account by using the results in [4] where it was shown that the integral neutron albedo dose from the ground surface for a fission source in air is given by the expression

$$A(\beta) = 0.435 \frac{\Sigma_r - \Sigma_H}{\Sigma_r} \cos^{2/3}\beta, \tag{5}$$

where Σ_G and Σ_H are the total macroscopic neutron cross sections of soil and of the hydrogen contained in a given soil; β is the angle of incidence of the neutrons at the surface of the ground measured from the normal.

Since part of the total dose at a detector located near the surface of the ground is produced by neutrons reflected from the ground, the value of the coefficient K_α in Eq. (3) will be different than that for an absolutely black ground. It can be found from the equation:

$$\int\int [1 + A(\beta)]\, K_\alpha (0.033 + 0.4045e^{-0.03345\Theta})\,d\Theta\,d\varphi = 1, \tag{6}$$

whose integration is carried out over the upper half-space. Values of the coefficient K_α calculated by this equation are given in the figure for soils of different moisture content, which determines the hydrogen content, and for water.

In conclusion, we note that the angular dose distribution of neutrons reflected from the ground is described by a cosine law according to [4].

LITERATURE CITED

1. R. French, Health Phys., 8, 229 (1962).
2. R. Ritchie and G. Hurst, Health Phys., 1, 390 (1959).
3. M. Wells, Trans. ANS, 6, 436 (1963).
4. R. Freanch and M Wells, Nucl. Sci. Engng, 19, 441 (1964).

SPECTRAL DISTRIBUTION IN THE SURFACE ATMOSPHERE OF γ-RAYS FROM A POINT SOURCE OF Co^{60} SHIELDED BY ALUMINUM

(UDC 621.039.58 : 539.121.73)

V. A. Ionov

Translated from Atomnaya Énergiya, Vol. 19, No. 4,
pp. 397-400, October, 1965
Original article submitted April 26, 1965

The γ-ray field in the surface layer of the atmosphere has been investigated by many people. The dose and angular distribution of intensity from a point source has been obtained [1, 2]. However, the spectral and spectral-angle functions have only been computed for extended sources [3, 4]; the corresponding functions for point radiation sources with an absorbing layer have not yet been obtained.

In this paper, the results of an experiment, schematically shown in Fig. 1, are described. The experiment was performed in the area of the high tower of the Institute of Applied Geophysics. A scintillation counter with an 80 x 60 mm NaI(Tl) crystal was installed on horizontal arms 6 m long which were extended from the working area of the tower. The Co^{60} source, with an activity of the order of 3 g-equiv Ra, was moved about along with an aluminum shield 2 x 2 m by means of a shipping container. The distance between the source and the surface of the ground was 15 cm. Energy spectrum measurements was made for heights H of 50 and 100 m, for source separations L of 25, 50, 100, 150, and 200 m, and for absorber thicknesses d of 0, 1, 2, 4, 8, and 12 cm.

The scintillation counter pulses were analyzed by an AI-100-1 instrument. The energy resolution of the spectrometer was 12.5% for the Cs^{137} line. The instrumental spectrogram was unfolded into a Compton distribution by means of a numerical matrix constructed by interpolation of calibration spectra from the isotopes Hg^{203}, Cr^{51}, Cs^{137}, Nb^{95}, Zn^{65}, and Co^{60}. The matrix steps were uniform over the entire energy range (ΔE = 146 keV). From computed data for a broad, parallel beam [5], the spectra were corrected for spectrometer efficiency. The results of the unfolding of the measured γ-ray spectra are given in Fig. 2 in the form of a spectral function I(E, H, L, d) normalized to the intensity of the direct beam:

$$J_0 = \frac{G}{4\pi H^2 (1 + \mathrm{tg}^2 \Theta)} e^{-\sqrt{1+\mathrm{tg}^2\Theta}\,(\mu_{air} H + \mu_{Al} d)},$$

where G is the source activity; Θ is the arctan L/H. The following values were assumed for the absorption coefficients: $\mu_{air} = 7.14 \cdot 10\ m^{-1}$, $\mu_{Al} = 0.15\ cm^{-1}$.

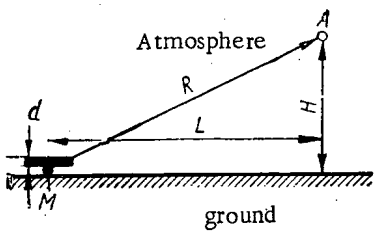

Fig. 1. Experimental geometry; M) Co^{60} source; A) isotropic detector; d) aluminum shield thickness; L) source separation from tower axis; H) detector height above ground; R) source-detector distance.

The statistical error in the measurements was 2-3%, and only in individual cases rose to 5-7%. The total error of the resultant spectral distributions was higher because of the errors introduced in unfolding the instrumental spectra, and was not more than 10% for d < 4 cm and 20% for d > 4 cm.

The error in the function I• can be determined from a comparison of the energy distribution I_{pl} for γ-radiation from an infinite, plane, isotropic source in air and the distribution which is obtained by integration of the γ-radiation from point sources on the ground surface (Fig. 3). In the curves shown, the intensity of the unscattered quanta $J_0(H, E_0)$ is arbitrarily shown in the form of a rectangle with base

•The energy distribution function I has dimensions MeV/Mev·cm^2·sec.

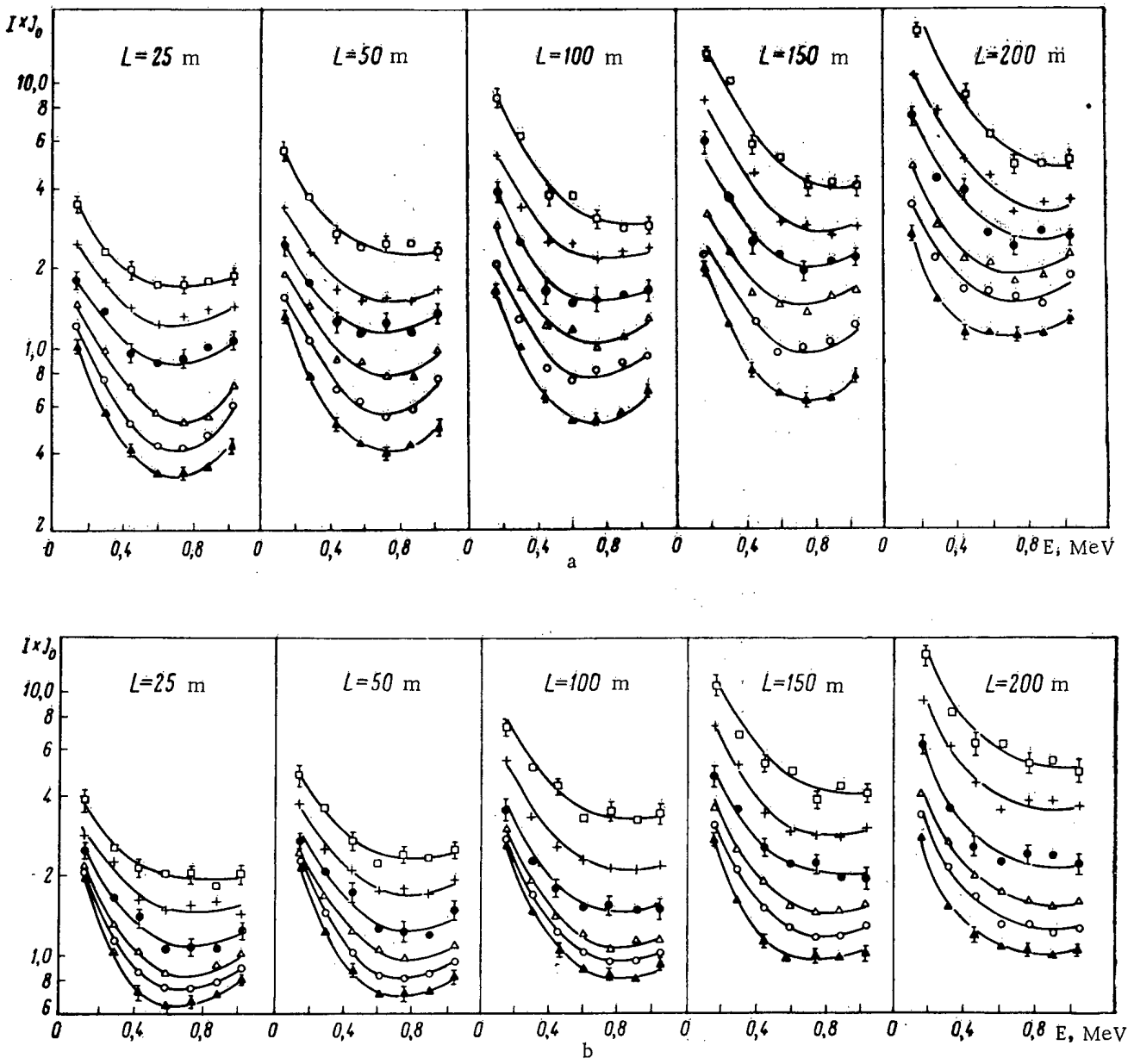

Fig. 2. Normalized spectral distributions of air-scattered γ-rays from a point source of Co^{60} located at a height of 50 (a) and 100 m (b) above the ground, for various values of L and aluminum absorber thicknesses, cm: ▲) 0; ○) 1; △) 2; ●) 4; +) 8; ○) 12.

ΔE = 0.05 MeV and height $J_0(H, E_0)\Delta E = J_0(H, E_0)$. The activity of the plane source was assumed to be σ = 1 MeV/cm^2 · sec. For the two values of H (50 and 100 m), the compared energy distributions agreed within limits of a few percent.

To compare the experimental results with the data in [2], the γ-ray dose in air from point sources on the ground was computed for d = 0.

The ratio $\alpha = P_1/P_2$ (P_1 and P_2 are the γ-ray doses in layered and homogeneous media, respectively), which was obtained by Monte-Carlo calculations of the field [2], and the corresponding experimental data are shown in the table.

The overestimate of 5-10% in the experimental data can be explained by the failure to include corrections for γ-ray scattering from the metallic structure of the tower and from parts of the shipping container in analyzing the

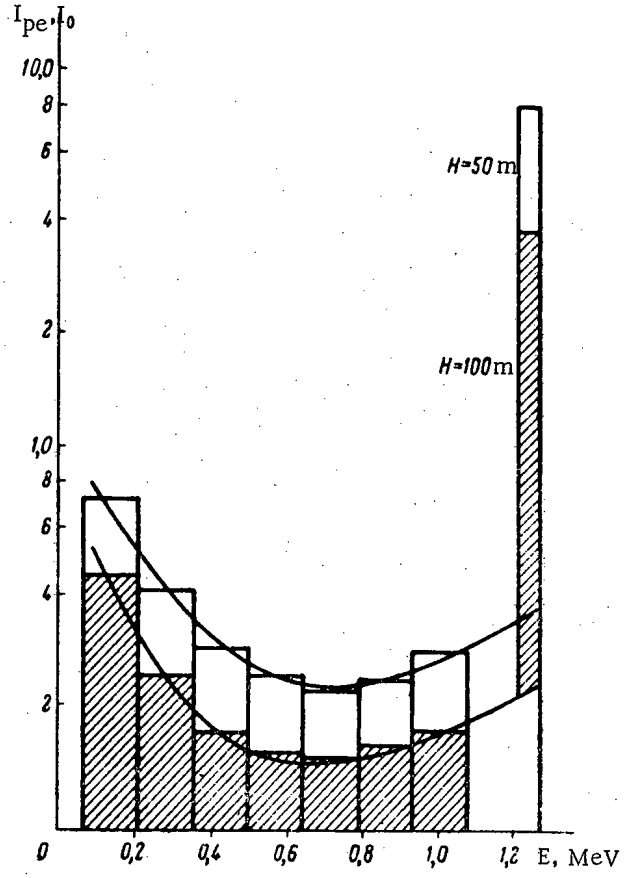

Fig. 3. A comparison of the γ-ray distributions in air I from an infinite, plane, isotropic source (plane source) obtained by interpolation of data in [3] (smooth curves) and from integration of the distribution function for a point source d = 0 (histogram) for heights of 50 and 100 m.

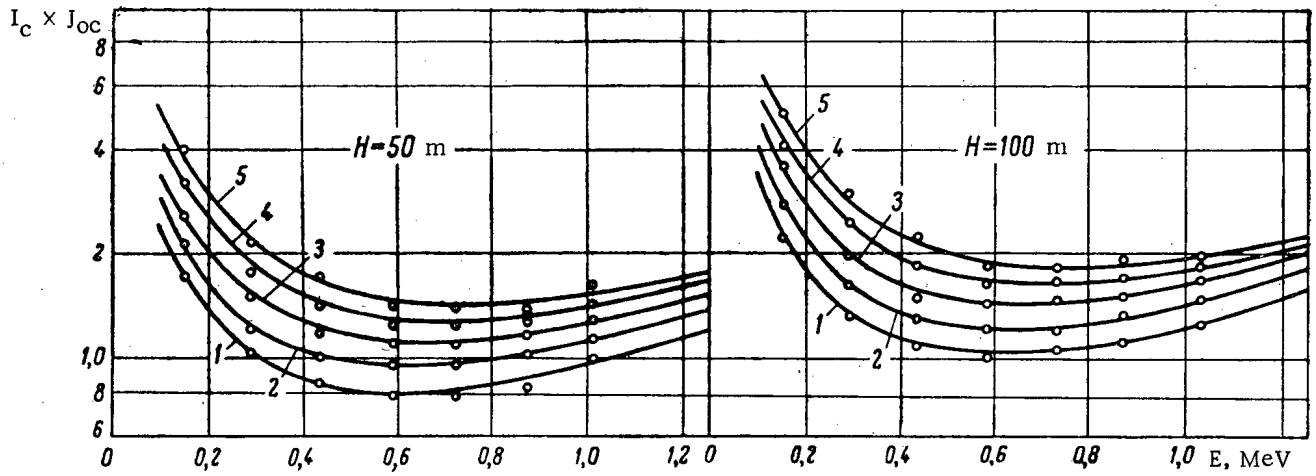

Fig. 4. Normalized distributions of γ-rays scattered in air from vertical columns at various values of L, m: 1) 25; 2) 50; 3) 100; 4) 150; 5) 200.

Relative Comparison of γ-Ray Doses in Layered and Homogeneous Media

Geometry	Experimental data	Monte-Carlo calculation [2]
$H=100$ m, $L=100$ m, $\mu R=1,0$	1,15	1,04
$H=50$ m, $L=150$ m, $\mu R=1,1$	1,05	1,0
$H=50$ m, $L=200$ m, $\mu R=1,46$	1,10	0,95
$H=100$ m, $L=200$ m, $\mu R=1,6$	1,08	1,0

results. In particular, in estimating the amount of albedo from the tower structure (diameter of tower structure 2.5 m; separation from detector, 8 m), a value of the order of 1-2% was obtained from the data in [6].

To calculate the energy distribution in air for γ-radiation from thick sources of finite dimensions (for example, portions of rock with increased activity), it is necessary to compute the radiating element in the form of a vertical column with elementary emission area at the surface.

In Fig. 4 are shown distributions of the γ-radiation from a vertical column which were obtained by integration of the γ-radiation from point sources shielded by 0-12 cm thicknesses of aluminum. The results, like the previous ones, are normalized to the intensity of the direct radiation from the column:

$$J_{0c}=\frac{J_0 H}{R^3}e^{-\mu_{air}R}.$$

A good approximation to the experimental curves is given by the expression

$$I_c(E, H, L)=k(0.80+0.0076)E^{-1.2}e^{(2.05-0.0023L)E}.$$

The author is deeply grateful to R. M. Kogan and I. M. Nazarov for valuable comments during the organization of the experiment and for discussions of the results, and also to V. A. Vorob'ev, A. V. Dmitriev, and Sh. D. Fridman for assistance.

LITERATURE CITED

1. O. I. Leipunskii and V. N. Sakharov, Atomnaya Énergiya, 6, 585 (1959).
2. M. Berger, J. Appl. Phys., 28, 1902 (1957).
3. R. M. Kogan and Sh. D. Fridman, Izv. AN SSSR, Ser. geofiz., No. 4, 530 (1960).
4. V. A. Vorob'ev, Atomnaya Énergiya, 16, 69 (1964).
5. W. Miller and W. Snow, Nucleonics, 19, No. 11, 174 (1961).
6. B. P. Bulatov and E. A. Garusov, Atomnaya Énergiya, 5, 12, 631 (1958).

All abbreviations of periodicals in the above bibliography are letter-by-letter transliterations of the abbreviations as given in the original Russian journal. *Some or all of this periodical literature may well be available in English translation.* A complete list of the cover-to-cover English translations appears at the back of this issue.

LIGHT PENCIL

(UDC 539.16.07)

A. A. Kurashov and V V. Paramonov

Translated from Atomnaya Énergiya, Vol. 19, No. 4,
pp. 400-401, October, 1965
Original article submitted May 21, 1965

In recent years, the number of problems in experimental nuclear physics which are solvable with the help of multidimensional analyzers and computers has expanded considerably [1, 2]; further, an instrument, the so-called light pencil, has proved to be extremely useful [3]. With its help, the experimenter, using a cathode-ray tube (CRT), can affect specific elements of the programmed memory of an analyzer.

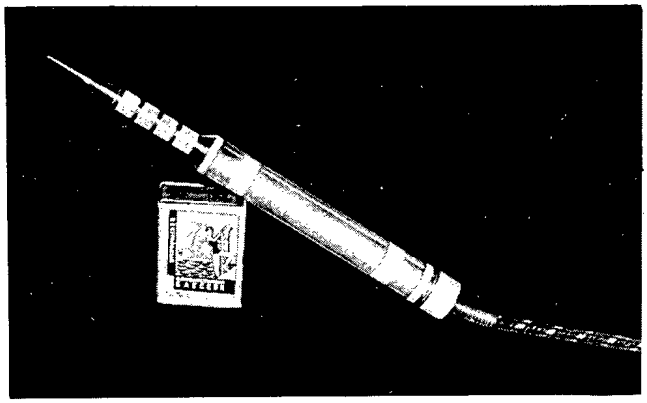

Fig. 1. Light pencil.

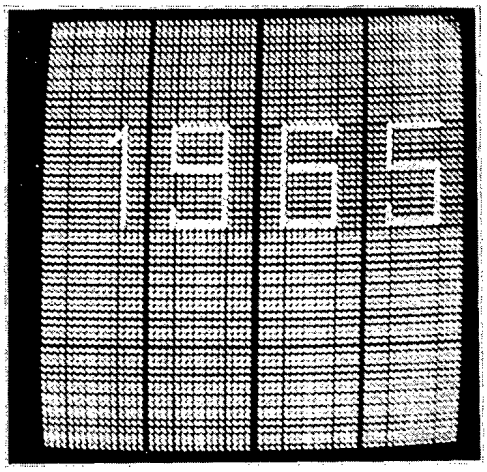

Fig. 2. Photograph of cathode ray tube screen operated in conjunction with a programmed memory. The bright points correspond to memory cells marked by the light pencil.

The operating principles of a memory which is programmed by means of the light pencil consist of the following. On the CRT, a point raster is produced, the number of points of which equals the number of cells in the memory. The motion of the beam of the CRT occurs synchronously with the operation of the address register of the memory in accordance with a program of continuous generation of data received. The experimenter directs the light pencil to the desired point of the raster, and the light pencil emits an electrical impulse at the moment when the electrical beam is at the given point. This pulse is transmitted to the memory together with a simultaneous instruction to write a "1" in the corresponding cell. Successively applying the light pencil to the required points of the raster, the experimenter may mark memory cells. Then, each time the address register selects a marked memory cell a "1" will be read out and rewritten. The signal from the readout of the one will also be an instruction through which further operations will be performed.

The action of the experimenter on the programmed memory by means of the light pencil makes it possible to single out for recording only data that is of interest and, thus to reduce the amount of recorded information, i.e., the number of units in the working memory. It is also possible to set up a program to extract or analyze the data.

A photoelement, photodiode, phototransistor, etc., can serve as the sensing element in the light pencil. In the cyclotron laboratory of the I V. Kurchatov Institute of Atomic Energy, a light pencil with an FÉU-60 photomultiplier as sensor is used (Fig. 1). The photomultiplier is located in a dural housing 17 mm in diameter. The CRT rectifier serves as a source of power. The working end of the pencil is made up in the form of a cone with an opening 0.5 mm in diameter. The distance from the

end of the pencil to the photocathode is 85 mm. The signal amplitude at the FÉU anode is 0.2-0.5 V. Experience has shown that it is not necessary to use a light pipe to fill the space between the end of the pencil and the FÉU photocathode. In scattered light, the pencil does not produce spurious signals, making it possible to use the pencil with normal illumination.

The spectral distribution of the energy emitted by the CRT phosphor during excitation should have a maximum in the wave length region corresponding to the greatest sensitivity of the photomultiplier photocathode (~4500 A). Type A, B, V, and M phosphors have a such a characteristic. The fluorescence time constant of the phosphors is 50-60 μsec. The rise time of the pulse at the FÉU anode has the same time constant. To avoid error in selecting the associated memory cell because of delay in shaper operation, its threshold is set at a sufficiently low level.

An example of writing done with the light pencil is shown in Fig. 2.

LITERATURE CITED

1. D. Bromley et al., Proceedings of the Conference on Utilization of Multiparameter Analyzers in Nuclear Physics. Grossinger, New York (1962).
2. D. Bromley, Nucl. Instrum. and Methods, 28, 160 (1964).
3. J. Kane, Nucl. Instrum. and Methods, 25, 141 (1963).

HUMAN BIOLOGICAL DOSE FROM INTERNAL RADIATION PRODUCED BY Sr^{90}

(UDC 577.391.087)

V. M. Malykhin, A. A. Moiseev, and V. P. Shamov

Translated from Atomnaya Énergiya, Vol. 19, No. 4,
pp. 401-403, October, 1965
Original article submitted February 18, 1965

Calculations of the accumulation of Sr^{90} in the body of the "standard" man [1] and of the skeletal burden as a function of the time of intake of Sr^{90} along with food play an important role in predicting the internal radiation levels of the population in future years in association with the observed clearing nuclear test products from the atmosphere.

To simplify such calculations, one can assume that the deposition of Sr^{90} from the atmosphere is basically complete at the time selected for the beginning of the reporting period and that contamination occurs mainly by plant uptake of Sr^{90} from the soil through the root system. Further, it is assumed that the Sr^{90} content in objects in the environment decreases exponentially. Because of the complexity of the calculations, washout of Sr^{90} from the soil is not taken into account. For $\lambda_w \approx 0.015\ yr^{-1}$ [2], such an approximation overestimates doses and levels of accumulation by no more than 20-30%.

It has been shown in several papers [3-6] that the accumulation of osteotropic isotopes in the human body and the resultant dose burden are better described by a power function model than by the widely used exponential model.

Because of this, in calculating q (nCi), the Sr^{90} content in the human body, we used the expression:

$$q(t)=\frac{1}{100}Rf_1f_2'Ae^{-\lambda(t-1)}\frac{t^{1-n}-1}{1-n}=BRe^{-\lambda(t-1)}(t^{1-n}-1), \quad (1)$$

where R is the Sr^{90} content in the human food ration, assumed to be 1.0 pCi/day at the initial time t (days); $f_1=f_2$ = 0.3 are the fractions of the isotope which are transferred from the gastrointestinal tract to the blood and from the blood to the critical organ, respectively; A and n are numerical parameters of the power function model; B is a constant; $\lambda = 7 \cdot 10^{-5}\ day^{-1}$ is the physical decay constant of the isotope.

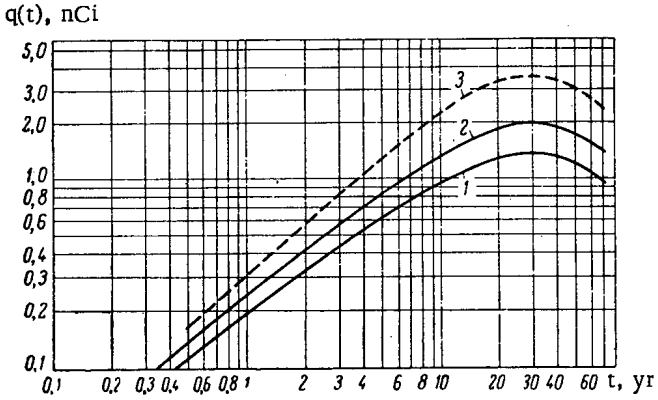

Fig. 1. Sr^{90} content, q(t), in the human body as a function of time t for an initial food ration activity of 1 pCi Sr^{90}: 1) power function model, A = 0.522, n = 0.175 [3]; 2) power function model, A = 0.515, n = 0.216 [4]; 3) exponential model.

Results of the calculations of the levels of Sr^{90} accumulation in human skeletal tissue, q(t), for numerical values of the parameters A and n recommended in [3, 4] are shown in Fig. 1.

The value of the human biological dose from internal radiation, D (rem), is found by integration of the "burden" q(t):

$$D=\int_{t_0=1}^{t} q(\tau)P_1\,d\tau. \quad (2)$$

The weighting factor P_1 is the dose rate resulting from 1 nCi content of Sr^{90} in the body;

$$P_1=\frac{18.6\Sigma E\ \mathrm{RBE})n_i}{m},$$

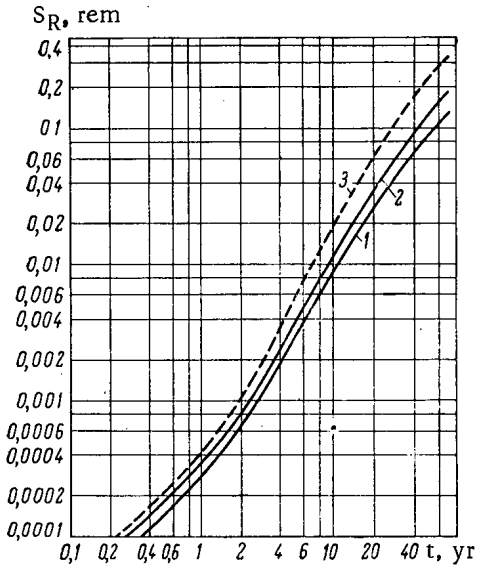

Fig. 2. Time dependence of the dose coefficient $S_R(t)$ for an initial food ration Sr^{90} activity of 10 pCi (see Fig. 1 for meaning of symbols on curves).

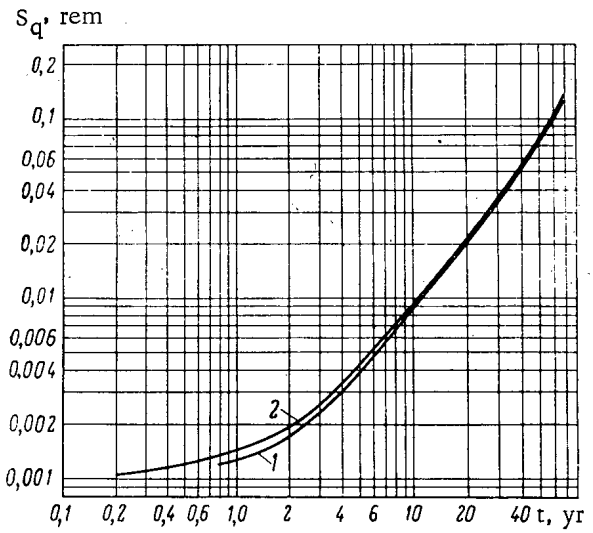

Fig. 3. Time dependence of the dose coefficient $S_q(t)$ for a Sr^{90} body burden of 1 nCi at time t (see Fig. 1 for meaning of symbols on curves).

where RBE is the coefficient for relative biological effectiveness. In the case under consideration, the mass of the organ (skeleton) $m = 7 \cdot 10^3$ g; for Sr^{90}, the effective energy $\Sigma E(RBE)n_i = 5.5$ MeV/disintegration; $P_1 = 4.6 \cdot 10^{-3}$ rem/yr or $4 \cdot 10^{-5}$ rem/day [1]. Substituting expression (1) in relation (2) and integrating over time, we obtain

$$D = BRP_1 \left\{ \frac{e^{\lambda t_0}}{\lambda^{2-n}} [\Gamma(2-n;\ \lambda t) - \Gamma(2-n;\ \lambda t_0)] - \frac{1-e^{-\lambda(t-1)}}{\lambda} \right\}, \tag{3}$$

where Γ is the incomplete gamma-function.

For an arbitrary amount of Sr^{90} in the initial food ration, R (pCi/day), the value of the dose can be represented in the form:

$$D = S_R(t)\, R.$$

The coefficient $S_R(t)$ is the absorbed dose of internal radiation accumulated after a time t (days) following the consumption of a food ratio which contained 1 pCi Sr^{90} at t = 0. Results of the calculation of the dose coefficient $S_R(t)$ are given in Fig. 2.

The biological dose D' can also be computed from the content q (nCi) of the isotope under consideration in the body at the time of observation t. Solving Eq. (1) for R, and substituting its value in relation (3) we obtain:

$$D' = \frac{q(t)\, P_1}{e^{-\lambda t}(t^{1-n}-1)\lambda^{2-n}} \{\Gamma(2-n;\ \lambda t) - \Gamma(2-n;\ \lambda t_0) - \lambda^{1-n} e^{-\lambda t_0}[1-e^{-\lambda(t-1)}]\}. \tag{4}$$

This relation can be written in the form:

$$D' = S_q(t)\, q.$$

The coefficient $S_q(t)$ is the absorbed dose during a time t when the Sr^{90} content in skeletal tissue at the time of observation is 1 nCi. The time dependence of the dose coefficient S_q is shown in Fig. 3.

To estimate the effect of the type of model used to describe Sr^{90} metabolism in the body on the value of the dose, calculations were also made in accordance with the often used exponential model with an effective biological half-life of $6.4 \cdot 10^3$ days [1]. These results are shown in Figs. 1 and 2 by dashed lines.

The coefficients $S_R(t)$ we have computed make it possible to determine the tissue dose for arbitrary levels of R (pCi/day), the initial (t = 0) Sr^{90} content in the food ration, or of the amount q (nCi) of that isotope in the body at time of measurement t, and they can be used for predicting irradiation of the skeleton by Sr^{90} which has been deposited in global radioactive fallout.

LITERATURE CITED

1. Radiation Shielding [in Russian], Moscow, Gosatomizdat (1961).
2. Report of the UN Scientific Committee on the Effects of Atomic Radiation, A/5216 (1962).
3. S. Cohn et al., Radiation Res., 17, 173 (1962).
4. M. Bishop et al., Internat. J. Radiation Biol., 2, 125 (1960).
5. S. Susumu et al., Health Phys., 9, 529 (1963).
6. S. Cohn et al., Radiation Res., 19, 104 (1963).

XVIII SESSION OF THE LEARNED COUNCIL OF THE JOINT INSTITUTE FOR NUCLEAR RESEARCH

V. Biryukov and Yu. Ryabov

Translated from Atomnaya Énergiya, Vol. 19, No. 4,
pp. 404-406, October, 1965

The XVIII Session of the Learned Council of the Joint Institute for Nuclear Research convened May 31 through June 4, 1965 in Dubna. Chairing the session was the Director of the Joint Institute, Academician N N. Bogolyubov, Vice-Director, Professor J. Ulehla, and Vice-Director Professor E. Fenyves. The main point on the agenda of the session consisted of scientific reports on the results of research by scientists on the Joint Institute staff or from laboratories of member-nations of the Joint Institute.

Members of the Learned Council heard seven reports presented in competition for the Joint Institute awards for outstanding research. Representing a panel of authors, physicists at the Joint Institute and at institutes in Bulgaria and Czechoslovakia, M. G. Shafranova reported the findings resulting from a complex of research entitled "Development of research techniques on elastic scattering of high-energy protons and π-mesons on protons and nuclei in the coulomb interference region; discovery of constructive interference in pp-scattering and investigation of the energy dependence of the real part of the amplitude of elastic pp-scattering." One of the techniques involves the use of multiple traversals of an internal proton beam in an accelerator through a thin hydrogenous target, with recording of the recoil protons. A special set of operating conditions has been elaborated for a cloud chamber in a second method devised to permit recording of recoil protons in the chamber gas through which a beam of π-mesons with an intensity of about 10^4 per acceleration cycle was passed. Detailed investigations of elastic pp-scattering over the course of several years revealed an interesting effect in the region of very low scattering angles: the differential cross section is greater than values based on the simple diffraction theory of spinless particles. In this angular region electromagnetic interaction plays a substantial role, so that interference between the coulomb amplitude and nuclear amplitude becomes possible. Analysis of the results leads us to infer the existence of a negative real part in the scattering amplitude, and so the existence of constructive interference in pp-scattering. Experimental results are in agreement with predictions based on dispersion relations. The energy dependence of the effect was studied subsequently, and the ratio of the parts of the complex amplitude α-ReA/ImA were found to vary from -0.17 ± 0.07 (at $E_{kin} = 2$ GeV) to -0.25 ± 0.07 (at $E_{kin} = 10$ GeV). The authors arrived at an estimate of the real part of the amplitude in their study of elastic πp-scattering also. Here the nature of the nuclear forces is the same as in pp-scattering, and is again in agreement with dispersion relations predictions.

"The quasi-potential method in field theory" was the title of a paper by R. N. Faustov reporting on work proposed by theoreticians of the Joint Institute. This method is being developed with success at the Dubna Joint Institute for Nuclear Research over the past several years; the Dubna work in this area has won wide acclaim. The authors demonstrated that a system of two interacting particles can be described in quantum field theory by a Schrödinger type equation with generalized complex potential dependent on the energy. The general properties of the quasi-potential were investigated. It was found that a local potential can be constructed for bound states as a superposition of Yukawa potentials with energy-dependent intensities. The authors developed a method for studying the analytic properties of partial amplitudes in the l-plane and studied the asymptotic properties of the total scattering amplitude, demonstrating that the scattering amplitude in field theory is non-Reggeian in the general case. The quasi-potential method is being applied to the study of the amplitudes of multichannel reactions. The method has proved a highly effective tool in computing energy levels of bound states in quantum electrodynamics.

A one-meter bubble chamber immersed in a magnetic field has been built at the Nuclear Problems Laboratory. A report on the device was presented by Yu. A Budagov. The chamber, featuring a sensitive volume of 200 liters, is filled with propane or with some other heavy liquid, and exhibits high recording efficiency for γ-rays. The operating cycle lasts from 9 to 1 sec. The authors used their original designs in building the chamber. The chamber is placed in a magnet of 17 kOe field strength and a magnetic channel was set up to bombard the chamber with a beam of π-mesons. Research designed to analyze hydrodynamical processes in bubble chambers has been rewarded with a

general method for hydrodynamical calculations of bubble chambers of any dimensions. The possibility of achieving a high-efficiency resonance mode of operation of bubble chambers at frequencies to 50 cycles per second has been demonstrated. The designs are being used to build bubble chambers in other institutes. About 60,000 plates have been taken using this chamber.

V. S. Evseev reported to the Learned Council on the results of experiments geared to detect the maximum possible asymmetry in the angular distribution of neutrons emitted in the absorption of polarized μ-mesons by nuclei. Measurements of the asymmetry factor in synchrocyclotron experiments on low-energy neutrons (about 10 MeV) yielded an unexpectedly high value (about -0.35) exceeding the theoretical prediction by a factor of 1.5 to 2. Further investigation showed a growth in the asymmetry factor with increased neutron energy, and the maximum asymmetry possible, $-(1.00 \pm 0.15)$, was reached in the 20-30 MeV region. This team of scientists also studied the angular distribution of neutrons of about 40 MeV energy emitted in μ-capture by sulfur nuclei. Here the asymmetry factor again came out close to -1. This value is a whole order of magnitude higher than the calculated results based on the universal weak interaction theory (-0.1). Attempts to account for this phenomenon have been fruitless to date.

N. I. Petrov delivered a report on a broad range of studies on the decay properties of K_2^0-mesons. Proton synchrotron experiments have been underway for a half decade and more, with the participation of a large team of Joint Institute physicists and colleagues from the Academy of Sciences of the Georgian SSR. Over 14 thousand V_{e3}^0-events have been recorded with two cloud chambers 40 cm and 1 meter in diameter in a magnetic field, yielding valuable findings for the theory of weak interactions. The study of K_{e3}^0-decay events showed that a vector variant is indeed realized in decays of K_2^0-mesons, in consonance with the theory of (V$-$A)-interaction. An investigation of two-particle decay events showed that the contribution of neutral currents is drastically depressed (down to a 10^{-4} fraction of the charged currents in fact). A more direct proof of the existence of a K_2^0-decay into two charged pions and one neutral pion was obtained; the mode of decay into three neutral pions, elusive as it is, was detected. Relative decay rates of the K_2^0-meson by different decay schemes were measured for the first time; this prompted some inferences on the selection rules in K_2^0-decay events. The antigravitation hypothesis was verified experimentally in inclined beams of K_2^0-mesons; the gravitational masses of particles and antiparticles were found to be of like sign. The report cited results of other investigations of the properties of K_2^0-mesons.

A new phenomenon: spontaneous fission of the nuclide Am^{242} found in an isomeric state, has been studied with the multiply charged ion cyclotron. S. M. Polikanov reported. U^{238} bombarded by accelerated Ne^{22} and O^{16} ions revealed a nuclide fissioning with an unusually short half-life (about 13 msec). Physicists later used Pu and Am isotopes as targets. The experiments confirmed the supposition that decay of a nucleus in an isomeric state is involved here, and found the atomic number of this nuclide $Z \leq 242$. To check out the supposition that the effect is accounted for by fission of the nuclide Am^{242}, Am^{243} was bombarded by 14 MeV neutrons. An isomer of Am^{242} with that same half-life ($\approx$ 13 msec) as in the synthesis reaction using charged heavy ions was found in the $Am^{243}(n, 2n)Am^{242}$ reaction. This abrupt increase in spontaneous fission (by a factor of 10^{20}) is a qualitative new effect, and further investigation may yield highly interesting data on the structure of the nucleus and on the mechanism of fission of nuclei.

G. I. Zabiyakin reported on the development of multichannel recording equipment and on the establishment of a measuring center at the Neutron Physics Laboratory. A complex line of electronic equipment for multichannel spectrometric measurements and for processing a huge volume of experimental information has been underway at this laboratory for the past several years. Detectors and electronic equipment with remote controls for presampling of data have been installed in measuring bays along the neutron guide of the pulsed reactor and near the electrostatic generator. Coded information is fed through the converting units to memory devices where it can be picked up to be printed out on a digital printer, tape punch, or can be sent by cable to the Computing Center of the Joint Institute to be processed on high-speed computers. The measuring center is presently capable of recording data coming in from seven independent experiments. Complex physical investigations have been carried out using the equipment available at the measuring center.

The Learned Council considered the proposal of the appointed jury and adopted a resolution to award the 1964 Joint Institute for Nuclear Research prize to the authors of the first three papers mentioned above.

Some research recently completed at the Institute was also reported on the Learned Council. V. G. Zinov gave an account of experiments on atomic capture of μ-mesons and on μ-mesic molecular processes in work with the synchrocyclotron. L. L. Nemenov reported on experimental and theoretical investigations of the formation of hard

γ-photons in pion-nucleon collisons. The results of the first experiments with polarized resonance neutrons were reported by Yu. V. Taran. Theoretical work on a dynamical model of compound particles, and on symmetries of elementary particles, was reported on by Nguyen Van Hieu.

A new accelerator, a microtron acting as injector at the pulsed reactor, has been commissioned at the Joint Institute for Nuclear Research. F. L. Shapiro reported to the Council members on this machine. The microtron principle was suggested about two decades ago by V. I. Veksler. But microtrons achieving high energies and high beam intensities in practical work have been designed and put into successful operation only recently in the Soviet Union. The microtron commissioned at Dubna is a further extension of the method. It is capable of accelerating electron beams to 30 MeV at currents to 60 mA per pulse. The accelerated beam is focused on a target in the core of the pulsed reactor and acts as a source of fast neutrons to be multiplied by the reactor. The shortened burst time of the pulsed reactor greatly enhances the resolving power of the reactor, thereby opening up important new opportunities for research.

At the low-energy nuclear physics panel session of the Learned Council, Professor I. M. Frank delivered a short report on the activities of the low-energy section over the 1960-1965 period. Proposals advanced by the Hungarian organizing committee to schedule the IV workshop conference on the physics and engineering of research reactors in Budapest were discussed and confirmed.

The members of the section heard 11 scientific papers presented by representatives of member-nations and Dubna Joint Institute laboratories. I. V. Sizov reported on the commissioning of the EG-5 electrostatic generator in the Neutron Physics Laboratory of the Joint Institute for Nuclear Research, and gave information on the first physical measurements carried out with the aid of that machine. The EG-5 is so situated that measurements may be conducted simultaneously on six beams in two experimental rooms. At the present time the EG-5 is capable of accelerating protons, deuterons, He^3 and He^4 ions to 4.0 MeV. The stability of the energy of the beam of accelerated particles is within $\pm 0.1\%$. The beam current on a target placed 10 m away from the magnetic analyzer is 20-30 μA in the case of protons, 10-12 μA in the case of He^4 ions. Measurements of the differential cross sections of the $O^{12} + He^3$ reaction in the He^3 ion energy range from 1.4 to 3.55 MeV are being carried out with the EG-5 electrostatic accelerator.

A paper by J. Urbanec (CSSR) entitled "Anomaly in intensities of hard gammas in resonance neutron capture" noted that anomalously high transition rates to the ground state and the first excited state were detected in experiments using the pulsed fast reactor of the Joint Institute, at the $E_n = 24.5$ eV resonance. The transition energies are 9.23 and 8.42 MeV, respectively. This implies that the resonance is a very strong p-wave resonance; in case it is a S-wave resonance, we can infer that the use of hard gammas to identify the parity of the capture levels is of dubious value in some instances. The pulse spectra of scintillation and germanium spectrometers were recorded with the aid of a multidimensional analyzer with magnetic tape memory (128 amplitude and 256 time channels). 4096 amplitude channels were used in measurements with the termanium spectrometer. The resolution 0.12 μsec/m of the time-of-flight spectrometer was 0.12 μsec/m in measurements using the scintillation spectrometer and 0.6 μsec/m in measurements using the germanium spectrometer.

M. Petrascu (SRR [Socialist Republic of Rumania]) rendered an account of time-of-flight measurements of fission cross sections of Pu^{239} over the 0.001-0.5 eV range. A gas scintillation chamber with a mixture of 85% argon and 15% nitrogen was employed as detector. A layer of plutonium oxide ≈ 1 mg/cm^2 thick was used in the measurements. The product $\sigma_t \cdot v$ was shown to be constant within $\pm$ 10% over a broad range of energies from 0.1 to 0.001 eV.

A report by N. Martalogu (SRR) was devoted to inelastic scattering of 8.5 MeV protons on Ne^{20} and on S^{32} by measuring angular correlations of (p, p', γ).

M. Petrascu (SRR) reported measurements of angular correlations of γ-photons in the capture of thermal neutrons by mercury-199. Five unknown energy levels were identified. The spins of several levels and of the capture state were determined.

N. Martalogu (SRR) reported measurements of angular distributions and polarization of neutrons in the B^{11}(p, n)C^{11} reaction; he also cited results of measurements of the polarizations of elastically and inelastically scattered 5.8 MeV protons on Mg^{24}.

M. Petrascu (SRR) reported research on a scheme of I^{128} energy levels by the γ-γ-coincidence method.

A report by Ya. Grabovskii (Joint Institute for Nuclear Research), "Inelastic scattering of complex nuclei," discussed the relative role of the coulomb and nuclear mechanism in excitation of collective and single-particle

levels in inelastic scattering of complex nuclei in the energy region above the potential barrier. Results of this work will be useful in the interpretation of experimental data.

J. Burget (CSSR [Czechoslovak Socialist Republic]) reported on dynamic polarization of protons in irradiated polymers. Of the polymers investigated the best results were those for polycaprolactam. 4.8% polarization was achieved at $T^0 = 2.1°K$ and in a field H = 19 kOe.

A report by E. Sosnovskii (Joint Institute for Nuclear Research) on neutron diffraction experiments at the IBR reactor reported some experiments designed to clarify the capabilities of the IBR reactor in neutron diffraction and neutron radiography work. Thermal neutrons were scattered on polycrystalline specimens, and the energy spectrum of the scattered neutrons was measured for a fixed angle by the time-of-flight method. The method was checked by using samples of known structure: Al, Zn, ZnO, Si. Over the 1 to 6 A wavelength range high resolution and high aperture were reported. This method was applied to the study of the ferroelectric—antiferromagnetic substance $BiFeO_3$. Neutron diffraction patterns for this compound were obtained for temperatures 20° and 450°C and scattering angles $2\theta = 90°$ and $2\theta = 52°$.

This session of the Learned Council of the Joint Institute for Nuclear Research also discussed a number of organizational questions concerned with the activities of the Institute. The Learned Council examined and approved the developmental plan drawn up by the directors to cover the 1966-1970 five-year period.

INTERNATIONAL SYMPOSIUM ON ELECTRON AND PHOTON INTERACTIONS AT HIGH ENERGIES

V. S. Barashenkov

Translated from Atomnaya Énergiya, Vol. 19, No. 4,
pp. 406-408, October, 1965

Over 350 scientists from various countries, including 5 Soviet physicists, attended this symposium, held June 8-12, 1965. The site of the symposium was Hamburg, since the 6 GeV DESY electron synchrocyclotron, one of the most highly improved and powerful machines of its type, had been commissioned there only recently.

Experimental and theoretical work discussed by the symposium participants could be grouped in the main around four leading topics: the study of the electromagnetic structure of nucleus and atomic nuclei; verification of quantum electrodynamics at short distances; electro- and photoproduction of particles; improvements in experimental techniques. A separate session was reserved for a brief survey of the present status of research on strong interactions.

No substantially novel results were reported on the electromagnetic structure of nucleons. Experimental data on electron scattering by protons and deuterons were reported in contributions by K. Buchanan and M. Yarian from Stanford University and by a large team of physicists working around the DESY accelerator (H. Bahrend, H. Schopper, and others); these data improved the earlier available values of scattering cross sections slightly, but did not alter the total picture greatly in this area.

As noted in a review paper by R. Hofstadter, experimental data fit well with theoretical formulas for effective cross sections right up to very high values of transferred momentum q^2 if the neutron electrical form factor F_{En} is put equal to zero, and the three other nucleon form factors, viz. the electrical and magnetic form factors of the proton E_{Ep} and E_{Mp} and the magnetic form factor of the neutron E_{Mn} are chosen in mutual proportions:

$$F_{Ep}(q^2)=F_{Mp}(q^2)/2.79=F_{Mn}(q^2)/(1-1.91);$$
$$F_{En}(q^2)=0.$$

On the other hand, if we use pole formulas of the type

$$F_x(q^2)=\sum_{i=1}^{n}\left\{\frac{a_{xi}}{1+q^2/M_{xi}^2}+b_{xi}\right\},$$

which are derived under the assumption that the electromagnetic properties of the meson cloud of the nucleon are determined mostly by the lower $\pi-\pi$ resonance ρ, ω, and Φ ($n \leq 2$) in order to describe the values of form factors found from comparing experimental data, then agreement with experiment can be obtained successfully only in the case where the mass of the ρ-meson is assigned values M_ρ = 500 to 600 MeV, which falls markedly below the true value M_ρ = 765 ± 10 MeV. (In this formula, M_{xi} are the masses of the pion resonance; a_{xi} and b_{xi} are constants selected from comparison with experiment such that the constants b_{xi} determine the electric and magnetic charges on the cores of the proton and neutron.) The contradiction may be eliminated by assuming that at least one isovector $\pi-\pi$ resonance makes a substantial contribution to the electromagnetic properties of the nucleon. The mass of this resonance must be about 1200 MeV, which is reasonably close to the mass of the recently detected B-meson. But the properties of this meson have not been studied adequately as yet.

Another approach to overcoming the difficulties in the theoretical interpretation of the form factors was suggested in a report by the French physicists B. Dudelsack and P. Leman, who proposed the existence of two pion resonances ρ' and ρ'' having masses slightly less and slightly larger than the experimentally observed M_ρ = 765 MeV. The anomalously large width of the resonance ρ ($\Gamma \simeq 105$ MeV) does not exclude this variant in principle. In the formula for the isovector form factors, the second-order pole appears in this case in the form:

$$\frac{a_{Q'}}{1+q^2/M_{Q'}^2}+\frac{a_{Q''}}{1+q^2/M_{Q''}^2}\simeq\frac{a_Q}{(1+q^2/M_Q^2)^2},$$

and experimental values of $F_X(q^2)$ are successfully approximated by using the correct mass values for the ω, Φ, and ρ resonances.

Several theoretical and experimental papers dealt with Compton scattering on protons; included among these is an interesting paper by P. Baranov et al. (Lebedev Institute of Physics, USSR). At energies below or near the photoproduction threshold of the π-meson, experimental data show an excellent fit to theoretical calculations if consideration is given not only to the electromagnetic dimensions of the proton and to its anomalous magnetic moment, but also to its electrical and magnetic polarizabilities. There are some difficulties in interpreting the experiment in the higher-energy regions.

The discussion of work on bremsstrahlung accompanying electron scattering processes was given a prominent place on the agenda. Reliable separation of such "quasi-elastic" processes is very important for improving the precision of cross section measurements in purely elastic scattering, and in the final analysis for securing more reliable information on the electromagnetic form factors of the nucleon.

On the whole, however, the status of research on the electromagnetic structure of nucleons leaves very much to be desired from a theoretical vantage point; each process of electromagnetic interaction between elementary particles is characterized by its own specific form factors as matters now stand, and even in the simplest case of elastic $e-p$-scattering and $\gamma-p$-scattering no successful correlation with the space-time structure of the particle has been achieved (if we do not count the region of very low momentum transfer $q^2 \approx 0$). Some entirely novel approach to this problem which will yield a simpler and more straight forward physical explanation appears to be required.

The participants at the symposium devoted close attention to discussion of experiments on the study of the structure of atomic nuclei using electrons of around 1 GeV energy as tools. Here we take particular note of the experiments by D. Amaldi et al. from Frascati on inelastic electron scattering on C^{12} and Al^{27} nuclei, where the effect of nuclear shells is clearly manifested.

Work on verification of the familiar laws of quantum electrodynamics in small space-time regions is intimately related with investigations of the internal structure of elementary particles. This problem was the subject of a paper by a group of Cambridge by physicists (F. Pipkin, P. Blumenthal, and others) reporting experimental data on the generation of electron-positron pairs by gamma photons of $1-5$ GeV energy on carbon nuclei. The paper mentioned that the number of high-energy pairs generated in this process is far in excess of that predicted by the theory. This result, should it receive confirmation, will be the first experimental indication of violation of the laws of quantum electrodynamics. It should be noted, however, that despite the discussion unfolding at the symposium without spotting any experimental errors in this work, the majority of the participants entertain great doubts as to the validity of the Cambridge results. The experiments will be repeated.

In principle, the discrepancy between theory and experiment detected in the experiments by F. Pipkin and colleagues could be accounted for by the contribution of an additional channel for the production of some short-lived fermion of mass far greater than the electron mass (F. Low's hypothesis). A paper by a group of French physicists (C. Betournet, Nguyen Ngo, et al.) was devoted to an experimental study of this problem. By detecting recoil protons, they studied the reaction

$$e+p\to e'+p$$

in the mass region of the heavy fermion $M_{e'}$ = 100 to 570 MeV, and obtained no indication of the existence of such a particle.

Topics dealing with electric production and photoproduction of particles accounted for over forty papers at the symposium. A wealth of new experimental data recovering energies right up to 6 GeV was made available; special attention was given to research on the production of nucleon and meson resonances. Theoretical analysis of these resonance processes is carried out primarily with the aid of single-meson pole diagrams.

Highly detailed data on photoproduction of π-, K-, ρ, ω-mesons, on the nucleon resonance N_{33}^*, multiple particle production in the 0.5 to 5.9 energy range, etc. were presented in a series of papers by H. Crouch and colleagues discussing the results of Cambridge work using the 12-inch hydrogen bubble chamber.

The audience responded with keen interest to a paper submitted by I. Greenberg, V. Blanpeed, et al., from Cambridge indicating the existence of new hyperon resonances with masses M > 1900 MeV. Another interesting paper was submitted by M. Gettner, P. Rotwell et al., of the same laboratory, on a study of photoproduction of antineutrons in the reaction

$$\gamma + p \to \bar{n} + d.$$

The cross section of a reaction of this type is 10^{-31} to 10^{-32} cm^2 in the γ-ray energy range from 4 to 6 GeV.

A paper by Soviet physicists (A. Belousov, B. Tamm et al.), on the photoproduction of π^0- mesons on a helium nucleus at energies from 160 to 240 MeV was also received with interest. These authors determined the radius of the He^4 nucleus, investigated the applicability of the momentum approximation in describing a many-nucleon system, and reported some interesting experimental data.

Two sessions were reserved for discussion of experimental techniques. Here special attention was given to A. Ritson's paper (Stanford Univ.) on the status of work with the colliding-beam electron accelerator. The instability of the beam was overcome by the time of the symposium and experiments involving synchro-clashes of beams of about 300 MeV energy, corresponding to distances of about $2 \cdot 10^{-14}$ cm, had begun. There are already over 500 plates made of e − e-scattering at large angles; 2 to 4 events an hour are recorded on the average.

The magnetic systems are being adjusted in the Orsay 500-650 MeV storage rings.

Construction has been started on a new 10 GeV electron cyclic accelerator with an average current of about 10 μA, at Cornell. The accelerator is scheduled for operation in 2-3 years.

Work on the construction and improvement of linear electron accelerators is going ahead in high gear. A 200 m section has been put into service on the Stanford two-mile linear accelerator; 1.4 GeV was obtained at 10 μA current and an energy spread of 0.7%. The accelerator is expected to be ready for service in a year and a half or less. Orsay is continuing work on expanding the linear accelerator there to obtain beams of 2 GeV particles.

Several theoretical papers on deceleration processes in electron interactions were relevant to the discussion of colliding-beam experiments. Here we should mention a paper by Y. Tszay from Stanford Univ. on calculating the spectral and energy distributions of bremsstrahlung in electron-electron collisions, and a paper by V. Galitskii from Novosibirsk on double bremsstrahlung in colliding electron beams.

An important result was reported in an unscheduled report by M. Goldhaber on studies $K_2^0 \to \pi^+ + \pi^-$ decay events by the D. Fitch team at Princeton University. These physicists detected interference between amplitudes of the direct K_2^0-meson decay into a π-meson pair and decay via the regenerative channel with the formation of a K_1^0-meson. The existence of this interference furnishes unassailable proof that the observed two-pion decay is associated precisely with the K_2^0-meson, and that it is not open to interpretation as any other mode of decay of some particle unknown to us. In other words, the results reported by the A. Fitch group confirm the earlier supposition of nonconservation of combined CP-parity in K-decays.

After the conclusion of the symposium, the participants were invited to study the work of the DESY electron synchrocyclotron at close hand.

PULSED NEUTRON RESEARCH

M. V. Kazarnovskii, Yu. P. Popov, and I. P. Sadikov

Translated from Atomnaya Énergiya, Vol. 19, No. 4,
pp. 408-410, October, 1965

In IAEA symposium dealing with research on nonstationary neutron distributions using pulsed neutron sources as research tools was held May 10-14, 1965 at Karlsruhe (West Germany). Over 220 delegates were in attendance, representing 23 countries and 3 international agencies. About 90 papers were read at the 9 plenary sessions. These papers discussed both experimental and theoretical aspects of nonstationary transport of fast and thermal neutrons in both pure moderators and in breeding systems, as well as topics involved in the building and use of pulsed reactors and pulsed neutron sources.

In a highly informative tutorial review paper, N, Korngold (USA) discussed the present state of affairs in the theory of thermalization of neutrons from pulsed sources. G. Yang (USA) presented a review of recent achievements in the development of physical models employed to describe slow neutron scattering in various moderators.

Original papers centered on numerical calculations of time spectra of neutrons (S. Purohit, Sweden) and spectra in transitional regions (M. Williams, Britain, L. Maiorov et al., USSR), damping constants of neutron flux (G. Wood et al., USA) and some other integrated characteristics of neutron distributions for concrete models representing various moderators, as well as rigorous mathematical analysis of the eigenvalue spectrum of the neutron transport equation (S. Albertoni et al., Italy, R. Bednarz, Poland). The relationships between the various neutron thermalization and diffusion parameters (such as the thermalization time, diffusion length, diffusion coefficient, diffusion cooling factor, etc.) were analyzed in an interesting paper by S. Purohit and N. Sjostrand (Sweden).

A new method for solving the neutron transport equation in media with random inhomogeneities based on the Feynmann graph method attracted a good deal of interest (A. Stepanov, USSR).

K. Beckurts (West Germany) presented an excellent review of the present state of the art in experimental work on the time damping constants of neutron density, on thermalization time, and summarized recently published experimental data.

Results of original research projects designed to improve data on "classical" moderators (water, heavy water, beryllium, graphite, beryllia, zirconium hydride) and to study various organic substances which might find application as moderators, were also reported. Even though these projects have been in progress for over a decade, there are still no reliable results for water or for several crystalline moderators (in some instances, quite possibly, no damping constant exists to begin with). The interpretation of data referable to water is further hampered by the pronounced dependence of the neutron free path length on neutron velocity, which brings about uncertainties in estimates of the extrapolated boundary (z_0) and consequently, in the geometric buckling parameter. A team of British physicists (J. Walker et al.) have improved their experimental data and have found a reasonable measure of agreement between theoretical calculations and experiments carried out earlier by different methods and by different authors, by assigning the value $z_0 = 0.36$ cm. But the findings of an American team (E. Gertner et al.) measuring neutron spectra contradict these data.

Despite these difficulties, the accuracy of experiments of this type is such at present that the results of the experiments can be used to check models of scattering nuclei when the theoretical interpretation stands on sure ground. The reader should still bear in mind that the center of gravity of research in the leading laboratories is shifting to the study of asymptotic and nonstationary neutron spectra, and nonstationary neutron distributions.

A review by M. Poole (Britain) dealt with pulsed neutron sources for spectral measurements. The reporter stated that even though the present theory accounts for neutron thermalization adequately, there is some discrepancy with experiment when intense poisoning takes place and when transient effects are described. J. Beister et al. (USA) studied

the angular dependence of scattering of monoenergetic neutrons in ordinary water and in heavy water over a broad energy range (to 10 eV), and also studied scattering in zirconium hydride.

The presentation of some papers dealing with research on nonstationary neutron spectra (USSR, USA, Britain, West Germany) was an important event at the symposium.

Papers submitted by the Ransellaer group (E. Gertner et al., USA) presented research findings on neutron spectra in heavy water, the effect of coherent scattering on neutron thermalization in beryllium, asymptotic spectra in homogeneous neutron-multiplying media, and the space dependence of asymptotic spectra in water and in polyethylene.

The British scientists M. Poole and M. Widler presented data on measurements and calculations of nonstationary spectra in heavy water. A paper by J. Kahlfelz and W. Keichardt (West Germany) discussed studies of spectra in hydrogenous substances: the angular dependence of asymptotic neutron spectra in water was studied and nonstationary spectra were measured near equilibrium in zirconium hydride and in ice at 77° and 21°K. It is interesting to note that a sharp drop in the rate at which the neutron gas attains equilibrium was detected when the ice was cooled to ?1°K.

Reports by the V. Mostovoi team (USSR) included measurements of nonstationary spectra in graphite, beryllium, zirconium hydride, and water over a broad range of moderation times at different values of the geometrical buckling. The procedure described allows measurements to be taken with resolution substantially improved over that attained in similar arrangements reported in other countries.

It is evident from these papers that experimental techniques have undergone impressive improvements in the leading laboratories over the past two or three years (powerful pulsed neutron sources phased with mechanical choppers, for instance), so that some very interesting results on nonstationary spectra have come to light. This trend appears to become dominant in the present period, along with the study of doubly differential cross sections [differential in both energy and emission angles].

The symposium centered much attention on studies of neutron behavior in neutron-multiplying systems. Most of the papers dealt with subcriticality and neutron lifetimes. Three papers (G. Braun et al. France, B. Joshi et al., India; I. Zhezherum, USSR) discussed pulsed neutron sources employed in the study of the parameters of multiplying media (diffusion lengths, diffusion coefficient, neutron age, etc.).

A review paper by E. Gerelis (USA) made an analysis of current techniques for studying the subcriticality of systems using a pulsed neutron source.

Some of the papers dealt with studies of concrete systems (different geometries and concentrations of fuel and moderator, presence or absence of reflector, absorbing rods, boron poison, etc.). Several papers generalized and extended the methods. K. Preskitt et al. (USA) developed a method for solving the space-dependent reactor kinetics equation using matrix algebra. The effect of higher-order spatial harmonics and other factors affecting the interpretation of pulsed neutron source experiments was investigated theoretically.

Improved techniques of subcriticality measurements were verified experimentally in a paper co-authored by Israeli (T. Gozani) and Swiss (P. Dermarmelse et al.) investigators. They found subcriticality subject to measurement by these methods in the region to 10β* with error kept to within 2%.

We may conclude from these papers that the pulsed neutron source method appears to have become a fundamental technique in measurements of reactivity and neutron lifetime in subcritical systems.

F. Storrer (France) delivered a review paper on fast-neutron systems. 12 original reports dealt with the same topic. Experimental and theoretical work is proceeding in two main directions here: determination of neutron flux depression with time in various multiplying and nonmultiplying systems, and the study of neutron spectra in different assemblies. In the last case the time-of-flight method seems the most promising. Neutron spectra have been studied successfully in the energy range up to several megaelectron-volts by using nanosecond pulse techniques and flight distances as great as 50 meters. The neutron sources employed are deuteron accelerator drift tubes, linear electron accelerators and pulsed Van de Graaff accelerators with pulse duration of several nanoseconds.

* β is the delayed neutron fraction.

Investigations of the behavior of fast and intermediate neutrons in multiplying and nonmultiplying systems by means of pulsed neutron sources have become common place in France (R. Comte et al.), Sweden (B. Brunfalder et al), USA (G. Russel et al.), Britain (W. Peterson et al., D. Geiter et al.), Belgium (G. Dekonink et al.), West Germany (D. Borgwaldt, et al.). To these we add a paper by A. Bergman et al. (USSR) on slowing down of neutrons from a pulsed source in bulk volumes of lead, iron, and graphite. A brief survey of physical results on neutron slowing-down time in lead obtained with a neutron spectrometer accompanies experimental and theoretical investigations of the slowing-down process.

We should also mention a paper by G. Russell et al. (USA) on measurements of neutron spectra in massive media; this paper is of interest both for fast reactor calculations and for shielding calculations.

A theoretical paper by M. Stievenaar (Belgium) showed that many-group method calculations give excellent predictions of time values proper near a critical state. The calculations do not fit experimental results so closely in the case of highly subcritical assemblies.

The session devoted to pulsed reactors and pulsed neutron sources began with a review tutorial paper by T. Wimmet (USA) on structural features and performance of pulsed nonperiodic reactors of the Godiva type. The most recent variant of this reactor type, the Superdoll, will yield $2 \cdot 10^{18}$ fission events per neutrons burst at a burst duration of ≈ 1 msec.

Another interesting paper was submitted by W. Rajewski (Euratom) on the outlook for the development of pulsed periodic fast reactors, a prototype of which is the IBR reactor in the USSR. The reporter dwelt in detail on the SORA fast reactor project, designed to be pulsed by means of a rotating reflector. The average power output of this reactor is to be 1 MW, pulse duration 50 μsec, and pulse repetition rate 50 cps.

To study the behavior of materials subjected to high instantaneous temperatures, and to clarify some other questions, the Buffalo nuclear research center (USA) has built a pulsed reactor (Polestar) with pulse duration of 10 msec and 3600 MW peak power; the reactor average power is 5 MW.

Several papers on improvements in pulsed neutron sources were read later (improvements involved mostly use of the D − T reaction). A paper from West Germany reported new ion sources for incorporation in compact pulsed neutron sources with $\approx 10^{14}$ neutrons/sec instantaneous output and pulse width ≈ 5 μsec. Results of research using sealed neutron tubes manufactured by Phillips Ltd. (Netherlands) were reported. These tubes can be used to pulsed or sinusoidally modulated neutron fluxes of frequencies from 1 to 10^3 bursts per second.

Some papers discussed investigations of neutron transport from various nonstationary but nonpulsed neutron sources, such as sources periodically modulated, with statistical time distributions, etc. A review paper by R. Uhrig (USA) discussed the theory of neutron propagation from sources of this type in pure moderators and in multiplying media, and discussed the advantages and disadvantages of using them to measure neutron diffusion parameters and the characteristics of multiplying systems (reactivity, neutron lifetime, etc.). A theoretical analysis of pulsed and modulated neutron sources was offered by M. Cadillac et al. (France) and by S. Carno (Italy). One of the most interesting of these was a method involving a sinusoidally modulated neutron source. Neutron propagation was of a wave-like nature in this case. The damping ratio and the phase shift per unit length are related to the diffusion and slowing-down parameters of the medium. The use of this method for analyzing neutron thermalization in graphite was discussed by R. Perez and R. Booth (USA). The experimental results are in excellent agreement with Parks model calculations. This method appears to be a worthy supplement in measurements of damping ratio in pulsed experiments.

A paper by R. Haas et al. (Euratom) suggested a modification of the pulsed method for measuring damping ratio with a neutron source featuring a random pulse distribution (using spontaneous fission of Cf^{252}), and cited results of paraffin block measurements.

Some original papers (J. Will, USA; S. Bierman, USA: W. Rotter, Belgium; M. Edelman et al., West Germany) reported results on nuclear reactors and assemblies using pulsed and modulated neutron sources and a technique for recording and analyzing noise. The discussion of these papers revealed that the pulsed neutron source method was most effective in the study of subcritical facilities well below the critical state, and that the most reliable results in a delayed critical regime could be obtained by measuring reactor "noise."

The progress registered at the symposium was summarized in a concluding report delivered by Prof. M. Nelkin (USA).

SEMINAR ON APPLICATIONS OF ISOTOPES AND RADIATIONS IN INDUSTRY AND IN MEDICINE

V. Sinitsyn

Translated from Atomnaya Énergiya, Vol. 19, No. 4,
pp. 410-412, October, 1965

A seminar on applications of radioactive isotopes and nuclear radiation sources in industry and in medicine was held in Baku in May, 1965 to afford opportunities for an exchange of experiences and information in the acceptance of radioisotope techniques in the national economy of Azerbaidjan.

500-odd persons took part in the seminar; the directors and chief engineers of factories, plants, and planning offices of branches of industry, leading production men and power experts, heads of engineering and production sections, representatives of research and design organizations, faculty members of engineering colleges, staff members of industrial, in-plant, and industry-wide laboratories, and practicing physicians were included in the audience. Over 60 papers were read at the plenary and panel sessions.

A review tutorial paper delivered by chief engineer of V/O Izotop V. I. Sinitsyn stated that important advances have been achieved in our country in recent years in the development of new techniques for uses of radioactive isotopes and radiation techniques. There are now over three thousand organizations and plants in the USSR regularly using radioisotopes and nuclear radiations in their work. γ-Ray flaw detection techniques and activation analysis are in widespread use, the list of available radioisotope devices for process monitoring and control in the metallurgical, chemical, mining and ore processing industries, in light industry, in the food processing industry and in miscellaneous branches of the national economy is continually being expanded. The technique of labeled atoms is being exploited on an intensified scale in scientific and industrial research, and is prominent in studies of wear on machinery, mechanisms, and tools.

The reporter stated that the method of labeled atoms, radioisotope devices, high-level radiation sources, and similar means will continue their previous advances in the national economy in radiation chemical and radiation sterilization processes.

Applications of radioisotope devices and methods in the industry of Azerbaidjan were covered by S. R. Grobshtein, head of the engineering control board in the Council of the National Economy of the Azerbaidjani Republic. He noted the use of isotopes in Azerbaidjan in radiation chemistry, in semiconductor physics, in prospecting and exploration of minerals, in geophysical research, and in the development of oil fields and gas fields, in radiobiology and in medicine. Isotope work is being carried on in 15 science research institutes. But a special study showed that roughly 1000 process monitoring radioisotope devices are needed and can be profitably used in industrial plants in the Republic. The reporter mentioned shortcomings in the work of gaining acceptance for radioisotope techniques in production, and ways of overcoming those shortcomings.

The seminar placed great stress on applications of isotopes and radiation sources in the prospect exploration and development of oil deposits, gas deposits, and ore mines, and also in the chemical and petrochemical processing industries.

A. M. Melik-Zhakhnazarov et al., reported on developments in the nuclear magnetic logging method at the Azerbaidjani Institute of Petroleum and Chemistry, jointly with the Nuclear Geophysics and Geochemistry Research Institute. The nuclear magnetic logging technique is based on exploitation of the phenomenon of freely processing hydrogen nuclei in the earth's magnetic field. A strong polarizing magnetic field of short duration is established in the host rock around a borehole. The polarization is rapidly quenched after equilibrium magnetization of the hydrogen nuclei sets in. The excitation of free procession of hydrogen nuclei in the liquid about the direction of the earth's field sets up an electromotive force in the measuring sensor indicating the amount of liquid present in the stratum. The longitudinal relaxation time measured by a specially devised method makes it possible to distinguish water-bearing reservoirs from oil reservoirs, and to appraise the permeability and productivity of the strata.

S. L. Abramyan (of the Azneftegeofizika trust) stated in a paper entitled "Status and perspectives of the development of nuclear geophysics in the Azerbaidjani petroleum industry" that high precision is required in measurements in radioactive probing of boreholes in mesozoic deposits. Further improvements in precision in radioactive logging measurements will require more efficient and more exacting equipment capable of service in high-temperature environments, and improvements in techniques. The reporter made the point that Azneftegeofizika has successfully tried out a method for determining the absorption profile of strata and quality control of borehole casing using the short-lived isotope Mn^{52}. Further development of radioactive techniques for studying geological sections of boreholes must proceed on the pathway of utilizing new modifications of the pulsed neutron-neutron logging method and borehole spectrometry, and using short-lived isotopes.

A method of studying boreholes and cores based on the use of a suspension (clarified montmorillonite clay) activated by Fe^{59} has been developed by this trust and is now in use at oil fields in Azerbaidjan. A report on the method was presented by S. A. Aksel'rod, K. D. Mamedov et al. The gist of the method is that the solid phase of the slurry, containing Fe^{59}, is laid down on the walls of the stratum in proportion to the volume of liquid pumped through. As a result, the radioactivity measured along the well hole length (natural background taken into account) gives a picture of the absorption profile. The method presents a quantitative solution to the problems concerning determination of absorption profiles in injection wells, and makes it possible to monitor and control the flooding of an oil bed.

Activated slurries are also used to monitor hydraulic sections of an oil stratum. In this case the absorption profiles are taken twice in the well: before and after hydraulic fracturing. Comparing the before and after profiles provides an estimate of the loss zone absorbing the fracturing fluid as well as a picture of quantitative changes underway in the stratum.

A paper entitled "neutron parameters of host rock in the Apsheron productive series" by L. A. Putkaradze stated that the significance of neutron techniques in industrial geophysics gains from the need to monitor the development of oil fields and to single out producing strata in the course of switchovers to new productive locations. The possibilities and the range of applications of the various neutron techniques in investigating wells in areas where the oil-water contact breaks off in the section through the producing strata of the Apsheron peninsula may be evaluated on the basis of research opening the way for a study of the results of neutron interactions with the stratum material, thereby determining neutron diffusion and neutron slowing-down in the strata, and neutron activation of the material. The potentialities of neutron-neutron logging, neutron-gamma logging, pulsed neutron-neutron logging have been established on the basis of calculations for break-offs in the oil-water contact. The report also showed that finding producing strata in a section through the Apsheron series in a task that can be performed reliably only by pulsed neutron-neutron logging techniques.

A report on the design and operating characteristics of IGN-1 pulsed neutron generators and some results of their use under a variety of geological conditions (in the Ukraine, the Krasnodar district, and elsewhere) was delivered by D. F. Bespalov. New radioactive logging equipment for deep-hole work developed by Azneftegeofizika was described in a paper by V. L. Petrov and associates.

An interesting paper on applications of radioactive isotopes and radiation sources in medicine was presented by I. G. Logunova. She stated that new and more convenient types of radioactive preparations, made in the form of needles, beads, and other useful shapes, have been developed recently and have been incorporated into medical practice. New high-level γ-irradiation facilities are also available. Radioactive phosphorus, iodine, and colloidal gold solution are being widely used in radiation therapy. Various external exposure techniques are being used intensively in medical practice, with betatrons and linear accelerators as tools, thereby achieving a concentration of high-energy radiation in the region of the pathological focus and minimizing exposure of surrounding healthy tissues. Radioactive isotopes have proved highly effective in clinical diagnostics as well. They are playing a prominent role in the diagnosis of malfunctions of the thyroid gland, liver, kidneys, and other organs. The radioscanning method for obtaining information on the state of internal organs which cannot be secured by other means has an especially bright future. Medical radiology is securing a firm material and technological basis for its development.

The director of the principal isotopes laboratory of the Latvian Council of the National Economy, V. E. Banashek, the representative of the Azovstal' steel works O. I. Val'ter, and other seminar participants shared their experiences on applications of radioisotope techniques.

Representatives of research organizations told of the result of their work. For example, the MVTU [Moscow Engng. College] representative S. G. Purtov reported on the savings achieved in the use of radioisotope techniques

and instruments in industry. K. B. Zaborenko (MGK) gave an account of how labeled atoms are used in industry. Experience in the use of the AZhS-1 radioisotope fluid analyzer in oil refineries was detailed by Yu. G. Khachaturov (State chemical committee OKVA).

Several papers discussed applications of radioisotope techniques and instrumentation in metallurgy, machine tools, and metalworking. Outstanding among these papers were one by A. G. Sul'kin (VNIIRT [Radiation engineering research institute]) on γ-ray nondestructive testing methods and experience in the use of these methods in machine tool manufacture, others by I. S. Izakhnenko (TsNIITMASh [Central research institute for technology and machinery manufacture]), "Ionization techniques in γ-ray nondestructive testing," and by G. I. Gil'man (of the Ekonomaizer boiler works), "Experience in the use of radioisotope level indicators for automating pneumatic conveyor lines in foundry production." D. G. Tochil'nikov, representing the Leningrad Institute of Waterways, gave an account of applications of radioactive tracers in the study of wear and in efforts to lengthen the operating life of parts.

The seminar adopted a resolution containing detailed recommendations on promising work with radioactive materials in Azerbaidjan and aiding the incorporation of radiation techniques into the national economy of the Republic.

A CONFERENCE ON NOMOGRAPHY

M. V. Filippov

Translated from Atomnaya Énergiya, Vol. 19, No. 4,
p. 412, October, 1965

The first intercollegiate nomographical conference was held in Moscow in June, 1965. Leading nomographists and faculty and staff members of engineering colleges and of many other institutions prominent in the creative study of nomographic work took part and gave to the conference the significance of a representative All-Union forum on the topic.

The conference heard and discussed sixty-odd papers of both theoretical and applied bent. Interest centered on the review papers delivered by M. V. Pentkovskii on certain aspects of the development of modern concepts in nomography, G. S. Khovanskii on the construction of transparent nomograms, I. A. Vil'ner on nomographing functions of a complex variable. A report on experience in the use of nomograms in magnetohydrodynamics problems shed new light on nomographing problems in a field closely bordering on nuclear power. Much of the content of the numerous papers presented had been published in three special nomographical collections issued in recent years by the Computing Center of the USSR Academy of Sciences. There are plans for also publishing the most interesting reports and papers submitted to the conference and not available elsewhere. Scientists and nuclear engineers interested in using the latest advances in nomography in their work will undoubtedly find much interesting material in the conference proceedings, much of which should contribute to great savings in calculations and to presenting a clear and lucid analysis of many important functional relationships.

SOVIET JOURNALS AVAILABLE IN COVER-TO-COVER TRANSLATION

This list includes all Russian journals which—to the publisher's knowledge—were available in cover-to-cover translation on June 30, 1965, or for which definite and immediate plans for cover-to-cover translation had been announced by that date. The list reflects only *current* publication arrangements, but the date and issue listed for first publication refer to translations available from any source. Thus, earlier volumes of a translation journal may have been published by an organization other than that listed as the current publisher, and possibly under a different title (and, for *Doklady Akademii Nauk SSSR*, in a different arrangement of sections).

Five bits of information are furnished, separated by bullets:

1. The abbreviation(s) by which the journals are most frequently referred to in Russian bibliographies (if the name of the journal is customarily spelled out, no abbreviation is given).
2. The transliterated full name of the journal.
3. The full name of the translation journal (in bold type).
4. The year, volume (in parentheses), and issue of first publication of the translation (parentheses are empty if the Russian journal does not use volume numbers).
5. The current publisher of the translation [AGI—American Geological Institute, AGU—American Geophysical Union, AIP—American Institute of Physics, CB—Consultants Bureau, CH—Clearing House for Federal Scientific and Technical Information, CS—The Chemical Society (London), FP—Faraday Press, IEEE—Institute of Electrical and Electronic Engineers, ISA—Instrument Society of America, PP—Pergamon Press].

For convenience in locating bibliographic references the journals are listed in alphabetical order of the *abbreviated* titles.

AÉ • Atomnaya énergiya • **Soviet Journal of Atomic Energy** • 1956(1)1 • CB

Akust. zh. • Akusticheskii zhurnal • **Soviet Physics—Acoustics** • 1955(1)1 • AIP

Astrofiz. • Astrofizika • **Astrophysics** • 1965(1)1 • FP

Astr(on). zh(urn). • Astronomicheskii zhurnal • **Soviet Astronomy—AJ** • 1957(34)1 • AIP

Avtomat. i telemekh. • Avtomatika i telemekhanika • **Automation and Remote Control** • 1956(27)1 • ISA

Avto(mat). svarka • Avtomaticheskaya svarka • **Automatic Welding** • 1959(12)1 • British Welding Research Association

Avtometriya • **Autometry** • 1965(1)1 • CB

Biokhim. • Biokhimiya • **Biochemistry** • 1956(21)1 • CB

Byul. éksp(erim). biol. (i med.) • Byulleten' éksperimental'noi biologii i meditsiny • **Bulletin of Experimental Biology and Medicine** • 1959(41)1 • CB

DAN (SSSR) • *see* Doklady AN SSSR

Defektoskopiya • **Soviet Defectoscopy** • 1965(1)1 • CB

Diff. urav. • Differentsial'nye uravneniya • **Differential Equations** • 1965(1)1 • FP

Dokl(ady) AN SSSR; DAN (SSSR) • Doklady Akademii Nauk SSSR • The translation of Doklady is published in various journals, according to subject matter. The sections of Doklady contained in each of the translation journals are listed in parentheses.

Doklady Biochemistry (biochemistry) • 1957(112)1 • CB

Doklady Biological Sciences Sections (anatomy, cytology, ecology, embryology, endocrinology, evolutionary morphology, parasitology, physiology, zoology) • 1957(112)1 • CB

Doklady Biophysics (biophysics) • 1957(112)1 • CB

Doklady Botany (botany, phytopathology, plant anatomy, plant ecology, plant embryology, plant physiology, plant morphology) • 1957(112)1 • CB

Doklady Chemical Technology (chemical technology) • 1956(106)1 • CB

Doklady Chemistry (chemistry) • 1956(106)1 • CB

Doklady Earth Sciences Sections (geochemistry, geology, geophysics, hydrogeology, lithology, mineralogy, paleontology, permafrost, petrography) • 1959(124)1 • AGI

Doklady Physical Chemistry (physical chemistry) • 1957(112)1 • CB

Doklady Soil Science (soil science) • 1964(154)1 • Soil Science Society of America

Soviet Mathematics—Doklady (mathematics) • 1960(130)1 • American Mathematical Society

Soviet Oceanography (oceanology) • 1959(124)1 • AGU

Soviet Physics—Doklady (aerodynamics, astronomy, crystallography, cybernetics and cor..rol theory, electrical engineering, energetics, fluid mechanics, heat engineering, hydraulics, mathematical physics, mechanics, physics, technical physics, theory of elasticity • 1956(106)1 • AIP

Élektrokhimiya • **Soviet Electrochemistry** • 1965(1)1 • CB

Élektrosvyaz' • combined with Radiotekhnika in **Telecommunications and Radio Engineering** • 1957(16)1 • IEEE

Élektrotekh. • Élektrotekhnika • **Soviet Electrical Engineering** • 1965 (36)1 • FP

Éntom(ol). oboz(r). • Éntomologicheskoe obozrenie • **Entomological Review** • 1958(37)1 • Entomological Society of America

Fiz. goreniya i vzryva • Fizika goreniya i vzryva • **Combustion, Explosion, and Shock Waves** • 1965(1) • FP

Fiziol(ogiya) rast. • Fiziologiya rastenii • **Soviet Plant Physiology** • 1957(4)1 • CB

Fiz.-khim. mekh(anika) mater(ialov); FKhMM • Fizikokhimicheskaya mekhanika materialov • **Soviet Materials Science** • 1965(1)1 • FP

Fiz. met. i metallov.; FMM • Fizika metallov i metallovedenie • **Physics of Metals and Metallography** • 1957(5)1 • Acta Metallurgica

Fiz.-tekhn. probl. razr. polezn. iskopaem. • Fizikotekhnicheskie problemy razrabotki poleznykh iskopaemykh • **Soviet Mining Science** • 1965(1)1 • CB

Fiz. tv(erd). tela; FTT • Fizika tverdogo tela • **Soviet Physics—Solid State** • 1959(1)1 • AIP

FKhMM • *see* Fiz.-khim. mekhanika materialov

FMM • *see* Fiz. met. i metallov.

FTT • *see* Fiz. tverd. tela

Geliotekh. • Geliotekhnika • **Applied Solar Energy** • 1965(1)1 • FP

Geol. nefti i gaza • Geologiya nefti i gaza • **Petroleum Geology** • 1958 (2)1 • Petroleum Geology, Box 171, McLean, Va.

Geomagnet. i aéronom. • Geomagnetizm i aéronomiya • **Geomagnetism and Aeronomy** • 1961(1)1 • AGU

Inzh.-fiz. zh. • Inzhenerno-fizicheskii zhurnal • **Journal of Engineering Physics** • 1965(8)1 • FP

Inzh. zh. • Inzhenernyi zhurnal • **Soviet Engineering Journal** • 1965(5)1 • FP

Iskusstv. sputniki Zemli • Iskusstvennye sputniki Zemli • **Artificial Earth Satellites** • 1958(1)1 • CB [superseded by Kosmich. issled.]

Izmerit. tekhn(ika) • Izmeritel'naya tekhnika • **Measurement Techniques** • 1958(7)1 • ISA

Izv. AN SSSR, o(td.) kh(im.) n(auk) (*or* ser. khim.) • Izvestiya Akademii Nauk SSSR: Otdelenie khimicheskikh nauk (*or* Seriya khimicheskaya) • **Bulletin of the Academy of Sciences of the USSR: Division of Chemical Science** • 1952(16)1 • CB

Izv. AN SSSR, ser. fiz(ich). • Izvestiya Akademii Nauk SSSR: Seriya fizicheskaya • **Bulletin of the Academy of Sciences of the USSR: Physical Series** • 1954(18)3 • Columbia Technical Translations

Izv. AN SSSR, ser. fiz. atm. i okeana • Izvestiya Akademii Nauk SSSR: Seriya fiziki atmosfery i okeana • **Izvestiya, Atmospheric and Oceanic Physics** • 1965( )1 • AGU

Izv. AN SSSR, ser. fiz. zemli • Izvestiya Akademii Nauk SSSR: Seriya fiziki zemli • **Izvestiya, Physics of the Solid Earth** • 1965( )1 • AGU

Izv. AN SSSR, ser. geofiz. • Izvestiya Akademii Nauk SSSR: Seriya geofizicheskaya • **Bulletin of the Academy of Sciences of the USSR: Geophysics Series** • 1957(7)1 • AGU [superseded by Izv. AN SSSR, ser. fiz. atm. i okeana and Izv. AN SSSR, ser. fiz. zemli]

Izv. AN SSSR, ser. geol. • Izvestiya Akademii Nauk SSSR: Seriya geologicheskaya • **Bulletin of the Academy of Sciences of the USSR: Geologic Series** • 1958(23)1 • AGI

Izv. AN SSSR, ser. neorgan. mat(er). • Izvestiya Akademii Nauk SSSR: Seriya neorganicheskie materialy • **Inorganic Materials** • 1965(1) 1 • CB

Izv. AN SSSR, tekhn. kiber(netika) • Izvestiya Akademii Nauk SSSR: Tekhnicheskaya kibernetika • **Engineering Cybernetics** • 1963(1)1 • IEEE

Izv. v(yssh.) u(ch.) z(av.) aviats. tekh. • Izvestiya vysshikh uchebnykh zavedenii. Aviatsionnaya tekhnika • **Aviation Engineering** • 1963(6)1 • CH

Izv. v(yssh.) u(ch.) z(av.) fiz. • Izvestiya vysshikh uchebnykh zavedenii. Fizika • **Soviet Physics Journal** • 1965(8)1 • FP

Izv. v(yssh.) u(ch.) z(av.) geodez. i aérofot. • Izvestiya vysshikh uchebnykh zavedenii. Geodeziya i aérofotos"emka • **Geodesy and Aerophotography** • 1959(4)1 • AGU

Izv. v(yssh.) u(ch.) z(av.) priborostr. • Izvestiya vysshikh uchebnykh zavedenii. Priborostroenie • **Izvestiya VUZOV. Instrument Building** • 1962(5)1 • CH

Izv. v(yssh.) u(ch.) z(av.) radiofiz. • Izvestiya vysshikh uchebnykh zavedenii. Radiofizika • **Izvestiya VUZOV. Radiophysics** • 1958(1)1 • CH

Izv. v(yssh.) u(ch.) z(av.) radiotekhn(ika) • Izvestiya vysshikh uchebnykh zavedenii. Radiotekhnika • **Izvestiya VUZOV. Radio Engineering** • 1959(2)1 • CH

Izv. v(yssh.) u(ch). z(av.) tekh. teks. prom. • Izvestiya vysshikh uchebnykh zavedenii. Tekhnologiya tekstilnoi promyshlennosti • **Technology of the Textile Industry, USSR** • 1960(4)1 • The Textile Institute (Manchester)

Kauch. i rez. • Kauchuk i rezina • **Soviet Rubber Technology** • 1959 (18)3 • Maclaren and Sons Ltd.

Khim. getero(tsik). soed. • Khimiya geterotsiklicheskikh soedinenii • **Chemistry of Heterocyclic Compounds** • 1965(1)1 • FP

Khim. i neft. mash(inostr). • Khimicheskoe i neftyanoe mashinostroenie • **Chemical and Petroleum Engineering** • 1965( )1 • CB

Khim. i tekhnol. topliv i masel • Khimiya i tekhnologiya topliv i masel • **Chemistry and Technology of Fuels and Oils** • 1965( )1 • CB

Khim. prirod. soed. • Khimiya prirodnykh soedinenii • **Chemistry of Natural Compounds** • 1965(1)1 • FP

Kib. • Kibernetika • **Cybernetics** • 1965(1)1 • FP

Kinet. i katal. • Kinetika i kataliz • **Kinetics and Catalysis** • 1960(1)1 • CB

Koks i khim. • Koks i khimiya • **Coke and Chemistry, USSR** • 1959( )8 • Coal Tar Research Assn. (Leeds, England)

Kolloidn. zh(urn). • Kolloidnyi zhurnal • **Colloid Journal** • 1952(14)1 • CB

Kosmich. issled. • Kosmicheskie issledovaniya • **Cosmic Research** • 1963(1)1 • CB

Kristallog. • Kristallografiya • **Soviet Physics—Crystallography** • 1957 (2)1 • AIP

Liteinoe proiz(-vo). • Liteinoe proizvodstvo • **Russian Castings Production** • 1961(12)1 • British Cast Iron Research Association

Mag. gidrodin. • Magnitnaya gidrodinamika • **Magnetohydrodynamics** • 1965(1)1 • FP

Mekh. polim. • Mekhnika polimerov • **Polymer Mechanics** • 1965(1)1 • FP

Metalloved. i term. obrabotka metal.; MiTOM • Metallovedenie i termicheskaya obrabotka metallov • **Metal Science and Heat Treatment** • 1958(6)1 • CB

Metallurg • **Metallurgist** • 1957( )1 • CB

Mikrobiol. • Mikrobiologiya • **Microbiology** • 1957(26)1 • CB

MiTOM • *see* Metalloved. i term. obrabotka metal.

Ogneupory • **Refractories** • 1960(25)1 • CB

Opt. i spektr.; OS • Optika i spektroskopiya • **Optics and Spectroscopy** • 1959(6)1 • AIP

Osnovan. fund. i mekh. gruntov • Osnovaniya fundamenty i mekhanika gruntov • **Soil Mechanics and Foundation Engineering** • 1964 ( )1 • CB

Paleon. zh(urn). • Paleontologicheskii zhurnal • **Journal of Paleontology** • 1962( )1 • AGI

Plast. massy • Plasticheskie massy • **Soviet Plastics** • 1960(8)7 • Rubber and Technical Press, Ltd.

PMM • *see* Prikl. matem. i mekhan.

PMTF • *see* Zhur. prikl. mekhan. i tekhn. fiz.

Pochvovedenie • **Soviet Soil Science** • 1958(53)1 • Soil Science Society of America

Poroshk. met. • Poroshkovaya metallurgiya • **Soviet Powder Metallurgy and Metal Ceramics** • 1962(2)1 • CB

Priborostroenie • **Instrument Construction** • 1959(4)1 • Taylor and Francis, Ltd.

Pribory i tekhn. éksp(erimenta); PTÉ • Pribory i tekhnika éksperimenta • **Instruments and Experimental Techniques** • 1958(3)1 • ISA

Prikl. biokhim. i mikrobiol. • Prikladnaya biokhimiya i mikrobiologiya • **Applied Biochemistry and Microbiology** • 1965(1)1 • FP

Prikl. matem. i mekh(an).; PMM • Prikladnaya matematika i mekhanika • **Applied Mathematics and Mechanics** • 1958(22)1 • PP

Probl. pered. inform. • Problemy peredachi informatsii • **Problems of Information Transmission** • 1965(1)1 • FP

Probl. severa • Problemy severa • **Problems of the North** • 1958( )1 • National Research Council of Canada

PTÉ • *see* Pribory i tekhn. éksperimenta

Radiokhim. • Radiokhimiya • **Soviet Radiochemistry** • 1962(4)1 • CB

Radiotekh. • Radiotekhnika • combined with Élektrosvyaz' in **Telecommunications and Radio Engineering** • 1961(16)1 • IEEE

Radiotekhn. i élektron(ika) • Radiotekhnika i élektronika • **Radio Engineering and Electronic Physics** • 1961(6)1 • IEEE

Stal' • **Stal' in English** • 1959(19)1 • The Iron and Steel Institute

Stanki i instr. • Stanki i instrument • **Machines and Tooling** • 1959 (30)1 • Production Engineering Research Association

Stek. i keram. • Steklo i keramika • **Glass and Ceramics** • 1956(13)1 • CB

Svaroch. proiz(-vo). • Svarochnoe proizvodstvo • **Welding Production** • 1959(5)4 • British Welding Research Association (London)

Teor. i éksperim. khim. • Teoreticheskaya i éksperimental'naya khimiya • **Theoretical and Experimental Chemistry** • 1965(1)1 • FP

Teor. veroyat. i prim. • Teoriya veroyatnostei i ee primenenie • **Theory of Probability and Its Application** • 1956(1)1 • Society for Industrial and Applied Mathematics

Teploénergetika • **Thermal Engineering** • 1964(11)1 • PP

Teplofiz. vys(ok). temp. • Teplofizika vysokikh temperatur • **High Temperature** • 1963(1)1 • CB

Tsvet. metally • Tsvetnye metally • **The Soviet Journal of Nonferrous Metals** • 1960(33)1 • Primary Sources

Usp. fiz. nauk; UFN • Uspekhi fizicheskikh nauk • **Soviet Physics—Uspekhi** • 1958(66)1 • AIP

Usp. khim.; UKh • Uspekhi khimii • **Russian Chemical Reviews** • 1960(29)1 • CS

Usp. mat. nauk; UMN • Uspekhi matematicheskaya nauk • **Russian Mathematical Surveys** • 1960(15)1 • Cleaver-Hume Press, Ltd.

Vest. Akad. med. nauk SSSR • Vestnik Akademii meditsinskikh nauk SSSR • **Vestnik of USSR Academy of Medical Sciences** • 1962(17)1 • CH

Vest. mashinostroeniya • Vestnik mashinostroeniya • **Russian Engineering Journal** • 1959(39)4 • Production Engineering Research Association

Vest. svyazi • Vestnik svyazi • **Herald of Communications** • 1954(14)1 • CH

Vysoko(molek). soed(ineniya) • Vysokomolekulyarnye soedineniya (SSSR) • **Polymer Science (USSR)** • 1959(1)1 • PP

Yadernaya fizika • **Soviet Journal of Nuclear Physics** • 1965(1)1 • AIP

Zashch(ita) met(allov) • Zashchita metallov • **Protection of Metals** • 1965(1)1 • CB

Zav(odsk). lab(oratoriya); ZL • Zavodskaya laboratoriya • **Industrial Laboratory** • 1958(24)1 • ISA

ZhÉTF pis'ma redaktsiyu • **JETP Letters** • 1965(1)1 • AIP

Zh(ur). anal(it). khim(ii); ZhAKh • Zhurnal analiticheskoi khimii • **Journal of Analytical Chemistry** • 1952(7)1 • CB

Zh(ur). éks(perim). i teor. fiz.; ZhÉTF • Zhurnal éksperimental'noi i teoreticheskoi fiziki • **Soviet Physics—JETP** • 1955(28)1 • AIP

Zh(ur). fiz. khimii; ZhFKh • Zhurnal fizicheskoi khimii • **Russian Journal of Physical Chemistry** • 1959(33)7 • CS

Zh(ur). neorg(an). khim.; ZhNKh • Zhurnal neorganicheskoi khimii • **Russian Journal of Inorganic Chemistry** • 1959(4)1 • CS

Zh(ur). obshch. khim.; ZhOKh • Zhurnal obshchei khimii • **Journal of General Chemistry of the USSR** • 1949(19)1 • CB

Zh(ur). org. khim.; ZhOrKh(im) • Zhurnal organicheskoi khimii • **Journal of Organic Chemistry of the USSR** • 1965(1)1 • CB

Zh(ur). prikl. khim.; ZhPKh • Zhurnal prikladnoi khimii • **Journal of Applied Chemistry of the USSR** • 1950(23)1 • CB

Zh(ur). prikl. mekhan. i tekhn. fiz. • Zhurnal prikladnoi mekhaniki i tekhnicheskoi fiziki • **Journal of Applied Mechanics and Technical Physics** • 1965( )1 • FP

Zh(ur). prikl. spektr. • Zhurnal prikladnoi spektroskopii • **Journal of Applied Spectroscopy** • 1965(2)1 • FP

Zh(ur). strukt(urnoi) khim.; ZhSKh • Zhurnal strukturnoi khimii • **Journal of Structural Chemistry** • 1960(1)1 • CB

Zh(ur). tekhn. fiz.; ZhTF • Zhurnal tekhnicheskoi fiziki • **Soviet Physics—Technical Physics** • 1956(26)1 • AIP

Zh(ur). vses. khim. ob-va im. Mendeleeva • Zhurnal vsesoyuznogo khimicheskogo obshchestva im. Mendeleeva • **Mendeleev Chemistry Journal** • 1965(10)1 • FP

Zh(ur). vychis. mat. i mat. fiz. • Zhurnal vychislitel'noi matematika i matematicheskoi fiziki • **USSR Computational Mathematics and Mathematical Physics** • 1962(1)1 • PP

ZL • *see* Zavodsk. laboratoriya

REVIEWS OF PLASMA PHYSICS
VOLUME 1

A comprehensive introduction to "classical" plasma physics, containing the following four important papers:

MOTION OF CHARGED PARTICLES IN ELECTROMAGNETIC FIELDS IN THE DRIFT APPROXIMATION

By D. V. Sivukhin

A development of the first-order approximation for the motion of a charged particle in strong magnetic fields with weak spatial inhomogeneities or in strong magnetic fields when weak electric fields are present. The solution of the equations of motion for the problem of a constant, uniform magnetic field provides the zero-th approximation to these special cases. Using this zero-th approximation as a basis, the first approximation is obtained, representing an estimate of the particles' motion in these electromagnetic fields which does not, however, account for small rapid oscillations of the particle about the trajectory characteristic of the smooth motion.

CONTENTS: Motion of a charged particle in a constant uniform magnetic field • Motion of the guiding center • Origin of the drifts • Smoothing and averaging of quantities containing rapidly varying terms • Complete system of equations of motion in the drift approximation • More exact system of equations of motion in the drift approximation • Derivation of certain auxiliary relations • Derivation of a compatible system of equations of motion in the drift approximation • Another approach to the equation of motion of the guiding center • Examples • Drift integrals of the motion in constant electric and magnetic fields • Liouville theorem in the drift approximation • Extension of drift theory to the case of strong transverse electric fields • References.

PARTICLE INTERACTIONS IN A FULLY IONIZED PLASMA

By B. A. Trubnikov

Reviews the kinetic effects associated with particle interactions in a fully ionized homogeneous gas. Special potential functions and electrostatic analogies are employed in the analysis. The motion of test particles in a plasma is considered, and a non-rigorous derivation of the kinetic equations is presented. Kinetic effects in high-temperature plasmas are also investigated.

CONTENTS: Test Particles in a Plasma: Force of friction due to scattering in a Coulomb field • Coulomb logarithm and the role of remote interactions • Average force acting on a particle in a plasma • Test particles in a plasma • Rate of change of the moments • Characteristic features of the Coulomb interaction: The potential functions χ and φ • Use of the scattering cross sections • **Kinetic Equation for Coulomb Particles:** Motion of particles in phase space • Expression for the flux • Force of dynamical friction and the diffusion tensor • Kinetic equation for the Coulomb interaction • Kinetic equation taking account of polarization of the medium • **Kinetic Effects in High-Temperature Plasmas:** Test particle in a medium of infinitely heavy field particles at rest • Solution of the kinetic equation for the preceding case: "basic" relaxation time • Spherically symmetric distribution of field particles • Runaway electrons • Maxwellian distribution of field particles: relaxation time • Plane flux in an equilibrium plasma • Energy transfer • Approach to equilibrium in a two-component plasma • References.

TRANSPORT PROCESSES IN A PLASMA

By S. I. Braginskii

Discusses transport processes in a fully ionized gas having a single species (simple plasma). The transport coefficients for a simple plasma are presented and given qualitative physical interpretations. They are then computed numerically from the kinetic equation. Some of the problems arising from the use of the transport equations to describe a plasma in a strong field are investigated. The application of the transport equations for particles of different species in analyses which assume a plasma model based on a single complex gas is also studied.

CONTENTS: Transport equations • Transport equations for a simple plasma (summary of results) • Kinetics of a simple plasma (qualitative description) • Kinetics of a simple plasma (quantitative analysis) • Certain paradoxes • Hydrodynamic description of a plasma • Multicomponent plasma • Examples • Appendix • References.

THERMODYNAMICS OF A PLASMA

By A. A. Vedenov

Examines the statistical thermodynamics of a system of particles characterized by Coulomb interactions. The difficulty of determing the thermodynamic quantities of nonideal systems when there is no small physical parameter in terms of which the quantities of interest can be expanded is noted, and for this reason, only weakly nonideal Coulomb gases are studied. In this case, the small parameter is the ratio of the mean Coulomb scattering amplitude to the mean distance between particles. The thermodynamic potential of the plasma is expanded in terms of this small parameter, and the leading terms of the virial expansions for both classical and quantum Coulomb systems are studied.

CONTENTS: Classical Coulomb system • Quantum Coulomb system • Degree of ionization of a plasma.

326 pages 1965 $12.50

(c/b) **CONSULTANTS BUREAU** 227 West 17th Street, New York, New York 10011